1331

ON THE SIGMA-NUCLEON INTERACTION

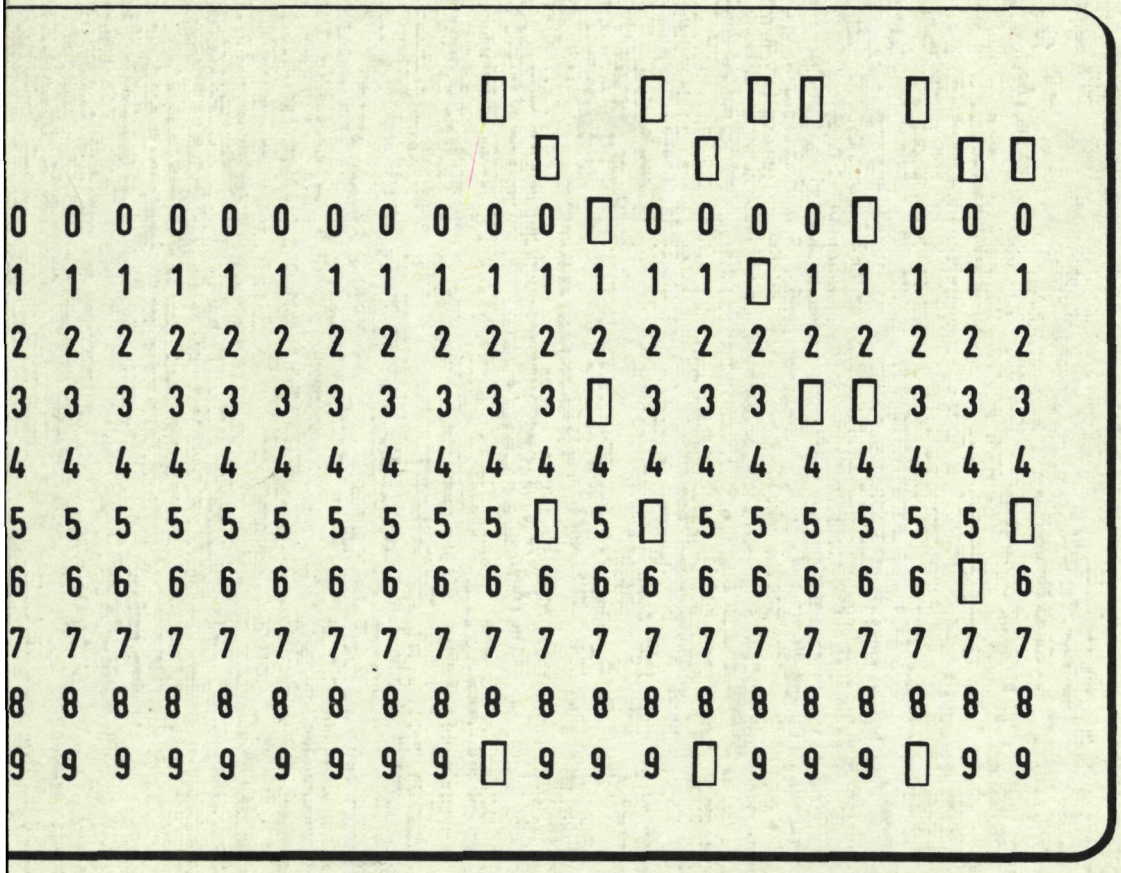

J.C. HELDER

ON THE SIGMA-NUCLEON INTERACTION

PROMOTOR: PROF.DR.IR. J.J. DE SWART

ON THE SIGMA-NUCLEON INTERACTION

PROEFSCHRIFT

TER VERKRIJGING VAN DE GRAAD VAN DOCTOR
IN DE WISKUNDE EN NATUURWETENSCHAPPEN
AAN DE KATHOLIEKE UNIVERSITEIT TE NIJMEGEN,
OP GEZAG VAN DE RECTOR MAGNIFICUS DR. A.Th.L.M. MERTENS,
HOOGLERAAR IN DE FACULTEIT DER GENEESKUNDE,
VOLGENS BESLUIT VAN DE SENAAT
IN HET OPENBAAR TE VERDEDIGEN
OP VRIJDAG 10 NOVEMBER 1967 DES NAMIDDAGS TE 2 UUR

DOOR

JAN CORNELIS HELDER
GEBOREN TE BARNEVELD

1967

OFFSETDRUK FACULTEIT DER WISKUNDE EN NATUURWETENSCHAPPEN

NIJMEGEN

Aan Anneke

Aan mijn moeder

CONTENTS

Gaarne wil ik op deze plaats hen bedanken die bij het tot stand komen van dit proefschrift in het bijzonder hun medewerking verleend hebben.
Drs. G. Fast heeft zijn enthousiasme voor het werken met rekenmachines op mij overgedragen. Ik ben hem en Dr. C. Dullemond dankbaar voor veel discussies.
De medewerkers van het U.R.C. hebben mij verbaasd door hun geduldige bemiddeling tussen mens en machine, die met elkaar in lastigheid wedijverden.
I wish to thank Dr. V. Hepp and Dr. H.G. Dosch for an enlightening discussion on the experimental results.
I am indebted to Dr. R. Piñon who corrected many offenses against the English grammar.
Het accurate typewerk van Mejuffrouw J.M.M. Korbeeck, de vermenging van precisie en artisticiteit van de afdeling Illustratie en het enthousiasme van de offsetdrukkerij waren onmisbaar voor de definitieve vormgeving van dit proefschrift.

CHAPTER 1
INTRODUCTION AND SUMMARY

We will be concerned in this thesis with Σ-hyperon-nucleon interactions. Both particles are considered to be elementary, and belong to the group of strongly interacting particles, or for short, the hadrons. In Table 1.1 we have summarized some properties [1] of those hadrons that are of interest to us.

Baryons $J^P = \frac{1}{2}^+$

	T	T_z	Y	Q	M
p	$\frac{1}{2}$	$\frac{1}{2}$	1	1	938.256
n	$\frac{1}{2}$	$-\frac{1}{2}$	1	0	939.550
Λ	0	0	0	0	1115.4
Σ^+	1	1	0	1	1189.41
Σ^0	1	0	0	0	1192.3
Σ^-	1	-1	0	-1	1197.08
Ξ^0	$\frac{1}{2}$	$\frac{1}{2}$	-1	0	1314.3
Ξ^-	$\frac{1}{2}$	$-\frac{1}{2}$	-1	-1	1320.8

Pseudoscalar mesons $J^P = 0^-$

	T	T_z	Y	Q	M
π	1	±1,0	0	±1,0	138.1
K	$\frac{1}{2}$	$\pm\frac{1}{2}$	±1	±1,0	496
η	0	0	0	0	584.7
X^0	0	0	0	0	959

Vector mesons $J^P = 1^-$

	T	T_z	Y	Q	M
ρ	1	±1,0	0	±1,0	763
K^*	$\frac{1}{2}$	$\pm\frac{1}{2}$	±1	±1,0	891
ω	0	0	0	0	782.8
ϕ	0	0	0	0	1019.5

Table 1.1. Properties of some hadrons. Given are spin J and parity P, the quantum numbers for isospin T and T_z, hypercharge Y, charge Q and mass M (in MeV/c^2).

In the theoretical investigations of the strong interactions two main lines of effort can be distinguished. Rather recently, the symmetry properties of the hadrons have been studied using group theoretical methods, whereas the more dynamical approaches, such as the use of potential models, techniques based on the use of dispersion relations, etc. have been used for a much longer time.

The hadrons can be arranged in multiplets by assigning them to the bases of irreducible representations of unitary groups. This way, one can find some order in the tremendous proliferation of elementary particles.

Also, relations for various properties of the hadrons can be predicted from these symmetry properties. This approach can be compared with the well known concept of isotopic spin, which treats for example the proton and the neutron on an equal footing, considering them as two states of one particle: the nucleon. This isospin multiplet can be assigned to a representation of SU(2).

The first successful higher symmetry scheme was the octet model [2] (unitary symmetry), proposed independently by Gell-Mann [3] and Ne'eman [4]. This theory is based on the use of the group SU(3), the group of unimodular and unitary transformations in a three dimensional complex linear vector space. After the success of SU(3), several higher symmetries for the strong interactions have been proposed, for example SU(6) [5].

Much work has been done using the more dynamical theories. We will consider in some detail the results of the investigations on the nucleon-nucleon (NN) interactions [6], since a theoretical study of the ΣN interactions bears much in common with these investigations. The low energy NN interactions have been studied first by using a phenomenological potential in conjunction with the Schrödinger equation. The most important result of these investigations is that the main features of this potential for ranges not too short can be described rather well by pion exchange potentials derived from meson theory [7]. For shorter distances phenomenological parts must still be added, such as a short range spin-orbit potential [8], and a repulsive hard core [9]. This is especially true for the experimental data at higher energy, that became more and more available. The strong central repulsion from the hard core and the spin-orbit term follow in a natural way if the exchange of vector mesons is assumed [10,11]. Encouraging results have been obtained in analyses of the NN interaction in terms of potentials derived from the one-meson-exchange Born terms [12]. In some of the more recent investigations [12] the same Born terms are used, but a unitary scattering amplitude is derived by employing dispersion relations. Usually the exchange of a scalar meson has to be included in these one-boson-exchange potentials. Experimentally, however, the existence of this meson is not certain.

Let us now consider the hyperon-nucleon (YN) interaction. Experimentally, this interaction is much less known than the NN interaction, since the experiments are much more difficult. Only recently have some experiments on low energy Λp and Σp scattering been done with reasonable accuracy (see Chapter 2 and the references given there). Since practically nothing is known about ΞN interactions, we will therefore not consider

the Ξ hyperons.

The theoretical work on low energy ΣN scattering is based on assumptions similar to those used for NN interactions. We will bypass the crude calculations for hyperon-nucleon (YN) interactions with very simple phenomenological potentials like square wells. More interesting are the investigations for which more realistic potentials have been used in the Schrödinger equation. It is in principle possible to relate the YN potentials to the NN ones. The now outdated global symmetry model [13] has been used [25] for this purpose. Calculations in this spirit have been done by several authors [14-17]. The use of SU(3) symmetry, on the other hand, to relate the YN and NN interactions has met severe difficulties caused by the large mass differences both between the mesons that generate the potential and between the interacting baryons [18]. For instance, the possibility of YN and YY bound states has been considered, yielding qualitatively satisfying results [19]. The more quantitative statements [20], however, seem to be heavily violated by the symmetry breaking. Another approach is the calculation of the YN potentials directly by means of meson-theoretical methods [21]. Extensive calculations for ΛN and ΣN interaction have been done by De Swart and Iddings [22,23]. They use the one and two pion exchange potentials calculated with the prescription of Brueckner and Watson [24]. Dispersion relation methods have been used by Dosch and Müller [26] for Σ^+p and Λn interactions. They derive, for S-waves, the effective range and shape dependent parameter as a function of the scattering length.

Since more accurate experiments (see Chapter 2) have resulted in substantial changes in previous data, and also have provided some new data, the theoretical work on the hyperon-nucleon interaction is now outdated, as far as the comparison with the experiments is concerned. Also recently developed theories like SU(3) and SU(6) have given an opportunity to extend the earlier theoretical work. On the other hand, calculations on hyperon-nucleon interactions can be used as a test for some predictions of these symmetry theories. Therefore, it seems worthwhile studying the YN interaction, using the recent theories for strongly interacting particles and to compare the results with the new experimental data.

In this thesis we will study low energy ΣN interactions up to the maximum energies for which the most recent experiments have been done, i.e., to energies of about 10 MeV in the laboratory. Since these experiments consider only $\Sigma^\pm$p scattering, we will restrict ourselves to these reactions. The ΛN interactions have been studied by Fast. We will use some of his results [27]

as input data for our calculations. Because of the similarity of the ΛN and the ΣN interaction, some parts of this thesis will run parallel to his work.

After a review of the experimental data in Chapter 2, we have described in Chapter 3, 4, and 5 the model we have employed for our calculations. Essentially it is based on the use of the Schrödinger equation in which a potential is inserted derived with meson-theoretical methods.

It is assumed that the potential describing the YN interactions can be derived using one-meson-exchange Born terms. We have included the potential due to the exchange of two pions using the prescription of Brueckner and Watson [24], since in the $\Lambda p \to \Lambda p$ interaction the exchange of one pion is impossible by isospin conservation, and also since the mass of the pion is so small that even for 2π-exchange potentials the range is a relatively long one. In Chapter 3 we have derived these potentials, considering the exchange of pseudoscalar and of vector mesons. In the same chapter the symmetry properties (SU(2), SU(3), SU(6)) have been discussed, from which relations can be found for the coupling constants.

The formalism for multichannel scattering [28] has been applied on Σp scattering in Chapter 4. In the Σp interaction a coupling exists between states of different orbital angular momentum due to the tensor part of the potential and coupling between channels where other particles are present. This implies that the Schrödinger equation can be reduced only to a set of coupled differential equations, up to six in the most complicated case.

The Coulomb potential has a considerable influence at these low energies. The implications of this long range potential on the scattering formalism are considered in Chapter 5. An effective range expansion for multichannel scattering, including a Coulomb potential, has been derived for general values of the orbital angular momentum.

In Chapter 6 we discuss the numerical methods and the structure of the computer programs we had to use in order to integrate the Schrödinger equation numerically and to compute the experimental quantities.

The following chapters give the results of the computations. In Chapter 7 we have first given an approximation for the inclusion of the Coulomb effects and compared the results with the exact computations. Then the $\Sigma^{\pm}$p scattering has been studied, using only potentials due to the exchange of pseudoscalar mesons. To these potentials we have added hard cores, whose radii had been determined by fitting the ΛN scattering lengths to the experimental values. Using the known value of the NNπ coupling constant, the other coupling constants are given by SU(3) symmetry in terms of one param-

eter, the F/(F+D) ratio α. A good fit with the experimental $\Sigma^- p$ data could be obtained for $\alpha \sim 0.5$, being close to the prediction of SU(6): $\alpha=0.4$. In the $\Sigma^- p \to \Lambda n$ angular distribution we obtained an enhancement in the forward direction in accordance with the experimental result.

One aspect of these calculations should be investigated further. Using the same potentials with the hard core radii derived from ΛN scattering also for the $\Sigma^+ p$ interaction, which is purely isospin T=3/2, whereas the ΛN system is purely T=1/2, we have obtained a singlet $\Sigma^+ p$ bound state in many cases. Such a bound state has not been found experimentally. The only evidence is an enhancement in the $\Sigma^+ p$ angular distribution in the forward direction. This could possibly be explained by assuming such a bound state that gives rise to a constructive Coulomb interference. We have shown that this implies the existence of a bound state with too much binding energy.

Rejecting the possibility of a $\Sigma^+ p$ bound state we had to drop the assumption that the T=1/2 and T=3/2 cores are equal. In Chapter 8 we have therefore developed an approximational method which enables us to treat a mixture of T=1/2 and T=3/2 states, with different cores in these states. The results of the previous chapter remain essentially the same.

In Chapter 9, finally, we have repeated the calculations of Chapter 7 and 8, but now using a potential due to the exchange of pseudoscalar and vector mesons. Employing the predictions of SU(6) for the coupling constants and using for the magnetic NNρ coupling constant a value derived from NN interactions, we were able to obtain a good agreement with the experiments.

A few remarks about the notation are in order. We will use units such that $\hbar = c = 1$. Unless otherwise stated, length are expressed in pion Compton wave lengths ($1\ m_\pi^{-1} = 1.41\text{fm} = 1.41 \times 10^{-13}\text{cm}$). Except in Chapter 3, we have denoted by p the momentum in the laboratory system, and by k the momentum in the c.m. system. We have used the symbol $\sim$ for "approximately equal", $\underset{\sim}{\sim}$ for "asymptotically equal", and $\propto$ for "proportional to".

CHAPTER 2
EXPERIMENTS

Experimentally, the hyperon-nucleon system is much more difficult to study than the corresponding nucleon-nucleon system. There are several reasons for this. Firstly, the bound state of a proton and a neutron, the deuteron, has given much insight into the NN interaction, but a bound state of two hyperons or of one hyperon with one nucleon has not been found. Secondly, the production of a beam of protons with a definite momentum has become fairly routine, and has resulted in scattering experiments with good statistics and over a wide range of energies. For hyperons this is not possible, since the mean lifetime of a hyperon is very short. The Λ and $\Sigma^{\pm}$ hyperons have lifetimes of the order of 10^{-10} sec., and the Σ^{o} hyperon, decaying electromagnetically, has a lifetime less than 10^{-14} sec. Therefore, a low energy $\Sigma^{\pm}$ hyperon traverses only a few mm before it decays. In most scattering experiments, the hyperons are produced in a hydrogen bubble chamber, after which they scatter with the hydrogen in the same chamber. However, because the path length traversed by a hyperon before decay is so short relative to the mean path length for collision in liquid hydrogen, a hyperon-proton collision will be very rare.

Although a bound state of a hyperon with one nucleon does not exist, bound states of a Λ hyperon with more nucleons do. Such a Λ-nucleus system is called a hyperfragment or hypernucleus [29]. A Σ hyperfragment is not generally expected to exist, for the Σ hyperon, being heavier than the Λ hyperon, would decay almost immediately via strong interactions according to the reactions $\Sigma^{-} + p \rightarrow \Lambda + n$ or $\Sigma^{+} + n \rightarrow \Lambda + p$. The only possibilities $\Sigma^{-}n$, and $\Sigma^{-}nn$ (or the charge symmetric states $\Sigma^{+}p$, and $\Sigma^{+}pp$), for which conservation of charge would prevent this decay, have not been observed. Consequently, the study of hyperfragments gives only information about the ΛN interaction.

An extensive discussion of the large amount of work that has been done on hyperfragments is beyond the scope of this thesis. We will only quote one result that can be derived from the hyperfragment data. From the analyses of the light hyperfragments De Swart and Dullemond [16] were able to estimate the singlet and triplet scattering lengths a_s and a_t and effective ranges r_s and r_t for the ΛN system. These parameters are very useful in describing the low energy ΛN interaction. They found

$$a_s = -(3.6\ ^{+3.6}_{-1.2})\ \text{fm} \qquad r_s \sim 2\ \text{fm}\ ,$$

$$a_t = -\ 0.53 \pm 0.12\ \text{fm} \qquad r_t \sim 5\ \text{fm}\ . \tag{2.1}$$

More recently, hyperon-nucleon scattering reactions have been studied in liquid hydrogen [30], deuterium [31] and propane [32] bubble chambers.

For the most recent experiment [33-41] the hyperons were produced in the Saclay 81 cm hydrogen bubble chamber at CERN, being exposed to a low energy K^- meson beam. The stopped K^- mesons produced hyperons according to the following reactions

$$\begin{aligned} K^- + p &\rightarrow \Sigma^- + \pi^+ \\ &\rightarrow \Sigma^+ + \pi^- \\ &\rightarrow \Sigma^0 + \pi^0 \\ &\rightarrow \Lambda + \pi^0\ . \end{aligned} \tag{2.2}$$

The Σ^0 decays almost immediately into $\Lambda + \gamma$.

Although all the reactions (2.2) for K^-p reactions at rest give a definite momentum for the produced hyperons, a small momentum spread is observed. This is because the $\Sigma^\pm$ hyperons slow down due to energy losses. Hence the Σ^- hyperon can be studied in the momentum interval $125\ \text{MeV/c} < p(\Sigma^-) < 173.4\ \text{MeV/c}$, and the Σ^+ hyperon in the interval $130\ \text{MeV/c} < p(\Sigma^+) < 181.5\ \text{MeV/c}$. The slight difference in these intervals is due to the small mass difference between Σ^+ and Σ^- hyperons. The lower limit is imposed because otherwise the residual range of the scattered particles becomes too short to enable an accurate measurement. Although the neutral Λ is not slowed down, the Λ's will still exhibit a momentum spread. The reaction $K^- + p \rightarrow \Lambda + \pi^0$ gives a unique Λ-momentum of 254 MeV/c, but the reactions $K^- + p \rightarrow \Sigma^0 + \pi^0$ followed by the decay $\Sigma^0 \rightarrow \Lambda + \gamma$, and $K^- + p \rightarrow \Sigma^- + \pi^+$ followed by the reaction $\Sigma^- + p \rightarrow \Lambda + n$ give Λ hyperons in the momentum interval $0\ \text{MeV/c} < p(\Lambda) < 250\ \text{MeV/c}$. Finally there is a small background of Λ's from in flight K^-p interactions. Hence a source of Λ hyperons extending to above 300 MeV/c exists [38].

Only a few of the produced hyperons will have an interaction with protons before they decay. Besides one has to apply severe cutoff criteria in order to avoid systematic errors caused by events that are difficult to detect or to insure an accurate measurement. Also the Coulomb scattering must be excluded. This reduces the number of events once more. For example, from 200,000 pictures one found 2500 elastic Σp scattering events. From this sample, after imposing the selection criteria, only 59 Σ^-p and 19 Σ^+p events

remained [36].

We will not consider here the ΛN interactions, but we only quote the values of the scattering lengths for the Λp interaction that give the best fit to the low energy experiments [42]. It is

$$a_s = -2.5 \pm 0.8 \text{ fm} \quad ,$$
$$a_t = -2.1 \pm 0.3 \text{ fm} \quad . \tag{2.3}$$

The triplet scattering length, in particular, differs substantially from the value given in (2.2). There is some evidence, however, that the triplet scattering length derived from the hyperfragment data could be greater than 0.53 fm [43].

As far as the ΣN interactions are concerned, only the $\Sigma^{\pm}$p scattering can be measured. There are also some results for Σ interactions with deuterium, obtained from K^- capture in a deuterium bubble chamber, but these reactions have poor statistics and are therefore less meaningful. As calculations [44] for these reactions require gross simplifications, hence making the results less certain, we will not use these results. We are left then with the following reactions. In a hydrogen bubble chamber the Σ^+ hyperon has only elastic interactions:

$$\Sigma^+ + p \to \Sigma^+ + p \quad . \tag{I}$$

The Σ^- hyperon, however, has inelastic interactions:

$$\Sigma^- + p \to \Lambda + n \tag{II^a}$$
$$\to \Sigma^o + n \quad , \tag{II^b}$$

as well as the elastic reaction:

$$\Sigma^- + p \to \Sigma^- + p \quad . \tag{II^c}$$

All these reactions can occur in the momentum interval given above. We will call these "reactions in flight". The reactions II^a and II^b also take place for stopped Σ^- hyperons. Since in a bubble chamber neutral particles cannot be seen, the scattering event has to be reconstructed from the secondary occurring particles. The Σ^o decays into $\Lambda + \gamma$, and the Λ hyperons can be seen if they decay as $\Lambda \to \pi^- + p$. Only the Λ hyperons having this decay mode are considered in the experiments.

We will first discuss the absorption reactions at rest. In this case

the Σ^- hyperon comes to rest in hydrogen and forms a Σ^-p atom due to the Coulomb potential. From measurements of the absorption time [45] and from calculations of this time for different capture mechanisms [46] one concludes that a Stark mixing effect leads to rapid capture from s-states of still rather high principal quantum number n. It is very important that this capture takes place from an s-state and that the capture from p-states does not occur frequently, which would be the case if the negatively charged particle were only cascading down. Therefore we may assume that the reactions II^a and II^b for Σ^- hyperons at rest occur from s-states. We will also make the reasonable assumption that 1/4 of the Σ^-p atoms are formed in a singlet state and 3/4 in a triplet state, and that there are no important transitions between singlet and triplet states during the deexcitation of the atom. One defines the capture ratio r_C by the expression

$$r_C = \frac{\# \Sigma^o}{\# \Sigma^o + \# \Lambda} \quad , \tag{2.4}$$

where $\# \Sigma^o$ is the number of Σ^o events found when the Σ^- is captured at rest, and similarly for $\# \Lambda$. In Chapter 4 we will relate this ratio to the cross sections using the assumptions mentioned above. The Σ^o hyperon in these reactions cannot be seen, but the Λ into which it decays can be distinguished from the Λ in reaction II^a by its kinematics. The first Λ has a kinematic energy in the interval $0.2 < E_\Lambda < 7.6$ MeV, whereas the second Λ has a unique kinetic energy of 36.8 MeV [36,37].

For Σ^-p interactions in flight one can also define the ratio

$$r_F = \frac{\# \Sigma^o}{\# \Sigma^o + \# \Lambda} \quad , \tag{2.5}$$

where now $\# \Sigma^o$ is the number of Σ^o, observed for interactions at the considered momentum. Of course, these reactions do not occur via a Σ^-p atom. Again the decay Λ can be distinguished from the directly produced Λ hyperon by its kinematics.

The total cross sections, angular distributions and polarizations were measured for the $\Sigma^\pm p$ reactions in flight. The total cross section can be measured for each of the reactions I and II.

The measurement of an angular distribution has only meaning if one has enough events. The difficulty of finding all scatter events with short recoils of the colliding particles makes a measurement of the angular distri-

bution for elastic Σp scattering not very reliable in the neighbourhood of $\cos\theta \lesssim 1$. On the other hand, for the reaction $\Sigma^- p \to \Lambda n$ the total angular region $-1 \leq \cos\theta \leq 1$ can be studied. The angular distribution for the reaction $\Sigma^- p \to \Sigma^0 n$ cannot be measured, since the Σ^0 decays almost immediately into $\Lambda + \gamma$. However, one could have some impression about the angular distribution of the Σ^0 hyperons, if the distribution of the Λ in the $\Sigma^- p$ rest system is anisotropic, if one assumes that the Λ decay is isotropic [35,36].

One also measures the polarization of the Λ in reaction II[a]. This is done by studying the angular distribution of the protons that arise from the decay $\Lambda \to p + \pi^-$ in the rest system of the Λ hyperon.

Measurements on Σp scattering have been done at Heidelberg [33-36] and Maryland [37-40]. In Table 2.1 we have quoted the latest results of the Heidelberg group [34-36]*. The total cross sections obtained by the Maryland group for $\Sigma^{\pm} p$ elastic scattering [40], $\sigma(\Sigma^- p \to \Sigma^- p) = 166 \pm 33$ mb at a mean laboratory momentum $\bar{p}(\Sigma^-) = 150$ MeV/c and $\sigma(\Sigma^+ p \to \Sigma^+ p) = 83 \pm 34$ mb at $\bar{p}(\Sigma^+) = 161.5$ MeV/c are in reasonable agreement with the results of Heidelberg.

$\Sigma^+ p$		$\Sigma^- p$			
p_{Σ^+}	σ_{Σ^+}	p_{Σ^-}	σ_{Λ}	σ_{Σ^0}	σ_{Σ^-}
153 ± 5	203 ± 117	140 ± 5	164 ± 25	125 ± 25	207 ± 85
163 ± 5	143 ± 58	150 ± 5	147 ± 19	111 ± 19	198 ± 48
173 ± 5	89 ± 28	160 ± 5	124 ± 14	115 ± 16	189 ± 32

Table 2.1 The total cross section (mb) for the $\Sigma^{\pm} p$ elastic and the $\Sigma^- p$ inelastic reactions for different laboratory momenta (MeV/c)

The angular distributions and the polarization of the Λ hyperon have been measured only by the Heidelberg group, since the number of events in Maryland was too small to permit such a measurement. The angular distributions are given in Fig. 2.1 - 2.3 and the polarization of the Λ in Table 2.2

* These results were obtained using the mean life times of the Σ hyperons, $\tau(\Sigma^+) = 0.794 \times 10^{-10}$ sec and $\tau(\Sigma^-) = 1.58 \times 10^{-10}$ sec (Tables of UCRL-8030 (rev.), March 1965) More recent results (Chung-Yun Chang, Nevis report CU-1932-251, Nevis-145, Feb 1966, Columbia University) give the values $\tau(\Sigma^+) = (0.830 \pm 0.018) \times 10^{-10}$ sec and $\tau(\Sigma^-) = (1.667 \pm 0.026) \times 10^{-10}$ sec These values would increase the cross sections with about 10% [36]

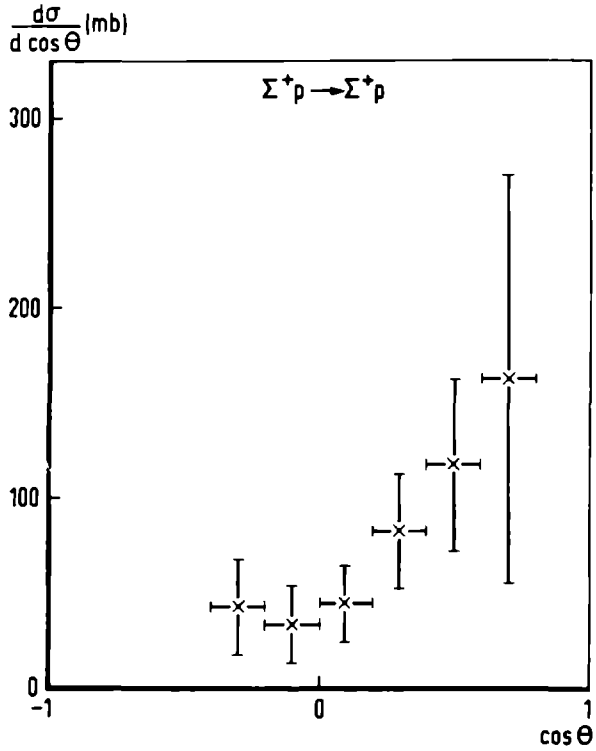

Fig. 2.1. The angular distribution for the reaction $\Sigma^+p \to \Sigma^+p$ in the momentum interval 148 MeV/c < $p(\Sigma^+)$ < 178 MeV/c

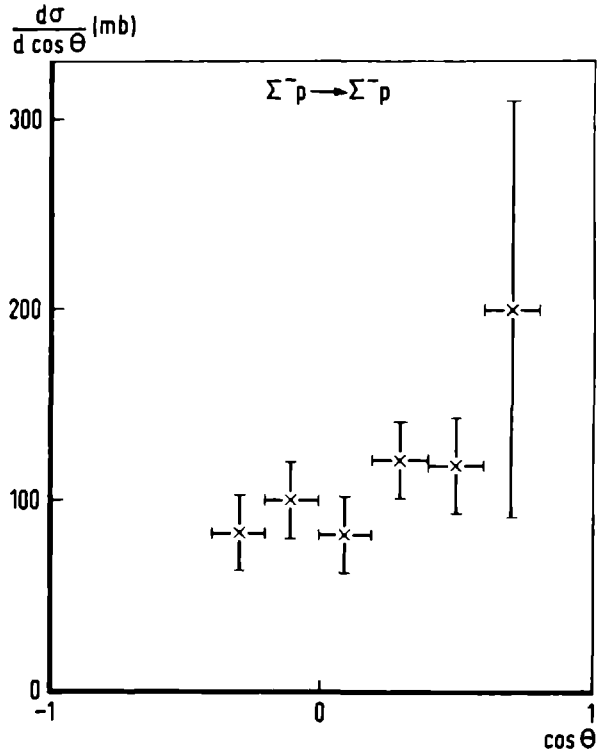

Fig. 2 2. The angular distribution for the reaction $\Sigma^-p \to \Sigma^-p$ in the momentum interval 135 MeV/c < $p(\Sigma^-)$ < 165 MeV/c.

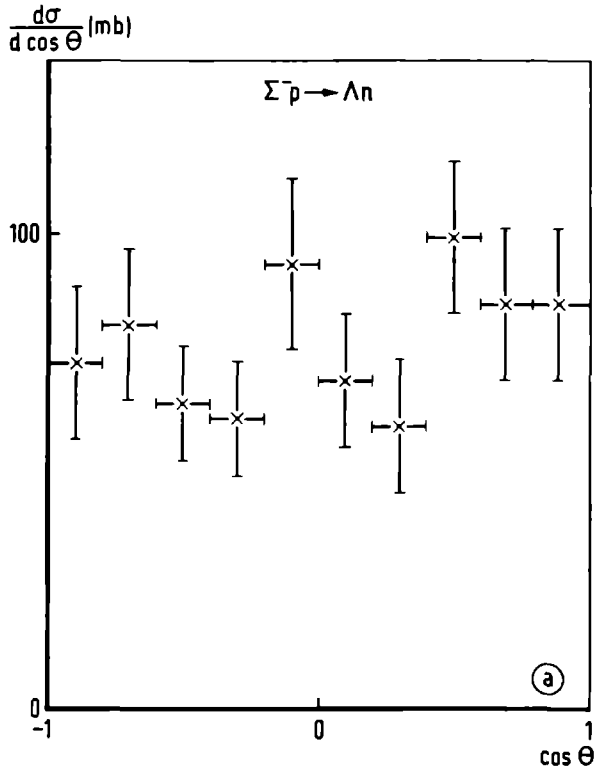

Fig. 2 3[a] The angular distribution for the reaction $\Sigma^-p \to \Lambda n$ in the momentum interval 100 MeV/c < $p(\Sigma^-)$ < 170 MeV/c

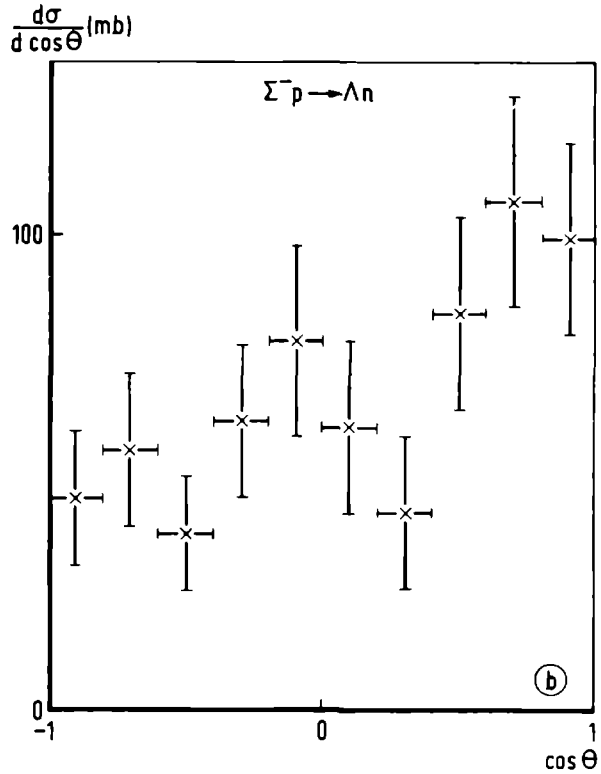

Fig 2 3[b] The angular distribution for the reaction $\Sigma^-p \to \Lambda n$ in the momentum interval 150 MeV/c < $p(\Sigma^-)$ < 170 MeV/c.

Momentum	Angles	Polarization
100 - 170	0° - 180°	-0.6 ± 0.4
100 - 170	0° - 90°	-0.3 ± 0.5
100 - 170	90° - 180°	-0.8 ± 0.6
0 - 100	0° - 180°	$+0.03 \pm 0.07$

Table 2 2 The polarization of the Λ hyperon in the reaction $\Sigma^{-}p \to \Lambda n$ for different Σ^{-} momentum intervals and for different angular regions of the Λ in the c m of the $\Sigma^{-}p$ system The polarization is in the direction of the normal $\underline{n} = (\underline{k}_{i} \times \underline{k}_{f})/|\underline{k}_{i} \times \underline{k}_{f}|$

We shall be using in the following chapters for the $\Sigma^{-}p$ cross sections the weighted averages

$$\sigma(\Sigma^{-}p \to \Lambda n) = 135 \pm 12 \text{ mb} \quad ,$$
$$\sigma(\Sigma^{-}p \to \Sigma^{0}n) = 115 \pm 12 \text{ mb} \quad ,$$
$$\sigma(\Sigma^{-}p \to \Sigma^{-}p) = 185 \pm 25 \text{ mb} \quad ,$$

all at a Σ^{-} laboratory momentum of 155 MeV/c, corresponding with E_{lab}=10MeV. For the $\Sigma^{+}p$ interactions we have not used the Maryland result, since this has been obtained with very weak selection criteria to gain statistics, but even then they have only 9 events. The average over the momentum intervals for the $\Sigma^{+}p$ total cross section is [34]

$$\sigma(\Sigma^{+}p \to \Sigma^{+}p) = 135 \pm 35 \text{ mb}$$

at $p(\Sigma^{+}) = 163$ MeV/c, corresponding with $E_{lab} = 11$ MeV.

The weighted average over the momentum intervals for the ratio in flight r_{F} is [35]

$$r_{F} = 0.47 \pm 0.03 \quad ,$$

practically independent of the momentum ($105 \leq p(\Sigma^{-}) \leq 165$), whereas one has for the corresponding ratio at rest [33,37,38,41]

$$r_{C} = 0.45 \pm 0.02 \quad .$$

Considering these experimental data we notice that the experimental $\Sigma^{-}p$ inelastic cross section at $p(\Sigma^{-}) = 155$ MeV/c

$$\sigma(\Sigma^- p \overset{\rightarrow \Sigma^0 n}{\rightarrow \Lambda n}) = 250 \pm 17 \text{ mb}$$

is very close to the S-wave unitarity limit for inelastic scattering π/k^2, which is about 255 mb at this momentum. This implies that we have almost maximal absorption, assuming that the main contribution comes from S-waves. The experimental elastic $\Sigma^- p$ cross section is also in the neighbourhood of π/k^2, as it should be for maximal absorption.

For the case of $\Sigma^+ p$ elastic scattering there is no absorption, so that the cross section could be as large as $4\pi/k^2$. Since the experimental value is much smaller, we conclude that the $\Sigma^+ p$ interaction is weak.

The angular distributions for $\Sigma^\pm p$ elastic scattering are consistent with isotropy, but there is some evidence for a forward peaking. It is not clear, however, if this is caused by Coulomb scattering. The angular distribution for $\Sigma^- p \rightarrow \Lambda n$ is almost isotropic, but when taking only events with $p(\Sigma^-) > 150$ MeV/c, an enhancement in the forward directions is obtained. The angular distribution from the Λ arising from the decay $\Sigma^- p \rightarrow \Sigma^0 n$ and $\Sigma^0 \rightarrow \Lambda + \gamma$ was consistent with isotropy, and hence no statement could be made about the Σ^0 angular distribution.

CHAPTER 3
THE DERIVATION OF THE POTENTIAL

3.1. Introduction.

We assume that the potential in the Schrödinger equation, which describes the hyperon-nucleon system, can be derived from meson theory. For the nucleon-nucleon interaction, the problem of the construction of a field theoretic potential has been extensively studied [7]. We will follow quite closely one of the methods used there.

From general considerations [47] it follows that the range R of a potential caused by the exchange of a meson with mass m is given by $R \sim m^{-1}$ (in units $\hbar = c = 1$). Therefore one can divide the range of the potential into different regions [48]. For large r ($r \gtrsim 1.5\ m_\pi^{-1}$) the behaviour of the potential is determined by the exchange of one pion. For shorter distances, $0.7\ m_\pi^{-1} \lesssim r \lesssim 1.5\ m_\pi^{-1}$, exchange of two pions and of heavier mesons must be taken into account. For still shorter distances the contribution from the exchange of more mesons becomes more and more important, but one may hope that the exchange of heavy mesons will at least partly represent this contribution.

At very short distances it is impossible to give a reliable calculation for the potentials. For the NN interaction a phenomenological hard core has been used to explain the experimental data [9]. This core occurs in most phenomenological and semiphenomenological nuclear potentials. We will also use a repulsive hard core. Its radius will be discussed later.

In this chapter we will calculate the one meson exchange potentials. The potential due to the exchange of two pions is also given. We will restrict ourselves to local potentials. It is known from NN calculations that the velocity dependence of the potential does not have much influence on the final results at low energies [49]. Other recoil effects are taken into account to some extent.

In our computations we will use two sets of potentials. First we will calculate the potentials due to the exchange of the SU(3) octet of pseudoscalar mesons π, K, and η. Their coupling constants with the baryons involved will be related by requiring SU(3) symmetry.

The exchange of vector mesons explains some important properties of the phenomenological NN potentials, like the spin-orbit potential. The se-

cond set consists therefore of the first set plus the potentials due to the exchange of the vector mesons ρ, K^*, ω, and ϕ. The exchange of the pseudoscalar X^o is also included, but we did not use the scalar mesons for which experimental evidence is still scarce. We also did not include the exchange of the heavier 2^+ mesons. The coupling constants will now be required to obey relations required by SU(6) symmetry.

For NN interactions, these potentials have been calculated by Hoshizaki, Lin and Machida [50]. Some of our results are also obtained by Protopapadakis [51].

An important consequence of the exchange of mesons carrying charge or hypercharge is that the particles in the final state can be different from those in the initial state. We give a few examples in Fig. 3.1. Consequently, when considering Σ^-p scattering, for example, one has a coupling with $\Sigma^o n$ and Λn states (reactions II^a and II^b in Chapter 2) due to these strong interactions.

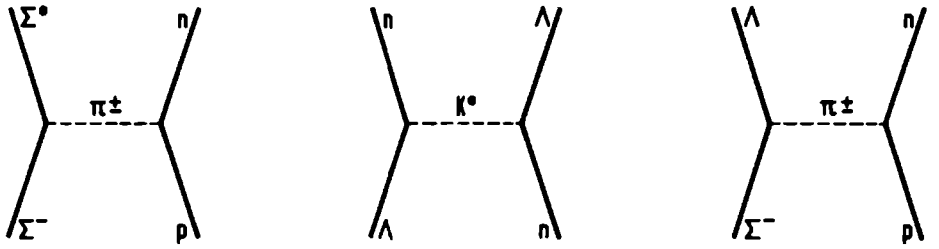

Fig. 3.1. Some diagrams illustrating the difference between initial and final states.

3.2. The calculation of the potentials in momentum space.

It is well known that if a two particle scattering process can be described by a Schrödinger equation, the potential can be related to the T-matrix by the Lippman-Schwinger equation

$$\langle a|T|b\rangle = \langle a|V|b\rangle + \Sigma_c \frac{\langle a|V|c\rangle\langle c|T|b\rangle}{E_b - E_c + i\varepsilon} \quad . \tag{3.1}$$

If one is able to calculate the T-matrix in the form of a series, e.g.,

$$T = g^2 T^{(2)} + g^4 T^{(4)} + \ldots \quad ,$$

and if we assume that we may write for the potential an analogous series

expansion

$$V = g^2 V^{(2)} + g^4 V^{(4)} + \ldots \quad ,$$

then one can write

$$\langle a|V^{(2)}|b\rangle = \langle a|T^{(2)}|b\rangle \quad , \tag{3.2a}$$

$$\langle a|V^{(4)}|b\rangle = \langle a|T^{(4)}|b\rangle - \Sigma_c \frac{\langle a|V^{(2)}|c\rangle\langle c|V^{(2)}|b\rangle}{E_b - E_c + i\epsilon} \quad , \tag{3.2b}$$

etc.

Except for the potential due to pion exchange, we will assume that $V=g^2V^{(2)}$ is a reasonably good approximation for the potential; hence $\langle a|V|b\rangle = \langle a|T^{(2)}|b\rangle$. The T-matrix will be obtained by relating it to the S-matrix, using the relation

$$\langle a|S|b\rangle = \delta_{ab} - 2\pi i\, \delta(E_a - E_b)\, \langle a|T|b\rangle \quad . \tag{3.3}$$

The S-matrix, finally, is calculated using Feynman rules. This yields the one meson exchange potential in momentum space. The essential assumption made here is that we may calculate the T-matrix in (3.1) by using a field theoretic calculation of the S-matrix.

Before we transform to coordinate space we will make some approximations. First we will neglect to some extent the recoil effects caused by the kinetic energy of the baryons. This is done as follows. Denoting the momentum of the exchanged meson by k and the momentum of the baryon with mass M in the c.m. by q, we make a development to powers of $(k/M)^2$ and $(q/M)^2$. The terms with powers of q/M will give rise to non-local potentials, or, what amounts to the same, velocity dependent potentials. This velocity dependence will be neglected, except that trivial dependence in the spin-orbit potential. The $(k/M)^2$ gives $-(m/M)^2$ after Fourier transformation. Therefore, we will neglect the recoil effects for the pseudoscalar mesons, but for the heavier vectormesons we have included terms of order $(k/M)^2$.

Furthermore, we have neglected the mass differences of the baryons, unless these differences would have a sizable influence.

The calculation of the two pion exchange potential is not unique, in the sense that different methods yield different results. We have chosen the prescription by Brueckner and Watson [24,22], which has the advantage that it has been tested for low energy nucleon-nucleon interaction and results, for that case, in a reasonable agreement with the experimental data.

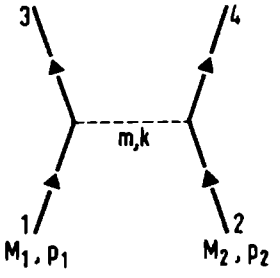

Fig 3 2 Diagram explaining the notation

Our notation is as follows. We number the baryons from 1 to 4 (Fig. 3.2) with mass M_i and fourmomentum p_i (and threemomentum $\underline{p}_i$). The exchanged meson has a mass m and fourmomentum k. Our metric is $p_i^2 = -M_i^2$.

We will first calculate the potentials due to the exchange of a pseudoscalar meson. The derivation we will give is strictly speaking valid only for the exchange of mesons with zero strangeness and isospin zero. For the other mesons some numerical factors have to be included. This will be considered later.

We take as interaction Hamiltonian

$$\mathcal{H}_I = i\, g_p\, \bar{\psi}\, \gamma_5\, \psi\, \phi \quad , \tag{3.4}$$

where $\bar{\psi}$ and ψ describe the creation and annihilation of the baryons and ϕ describes the meson fields. Using Feynman rules, we get for the second order S-matrix element (suppressing the spin indices)

$$\langle p_4,p_3|S^{(2)}|p_1,p_2\rangle = -i\,\frac{g_{13}\,g_{24}}{(2\pi)^2}\left(\frac{M_1\,M_2\,M_3\,M_4}{E_1\,E_2\,E_3\,E_4}\right)^{\frac{1}{2}}$$

$$\delta^{(4)}(p_1 + p_2 - p_3 - p_4)\;\bar{w}(p_3)\gamma_5\, w(p_1)$$

$$\frac{1}{(p_1-p_3)^2+m^2}\;\bar{w}(p_4)\gamma_5\, w(p_2) \quad . \tag{3.5}$$

In this formula g_{13} is the coupling constant between particle 1 and 3 and the pseudoscalar meson.

We use the Dirac representation for the γ matrices:

$$\underline{\gamma} = \begin{pmatrix} 0 & -i\underline{\sigma} \\ i\underline{\sigma} & 0 \end{pmatrix} \quad , \quad \gamma_4 = \begin{pmatrix} I & 0 \\ 0 & -I \end{pmatrix} \quad , \quad \gamma_5 = \begin{pmatrix} 0 & -I \\ -I & 0 \end{pmatrix} \quad , \tag{3.6}$$

and we have for the spinors the explicit representation

$$w(p) = \left(\frac{E+M}{2M}\right)^{\frac{1}{2}} \begin{pmatrix} u \\ \dfrac{\underline{\sigma}\cdot\underline{p}}{E+M}\, u \end{pmatrix} \quad , \tag{3.7}$$

where u is an ordinary Pauli spinor, describing the spin wave function of the baryon. Omitting the spinors u but giving the operators σ an index denoting the baryon on which it works, Eq. (3.5) reduces to

$$-i\,\frac{g_{13}\,g_{24}}{(2\pi)^2}\quad\left(\frac{(M_1+E_1)(M_2+E_2)(M_3+E_3)(M_4+E_4)}{16E_1E_2E_3E_4}\right)^{\frac{1}{2}}\ \delta^{(4)}(p_1+p_2-p_3-p_4)$$

$$\frac{1}{(p_1-p_3)^2+m^2}\quad\left(-\frac{\underline{\sigma}_1\cdot\underline{p}_1}{M_1+E_1}+\frac{\underline{\sigma}_1\cdot\underline{p}_3}{M_3+E_3}\right)\quad\left(-\frac{\underline{\sigma}_2\cdot\underline{p}_2}{M_2+E_2}+\frac{\underline{\sigma}_2\cdot\underline{p}_4}{M_4+E_4}\right)\quad . \tag{3.8}$$

We take the non-relativistic limit, i.e., we neglect $|\underline{p}|$ with respect to M, and we transform to the c.m. system, taking

$$\begin{aligned}\underline{p}_1 &= -\underline{p}_2 = \underline{p}\quad ,\\ \underline{p}_3 &= -\underline{p}_4 = \underline{p}'\quad ,\end{aligned} \tag{3.9}$$

and we define

$$\begin{aligned}\underline{k} &= \underline{p} - \underline{p}'\quad ,\\ \underline{q} &= (\underline{p} + \underline{p}')/2\ .\end{aligned} \tag{3.10}$$

Due to the transformation to the c.m. system we can replace the $\delta^{(4)}$ function by $(2\pi)^3\ \delta(E_1+E_2-E_3-E_4)$.

In the last two factors of (3.8) we neglect the mass difference between the two baryons and between the two hyperons by writing M' for the mean mass of the nucleons and M for the mean mass of the hyperons involved. In the propagator, however, we write $(p_1-p_3)^2 + m^2 = \underline{k}^2 + m^2_{eff}$ with $m_{eff} = m\sqrt{1-\gamma^2}$. This factor γ arises from the mass difference between the Σ and Λ hyperon and is extensively considered by De Swart and Iddings [22]. Using (3.1) and (3.3) the potential in momentum space due to the exchange of a pseudoscalar meson is

$$V_{PS} = -g_{13}g_{24}\,\frac{(\underline{\sigma}_1\cdot\underline{k})(\underline{\sigma}_2\cdot\underline{k})}{4MM'}\,\frac{1}{\underline{k}^2+m^2_{eff}}\quad . \tag{3.11}$$

For the vector mesons the interaction Hamiltonian is given by

$$\mathcal{H}_I = ig_V\,\bar{\psi}\,\gamma_\mu\psi\phi_\mu + (f_V/2m)\,\bar{\psi}\,\sigma_{\mu\nu}\psi(\partial_\nu\phi_\mu - \partial_\mu\phi_\nu) \tag{3.12}$$

with

$$\sigma_{\mu\nu} = \tfrac{1}{2}\,i(\gamma_\mu\gamma_\nu - \gamma_\nu\gamma_\mu)\quad . \tag{3.13}$$

The first term in (3.12) is called the electric interaction, the second the magnetic interaction. Using this interaction Hamiltonian, we obtain

for the second order S-matrix element

$$\langle p_4,p_3|S^{(2)}|p_1,p_2\rangle = -\frac{i}{(2\pi)^2}\left(\frac{M_1M_2M_3M_4}{E_1E_2E_3E_4}\right)^{\frac{1}{2}}\delta^{(4)}(p_1+p_2-p_3-p_4)$$

$$\bar{w}(p_3)\left[g_{13}\,\gamma_\mu + \frac{f_{13}}{m}\,\sigma_{\mu\rho}(p_{3_\rho} - p_{1_\rho})\right] w(p_1)$$

$$\frac{\delta_{\mu\nu} - (p_{3_\mu} - p_{1_\mu})(p_{4_\nu} - p_{2_\nu})/m^2}{(p_1-p_3)^2 + m^2}$$

$$\bar{w}(p_4)\left[g_{24}\,\gamma_\nu + \frac{f_{24}}{m}\,\sigma_{\nu\tau}(p_{4_\tau}-p_{2_\tau})\right] w(p_2) \quad . \tag{3.14}$$

Using the Dirac equation, we get

$$\bar{w}(p_3)\sigma_{\mu\nu}w(p_1)(p_{3_\nu}-p_{1_\nu}) = (M_1+M_3)\,\bar{w}(p_3)\gamma_\mu w(p_1) +$$

$$+ i\,\bar{w}(p_3)w(p_1)(p_{3_\mu}+p_{1_\mu}) \quad . \tag{3.15}$$

It follows also from the Dirac equation that the second term in the propagator gives contributions of order $(M_1-M_3)^2/m^2$, which we will neglect. So we can write for (3.14)

$$\frac{-i}{(2\pi)^2}\left(\frac{M_1M_2M_3M_4}{E_1E_2E_3E_4}\right)^{\frac{1}{2}}\delta^{(4)}(p_1+p_2-p_3-p_4)\,\frac{1}{(p_1-p_3)^2+m^2}$$

$$\bar{w}(p_3)\left[\left(g_{13} + \frac{M_1+M_3}{m}\,f_{13}\right)\gamma_\mu + \frac{if_{13}}{m}\,(p_{1_\mu}+p_{3_\mu})\right] w(p_1)$$

$$\bar{w}(p_4)\left[\left(g_{24} + \frac{M_2+M_4}{m}\,f_{24}\right)\gamma_\mu + \frac{if_{24}}{m}\,(p_{2_\mu}+p_{4_\mu})\right] w(p_2) \quad . \tag{3.16}$$

Using the Dirac representation (3.6) and defining the total spin $\underline{S}=\frac{1}{2}(\underline{\sigma}_1+\underline{\sigma}_2)$, we get, after transforming to the c.m. system,

$$\langle|S^{(2)}|\rangle = -2\pi i\left(\frac{N_1N_2N_3N_4}{E_1E_2E_3E_4}\right)^{\frac{1}{2}}\delta(E_1+E_2-E_3-E_4)\,\frac{1}{(p-p')^2+m^2}$$

$$\Bigg[G_{13}G_{24}\left\{\left(\frac{\underline{p}}{N_1}+\frac{\underline{p}'}{N_3}\right)\left(\frac{\underline{p}}{N_2}+\frac{\underline{p}'}{N_4}\right) + \left(1+\frac{\underline{p}\cdot\underline{p}'}{N_1N_3}\right)\left(1+\frac{\underline{p}\cdot\underline{p}'}{N_2N_4}\right) +$$

$$+ 2i\underline{S}\cdot[\underline{p}'\times\underline{p}]\left(\frac{1}{N_1N_4}+\frac{1}{N_2N_3}+\frac{\underline{p}\cdot\underline{p}'}{N_1N_2N_3N_4}\right) + i\,[\underline{p}'\times\underline{p}]\cdot\left(\frac{\underline{\sigma}_1}{N_1N_3}+\frac{\underline{\sigma}_2}{N_2N_4}\right) +$$

$$-(\underline{\sigma}_1\cdot\underline{\sigma}_2)\left(\frac{\underline{p}}{N_1}-\frac{\underline{p}'}{N_3}\right)\left(\frac{\underline{p}}{N_2}-\frac{\underline{p}'}{N_4}\right)+\underline{\sigma}_1\cdot\left(\frac{\underline{p}}{N_2}-\frac{\underline{p}'}{N_4}\right)\underline{\sigma}_2\cdot\left(\frac{\underline{p}}{N_1}-\frac{\underline{p}'}{N_3}\right)-\frac{\underline{\sigma}_1\cdot[\underline{p}'\times\underline{p}]\,\underline{\sigma}_2\cdot[\underline{p}'\times\underline{p}]}{N_1N_2N_3N_4}\Bigg\}+$$

$$-G_{13}\,\frac{f_{24}}{m}\left\{E_2+E_4+\frac{\underline{p}^2}{N_1}+\frac{\underline{p}'^2}{N_3}+\frac{N_1+N_3+E_2+E_4}{N_1N_3}\,(\underline{p}\cdot\underline{p}'+i\underline{\sigma}_1\cdot[\underline{p}'\times\underline{p}])\right\}$$

$$\left\{1-\frac{\underline{p}\cdot\underline{p}'+i[\underline{p}'\times\underline{p}]\cdot\underline{\sigma}_2}{N_2N_4}\right\}+$$

$$-G_{24}\,\frac{f_{13}}{m}\left\{E_1+E_3+\frac{\underline{p}^2}{N_2}+\frac{\underline{p}'^2}{N_4}+\frac{N_2+N_4+E_1+E_3}{N_2N_4}\,(\underline{p}\cdot\underline{p}'+i\underline{\sigma}_2\cdot[\underline{p}'\times\underline{p}])\right\}$$

$$\left\{1-\frac{\underline{p}\cdot\underline{p}'+i[\underline{p}'\times\underline{p}]\cdot\underline{\sigma}_1}{N_1N_3}\right\}+$$

$$+\frac{f_{13}f_{24}}{m^2}\left\{(\underline{p}+\underline{p}')^2+(E_1+E_3)(E_2+E_4)\right\}\cdot\Bigg\{\left(1-\frac{\underline{p}\cdot\underline{p}'}{N_1N_3}\right)\left(1-\frac{\underline{p}\cdot\underline{p}'}{N_2N_4}\right)+$$

$$+2i\underline{S}\cdot[\underline{p}'\times\underline{p}]\,\frac{\underline{p}\cdot\underline{p}'}{N_1N_2N_3N_4}-i[\underline{p}'\times\underline{p}]\left(\frac{\underline{\sigma}_1}{N_1N_3}+\frac{\underline{\sigma}_2}{N_2N_4}\right)$$

$$-\frac{\underline{\sigma}_1\cdot[\underline{p}'\times\underline{p}]\;\underline{\sigma}_2\cdot[\underline{p}'\times\underline{p}]}{N_1N_2N_3N_4}\Bigg\}\Bigg]\quad, \tag{3.17}$$

in which we have used

$$G_{13}=g_{13}+\frac{M_1+M_3}{m}\,f_{13}\quad,$$

and

$$N_1=M_1+E_1\quad,$$

etc.

Except in the propagator, we neglect again the mass difference between Λ and Σ hyperons by using M and M', as we did in the pseudoscalar case. Furthermore, we use the transformations (3.10). We will neglect, except in the term $[\underline{p}'\times\underline{p}]$, the $\underline{q}$, which gives rise to a non-local potential [52]. Consequently, we have $E_1 = E_2 = E$ and $E_3 = E_4 = E'$. We then get for the S-matrix element in the c.m. system

$$\langle|S^{(2)}|\rangle=-2\pi i\delta(2E-2E')\,\frac{(M+E)(M'+E')}{4EE'}\;\frac{1}{\underline{k}^2+m_{\text{eff}}^2}$$

$$\Bigg[G_{13}G_{24}\left\{\left(1-\frac{\underline{k}^2}{4N^2}\right)\left(1-\frac{\underline{k}^2}{4N'^2}\right)+\right.$$

$$+ i\underline{S}\cdot[\underline{k}\times\underline{q}]\left(\frac{4}{NN'} - \frac{\underline{k}^2}{2N^2N'^2}\right) +$$

$$+ i[\underline{k}\times\underline{q}]\left(\frac{\underline{\sigma}_1}{N^2} + \frac{\underline{\sigma}_2}{N'^2}\right) +$$

$$-(\underline{\sigma}_1\cdot\underline{\sigma}_2)\frac{\underline{k}^2}{NN'} + \frac{(\underline{\sigma}_1\cdot\underline{k})(\underline{\sigma}_2\cdot\underline{k})}{NN'} +$$

$$- \frac{\underline{\sigma}_1\cdot[\underline{k}\times\underline{q}]\,\underline{\sigma}_2\cdot[\underline{k}\times\underline{q}]}{N^2N'^2}\Bigg\} +$$

$$-G_{13}\frac{f_{24}}{m}\left\{2E'\left(1-\frac{\underline{k}^2}{4N^2}\right) + 2i\underline{\sigma}_1\cdot[\underline{k}\times\underline{q}]\left(\frac{N+E'}{N^2}\right)\right\}\left\{1+\frac{\underline{k}^2}{4N'^2} - \frac{i[\underline{k}\times\underline{q}]\cdot\underline{\sigma}_2}{N'^2}\right\} +$$

$$-G_{24}\frac{f_{13}}{m}\left\{2E\left(1-\frac{\underline{k}^2}{4N'^2}\right) + 2i\underline{\sigma}_2\cdot[\underline{k}\times\underline{q}]\left(\frac{N'+E}{N'^2}\right)\right\}\left\{1+\frac{\underline{k}^2}{4N^2} - \frac{i[\underline{k}\times\underline{q}]\cdot\underline{\sigma}_1}{N^2}\right\} +$$

$$+\frac{f_{13}f_{24}}{m^2}4EE'\left\{\left(1+\frac{\underline{k}^2}{4N^2}\right)\left(1+\frac{\underline{k}^2}{4N'^2}\right) - i\underline{S}\cdot[\underline{k}\times\underline{q}]\frac{\underline{k}^2}{2N^2N'^2} +\right.$$

$$\left.-i[\underline{k}\times\underline{q}]\left(\frac{\underline{\sigma}_1}{4N^2} + \frac{\underline{\sigma}_2}{4N'^2}\right) - \frac{\underline{\sigma}_1\cdot[\underline{k}\times\underline{q}]\,\underline{\sigma}_2\cdot[\underline{k}\times\underline{q}]}{N^2N'^2}\right\}\Bigg] \quad . \tag{3.18}$$

Since we have neglected the q-dependence in E, we have $E = (\frac{1}{4}\underline{k}^2+M^2)^{\frac{1}{2}}$ and we expand in powers of k/M:

$$E = M + \frac{\underline{k}^2}{8M} - \frac{\underline{k}^4}{32M^3} + \ldots \quad ,$$

$$\frac{1}{M+E} = \frac{1}{2M} - \frac{\underline{k}^2}{32M^3} + \ldots \quad , \tag{3.19}$$

etc.

Since the mass differences between the baryons are small, we have to a good approximation

$$\frac{1}{M^2} + \frac{1}{M'^2} = \frac{2}{MM'} \quad . \tag{3.20}$$

This yields, retaining only terms to order $1/M^2$,

$$\langle|S^{(2)}|\rangle = -2\pi i\delta(E_i-E_f)\frac{1}{\underline{k}^2+m_{eff}^2}\Bigg[g_{13}g_{24}\left\{1 - \frac{\underline{k}^2}{4MM'} +\right.$$

$$+ i[\underline{k}\times\underline{q}]\left(\frac{\underline{S}}{MM'}+\frac{\underline{\sigma}_1}{4M^2}+\frac{\underline{\sigma}_2}{4M'^2}\right)-(\underline{\sigma}_1\cdot\underline{\sigma}_2)\frac{\underline{k}^2}{4MM'}+(\underline{\sigma}_1\cdot\underline{k})(\underline{\sigma}_2\cdot\underline{k})\frac{\underline{k}^2}{4MM'}\Bigg\}+$$

$$+ g_{13}f_{24}\frac{2M'}{m}\Bigg\{\frac{\underline{k}^2}{8M^2}-\frac{\underline{k}^2}{8M'^2}-\frac{\underline{k}^2}{4MM'}+i[\underline{k}\times\underline{q}]\left(\frac{\underline{S}}{4MM'}-\frac{\underline{\sigma}_1}{2MM'}+\frac{\underline{\sigma}_2}{2M'^2}\right)+$$

$$-(\underline{\sigma}_1\cdot\underline{\sigma}_2)\frac{\underline{k}^2}{4MM'}+(\underline{\sigma}_1\cdot\underline{k})(\underline{\sigma}_2\cdot\underline{k})\frac{\underline{k}^2}{4MM'}\Bigg\}+g_{24}f_{13}\frac{2M}{m}\Bigg\{\frac{\underline{k}^2}{8M'^2}-\frac{\underline{k}^2}{8M^2}-\frac{\underline{k}^2}{4MM'}+$$

$$+ i[\underline{k}\times\underline{q}]\left(\frac{\underline{S}}{4MM'}+\frac{\underline{\sigma}_1}{2M^2}-\frac{\underline{\sigma}_2}{2MM'}\right)-(\underline{\sigma}_1\cdot\underline{\sigma}_2)\frac{\underline{k}^2}{4MM'}+\frac{(\underline{\sigma}_1\cdot\underline{k})(\underline{\sigma}_2\cdot\underline{k})}{4MM'}\Bigg\}+$$

$$+ f_{13}f_{24}\frac{4MM'}{m^2}\Bigg\{\frac{\underline{k}^4}{16M^2M'^2}+i[\underline{k}\times\underline{q}]\left(-\frac{7}{16}\frac{\underline{S}}{M^2M'^2}+\frac{\underline{\sigma}_1}{32M^4}+\frac{\underline{\sigma}_2}{32M'^4}\right)+$$

$$-(\underline{\sigma}_1\cdot\underline{\sigma}_2)\left(\frac{\underline{k}^2}{4MM'}-\frac{\underline{k}^4}{16M^2M'^2}\right)+(\underline{\sigma}_1\cdot\underline{k})(\underline{\sigma}_2\cdot\underline{k})\left(\frac{1}{4MM'}-\frac{\underline{k}^2}{16M^2M'^2}\right)+$$

$$-\frac{\underline{\sigma}_1\cdot[\underline{k}\times\underline{q}]\;\;\underline{\sigma}_2\cdot[\underline{k}\times\underline{q}]}{2M^2M'^2}\Bigg\}\Bigg] \quad . \tag{3.21}$$

It should be noted that in this expression a $(\underline{\sigma}_1-\underline{\sigma}_2)$ potential occurs, which is impossible for NN potentials. This potential is caused by two effects. Firstly, the mass difference between hyperons and nucleons gives a small contribution, but also the difference between $g_{13}f_{24}$ and $g_{24}f_{13}$ yields this potential. But, if the g and the f coupling constants obey the same symmetry properties, this potential disappears. In the following, we will neglect the $\underline{\sigma}_1-\underline{\sigma}_2$ potential. The possible consequences of a potential of this kind will be discussed in Chapter 4. We finally get then for the potential in momentum space, due to the exchange of a vector meson with zero hypercharge and isospin,

$$V_V=\frac{1}{\underline{k}^2+m_{eff}^2}\Bigg[\Bigg\{g_{13}g_{24}\left(1-\frac{\underline{k}^2}{4MM'}\right)-(g_{13}f_{24}+g_{24}f_{13})\frac{\underline{k}^2}{2m(MM')^{\frac{1}{2}}}+f_{13}f_{24}\frac{\underline{k}^2}{4m^2MM'}\Bigg\}+$$

$$+i\underline{S}\cdot[\underline{k}\times\underline{q}]\Bigg\{g_{13}g_{24}\frac{3}{2MM'}+(g_{13}f_{24}+g_{24}f_{13})\frac{2}{m(MM')^{\frac{1}{2}}}-f_{13}f_{24}\frac{3\underline{k}^2}{2m^2MM'}\Bigg\}+$$

$$-\underline{\sigma}_1\cdot\underline{\sigma}_2\Bigg\{g_{13}g_{24}\frac{\underline{k}^2}{4MM'}+(g_{13}f_{24}+g_{24}f_{13})\frac{\underline{k}^2}{2m(MM')^{\frac{1}{2}}}+f_{13}f_{24}\left(\frac{\underline{k}^2}{m^2}-\frac{\underline{k}^4}{4m^2MM'}\right)\Bigg\}+$$

$$+ (\underline{\sigma}_1\cdot\underline{k})(\underline{\sigma}_2\cdot\underline{k})\left\{ g_{13}g_{24}\,\frac{1}{4MM'} + (g_{13}f_{24}+g_{24}f_{13})\,\frac{1}{2m(MM')^{\frac{1}{2}}} + \right.$$

$$\left. + f_{13}f_{24}\left(\frac{1}{m^2} - \frac{\underline{k}^2}{4m^2MM'}\right)\right\} - \underline{\sigma}_1\cdot[\underline{k}\times\underline{q}]\,\underline{\sigma}_2\cdot[\underline{k}\times\underline{q}]\; f_{13}f_{24}\,\frac{2}{m^2MM'}\Bigg] \quad . \qquad (3.22)$$

The last term in this formula gives rise to the quadratic spin-orbit potential. This term will be left out of consideration. Because of the relation

$$(\underline{k}\cdot\underline{q})\{(\underline{\sigma}_1\cdot\underline{k})(\underline{\sigma}_2\cdot\underline{q})+(\underline{\sigma}_1\cdot\underline{q})(\underline{\sigma}_2\cdot\underline{k})\} = \underline{q}^2(\underline{\sigma}_1\cdot\underline{k})(\underline{\sigma}_2\cdot\underline{k})+k^2(\underline{\sigma}_1\cdot\underline{q})(\underline{\sigma}_2\cdot\underline{q}) +$$

$$+ \underline{\sigma}_1\cdot[\underline{k}\times\underline{q}]\,\underline{\sigma}_2\cdot[\underline{k}\times\underline{q}] - [\underline{k}\times\underline{q}]^2(\underline{\sigma}_1\cdot\underline{\sigma}_2) \qquad (3.23)$$

we see that this term includes non-local effects, and we have neglected them in this calculation. In addition, however, the range of the quadratic spin-orbit potential is shorter than the range of the other potentials, and hence its influence will be important only for higher energies.

For the mesons K and K^*, carrying hypercharge, the sign of (3.11) and (3.22) is opposite. This is caused by the fact that the hyperons and nucleons in the final state are changed with respect to the initial state [21]. Furthermore, in formula (3.22) one should change $\sqrt{MM'}$ into (M+M')/2, but this difference will be neglected.

Finally, the two pion exchange potentials in momentum space have been tabulated by De Swart and Iddings [22].

3.3. The potentials in coordinate space.

It can be shown [53] that the most general Hermitian potential for NN interactions in coordinate space can be written as

$$V = V_C + V_{\sigma\sigma}(\underline{\sigma}_1\cdot\underline{\sigma}_2) + V_T S_{12} + V_{SO}(\underline{L}\cdot\underline{S}) + V_Q Q_{12} \quad , \qquad (3.24)$$

if one assumes that the potential is invariant under translations, rotations, space reflections, time reversal, and exchange of the particles. The V_i can be a function of the relative position of the nuclei, of their relative momentum q, and of L^2:

$$V_i = V_i(r, q, L^2) \quad , \qquad (3.25)$$

and the operators S_{12} and Q_{12} are given by

$$S_{12} = 3\,\frac{(\underline{\sigma}_1\cdot\underline{r})(\underline{\sigma}_2\cdot\underline{r})}{r^2} - (\underline{\sigma}_1\cdot\underline{\sigma}_2) \quad ,$$

$$Q_{12} = \tfrac{1}{2}\,\{(\underline{\sigma}_1\cdot\underline{L})(\underline{\sigma}_2\cdot\underline{L}) + (\underline{\sigma}_2\cdot\underline{L})(\underline{\sigma}_1\cdot\underline{L})\} \quad . \tag{3.26}$$

For YN interactions the same assumptions as those leading to Eq. (3.24) hold, but we cannot require that the potential is invariant under the exchange of the particles. Hence we cannot exclude a $(\underline{\sigma}_1-\underline{\sigma}_2)\cdot\underline{L}$ potential. Due to the restrictions we have made in the last section the quadratic spin-orbit potential $V_Q Q_{12}$ and the $(\underline{\sigma}_1-\underline{\sigma}_2)\cdot\underline{L}$ potential will not be present in the potential we will use. We also have neglected the dependence of q.

Before we proceed to the actual calculation of these potentials from (3.11) and (3.22), we will discuss briefly the properties of the potentials in (3.24). The central potential needs no discussion. The spin-spin potential $V_{\sigma\sigma}$ is accompanied by the operator $(\underline{\sigma}_1\cdot\underline{\sigma}_2)$. We will use a basis in which this operator is diagonal. This is the so called singlet triplet basis, consisting of the simultaneous eigenfunctions of S^2 and S_z, where $\underline{S}$ is the total spin operator. For singlet states (s=0)$(\underline{\sigma}_1\cdot\underline{\sigma}_2)$ has the eigenvalue -3, and for triplet states (s=1) +1.

The tensor force $V_T S_{12}$ is an important part, and not only with respect to its magnitude. The fact that L^2 no longer commutes with the Hamiltonian is caused by the presence of this term in V. In Chapter 4 we will use the eigenfunctions ${}^{\mathcal{Y}}{}^{\ell s j}_{m}$ of J^2 and J_z, where the total angular momentum $\underline{J} = \underline{L} + \underline{S}$. For singlet states the eigenvalues of S_{12} are 0, but for triplet states we have in this representation

$$S_{12} = \begin{pmatrix} \frac{-2j+2}{2j+1} & 0 & \frac{6[j(j+1)]^{\frac{1}{2}}}{2j+1} & \ell = j-1 \\ 0 & 2 & 0 & \ell = j \\ \frac{6[j(j+1)]^{\frac{1}{2}}}{2j+1} & 0 & \frac{-2j-4}{2j+1} & \ell = j+1 \end{pmatrix} \quad . \tag{3.28}$$

From this matrix it can be seen that there is coupling between states having $\ell = j \pm 1$, but that there is no coupling between these states and states having $\ell = j$. This is a consequence of the conservation of parity.

The matrix elements for the spin-orbit operator $\underline{L}\cdot\underline{S}$ can be found, using $\underline{L}\cdot\underline{S} = \frac{1}{2}(J^2-L^2-S^2)$. This gives for the singlet states $\underline{L}\cdot\underline{S} = 0$, and for the triplet states, using the same representation as above,

$$\underline{L}\cdot\underline{S} = \begin{pmatrix} j-1 & 0 & 0 \\ 0 & -1 & 0 \\ 0 & 0 & -(j+2) \end{pmatrix} \quad , \tag{3.29}$$

so this potential does not give coupling between states of different orbital angular momentum.

We can obtain the potential in coordinate space from the potential in momentum space by means of the Fourier transformation

$$V(\underline{r},\underline{q}) = \frac{1}{(2\pi)^3} \int d^3k \; V(\underline{k},\underline{q}) e^{i\underline{k}\underline{r}} \quad . \tag{3.30}$$

The $\underline{q}$ in $V(\underline{r},\underline{q})$ denotes now a differential operator working on the baryon wave functions [52], hence giving rise to a non-local potential. Since we have neglected this $\underline{q}$-dependence from the start, this non-locality does not arise in our potentials.

Due to the presence of terms with k^2 and higher powers of k in (3.22), not all the integrals converge. This divergency is partly caused by the developments we have used (3.19), but they are also caused by the derivatives in the Hamiltonian (3.12). We can circumvent these divergencies by introducing a cut-off function v(k), being 1 for small values of k, but v(k) = 0 for values of k much larger than m. This procedure limits the validity of our derivation to not too small separations of the baryons. This is not so serious, since for short distances other errors are already present. Moreover, at very short distances the hard core will be the only remaining influence.

We will use the following integrals [52], in which the cut-off is understood:

$$\frac{1}{(2\pi)^3} \int d^3k \; f(\underline{k}^2) \frac{1}{\underline{k}^2+m^2} e^{i\underline{k}\underline{r}} = \frac{m}{4\pi} \phi(x) \; f(-m^2) \quad ,$$

$$\frac{1}{(2\pi)^3} \int d^3k \; f(\underline{k}^2) \frac{(\underline{\sigma}_1\cdot\underline{k})(\underline{\sigma}_2\cdot\underline{k})}{\underline{k}^2+m^2} e^{i\underline{k}\cdot\underline{r}} = -\frac{m^3}{4\pi}\left[\frac{1}{3}(\underline{\sigma}_1\cdot\underline{\sigma}_2)\phi(x)+S_{12}\chi(x)\right] f(-m^2),$$

$$\frac{1}{(2\pi)^3} \int d^3k \; f(\underline{k}^2) \frac{i\underline{S}\cdot[\underline{k}\times\underline{q}]}{\underline{k}^2+m^2} e^{i\underline{k}.\underline{r}} = -\frac{m^3}{4\pi}\left(\frac{1}{x}+\frac{1}{x^2}\right)\phi(x)(\underline{L}\cdot\underline{S})f(-m^2) \quad . \tag{3.31}$$

In this formulae $x = mr$,

$$\chi(x) = \frac{1}{3}\left(1+\frac{3}{x}+\frac{3}{x^2}\right)\frac{e^{-x}}{x} \quad , \text{ and } \quad \phi(x) = \frac{e^{-x}}{x} \quad .$$

The potential in coordinate space due to the exchange of a pseudoscalar meson, is therefore given by

$$V_{PS} = \frac{g^P_{13} g^P_{24}}{4\pi} m \left[\frac{1}{3}(\underline{\sigma}_1 \cdot \underline{\sigma}_2)\ \phi(x) + S_{12}\ X(x)\right] \quad . \tag{3.32}$$

Due to the exchange of a vector meson it is

$$\begin{aligned} V_V = \frac{m}{4\pi} \Bigg[& \left\{ g^V_{13} g^V_{24} \left(1 + \frac{m^2}{4MM'}\right) + (g^V_{13} f^V_{24} + g^V_{24} f^V_{13}) \frac{m}{2\sqrt{MM'}} + f^V_{13} f^V_{24} \frac{m^2}{4MM'} \right\} \phi(x) + \\ & - \left\{ g^V_{13} g^V_{24} \frac{3m^2}{2MM'} + (g^V_{13} f^V_{24} + g^V_{24} f^V_{13}) \frac{2m}{\sqrt{MM'}} + f^V_{13} f^V_{24} \frac{3m^2}{2MM'} \right\} \left(\frac{1}{x} + \frac{1}{x^2}\right) \phi(x) \underline{L}\cdot\underline{S} + \\ & + \left\{ g^V_{13} g^V_{24} \frac{m^2}{4MM'} + (g^V_{13} f^V_{24} + g^V_{24} f^V_{13}) \frac{m}{2\sqrt{MM'}} + f^V_{13} f^V_{24} \left(1 + \frac{m^2}{4MM'}\right) \right\} \\ & \left\{ \frac{2}{3} (\underline{\sigma}_1 \cdot \underline{\sigma}_2)\phi(x) - S_{12} X(x) \right\} \Bigg] \quad . \end{aligned} \tag{3.33}$$

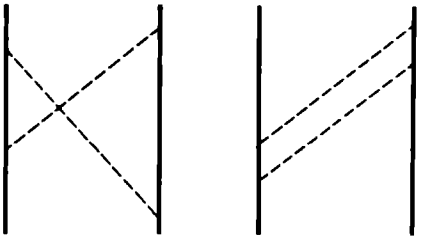

Fig. 3.3. Crossed and uncrossed diagrams for two pion exchange.

For completeness we quote the two pion exchange potentials [22]. They consist of two parts, ${}^{\times}V_{\pi\pi}$ and ${}^{/\!/}V_{\pi\pi}$, obtained from the diagrams in Fig. 3.3. The contributions of the crossed diagram are, apart from the coupling constants,

$$\begin{aligned} {}^{\times}V_{\pi\pi} = & - \frac{1}{2\pi} \left[\left(\frac{12}{x^2} + \frac{23}{x^4} \right) K_1(2x) + \left(\frac{4}{x} + \frac{23}{x^3} \right) K_o(2x) \right] + \\ & + \frac{4}{3\pi} \left[\left(\frac{2}{x^2} + \frac{3}{x^4} \right) K_1(2x) + \frac{3}{x^2} K_o(2x) \right] (\underline{\sigma}_1 \cdot \underline{\sigma}_2) + \\ & - \frac{1}{3\pi} \left[\left(\frac{4}{x^2} + \frac{15}{x^4} \right) K_1(2x) + \frac{12}{x^3} K_o(2x) \right] S_{12} \quad , \end{aligned} \tag{3.34}$$

and of the uncrossed diagram

$$\begin{aligned} {}^{/\!/}V_{\pi\pi} = & - {}^{\times}V^C_{\pi\pi} - \frac{2}{\pi} \left[\left(\frac{1}{x^2} + \frac{4}{x^3} + \frac{4}{x^4} \right) e^{-x} K_1(x) + \left(\frac{1}{x} + \frac{2}{x^2} + \frac{2}{x^3} \right) e^{-x} K_o(x) \right] + \\ & + {}^{\times}V^{\sigma\sigma}_{\pi\pi} - \frac{4}{3\pi} \left[\left(\frac{1}{x^2} + \frac{2}{x^3} + \frac{2}{x^4} \right) e^{-x} K_1(x) + \left(\frac{1}{x^2} + \frac{1}{x^3} \right) e^{-x} K_o(x) \right] (\underline{\sigma}_1 \cdot \underline{\sigma}_2) + \end{aligned}$$

$$+ {}^{x}V^{T}_{\pi\pi} + \frac{2}{3\pi}\left[\left(\frac{1}{x^2} + \frac{5}{x^3} + \frac{5}{x^4}\right) e^{-x}K_1(x) + \left(\frac{1}{x^2} + \frac{1}{x^3}\right) e^{-x}K_0(x)\right] S_{12} \quad . \tag{3.35}$$

The Bessel functions $K_n(x)$ are defined by

$$K_n(x) = \frac{\Gamma(n+\frac{1}{2})}{\pi^{\frac{1}{2}}} \left(\frac{2}{x}\right)^n \int_0^\infty \frac{\cos kx}{(k^2+1)^{n+\frac{1}{2}}}\, dk \quad . \tag{3.36}$$

3.4. The coupling constants.

Our first calculations (Chapter 7) were done with potentials obtained from the exchange of the pseudoscalar mesons π, K, and η. These potentials are given by (3.32), (3.34), and (3.35), but we have still to agree about the choice of the coupling constants.

It is generally accepted that the strong interactions are charge independent. This can be described conveniently by the well known isospin formalism. One defines an abstract space, the isotopic spin space or isospace, analogous to ordinary spin space. In this space one makes the following assignments for the field operators corresponding to the various particles: Λ and η are scalars in isotopic spin space, $\underline{\Sigma}$ and $\underline{\pi}$ are vectors, and Ξ, N, K and $\bar{K}$ are spinors. A charge independent interaction Hamiltonian should be a scalar in isospace. Assuming only Yukawa couplings between the baryons and the pseudoscalar mesons, the most general Hermitean interaction Hamiltonian that is a scalar in isospace and that conserves hypercharge and baryon number can be written as [54]

$$\begin{aligned}
\mathcal{H}_I = {} & g_{NN\pi}(\bar{N}_1 \underline{\tau} N_1)\cdot\underline{\pi} + g_{\Xi\Xi\pi}(\bar{N}_2 \underline{\tau} N_2)\cdot\underline{\pi} + g_{\Lambda\Sigma\pi}(\bar{\Lambda}\underline{\Sigma} + \bar{\underline{\Sigma}}\Lambda)\cdot\underline{\pi} - ig_{\Sigma\Sigma\pi}(\bar{\underline{\Sigma}} \times \underline{\Sigma})\cdot\underline{\pi} + \\
& + g_{NN\eta}(\bar{N}_1 N_1)\eta + g_{\Xi\Xi\eta}(\bar{N}_2 N_2)\eta + g_{\Lambda\Lambda\eta}\bar{\Lambda}\Lambda\eta + g_{\Sigma\Sigma\eta}(\bar{\underline{\Sigma}}\cdot\underline{\Sigma})\eta + \\
& + g_{N\Lambda K}\{(\bar{N}_1 K)\Lambda + \bar{\Lambda}(\bar{K} N_1)\} + g_{\Xi\Lambda K}\{(\bar{N}_2 K_c)\Lambda + \bar{\Lambda}(\bar{K}_c N_2)\} + \\
& + g_{N\Sigma K}\{(\bar{\underline{\Sigma}}\cdot(\bar{K}\underline{\tau} N_1) + (\bar{N}_1 \underline{\tau} K)\cdot\underline{\Sigma}\} + g_{\Xi\Sigma K}\{\bar{\underline{\Sigma}}\cdot(\bar{K}_c \underline{\tau} N) + (\bar{N}_2 \underline{\tau} K_c)\cdot\underline{\Sigma}\} \quad ,
\end{aligned} \tag{3.37}$$

where we have used the notation

$$N_1 = \begin{pmatrix} p \\ n \end{pmatrix} \quad , \quad N_2 = \begin{pmatrix} \Xi^0 \\ \Xi^- \end{pmatrix} \quad , \quad K = \begin{pmatrix} K^+ \\ K^0 \end{pmatrix} \quad , \quad K_c = \begin{pmatrix} \bar{K}^0 \\ -K^- \end{pmatrix} \quad ,$$

and the inner product $\underline{\Sigma}\cdot\underline{\pi} = \Sigma^{+}\pi^{-} + \Sigma^{o}\pi^{o} + \Sigma^{-}\pi^{+}$.
We have followed the usual convention by denoting p as the destruction operator of a proton or a creation operator of an antiproton, and we have suppressed the space and time dependence in this Hamiltonian.

We will use this Hamiltonian to include the isospin factors in the potential. Defining V_{AB} as a potential that couples the state containing hyperon A with the state containing hyperon B, we get for the coupling constants to be inserted in V_{AB}

	V_{π}	V_{K}	V_{η}
$V_{\Lambda\Lambda}$	0	$g^2_{\Lambda NK}P$	$g_{\Lambda\Lambda\eta}\, g_{NN\eta}$
$V_{\Lambda\Sigma^o}$	$-g_{\Lambda\Sigma\pi}\, g_{NN\pi}$	$-g_{\Lambda NK}g_{\Sigma NK}P$	0
$V_{\Lambda\Sigma^-}$	$\sqrt{2}g_{\Lambda\Sigma\pi}g_{NN\pi}$	$\sqrt{2}g_{\Lambda NK}g_{\Sigma NK}P$	0
$V_{\Sigma^o\Sigma^o}$	0	$g^2_{\Sigma NK}P$	$g_{\Sigma\Sigma\eta}\, g_{NN\eta}$
$V_{\Sigma^o\Sigma^-}$	$\sqrt{2}g_{\Sigma\Sigma\pi}g_{NN\pi}$	$\sqrt{2}g^2_{\Sigma NK}P$	0
$V_{\Sigma^-\Sigma^-}$	$-g_{\Sigma\Sigma\pi}\, g_{NN\pi}$	0	$g_{\Sigma\Sigma\eta}\, g_{NN\eta}$
$V_{\Sigma^+\Sigma^+}$	$g_{\Sigma\Sigma\pi}\, g_{NN\pi}$	$2g^2_{\Sigma NK}P$	$g_{\Sigma\Sigma\eta}\, g_{NN\eta}$

	$^{\times}V_{\pi\pi}$	$^{/\!/}V_{\pi\pi}$
$V_{\Lambda\Lambda}$	$3g^2_{\Lambda\Sigma\pi}\, g^2_{NN\pi}$	$3g^2_{\Lambda\Sigma\pi}\, g^2_{NN\pi}$
$V_{\Lambda\Sigma^o}$	$-2g_{\Lambda\Sigma\pi}\, g_{\Sigma\Sigma\pi}\, g^2_{NN\pi}$	$2g_{\Lambda\Sigma\pi}\, g_{\Sigma\Sigma\pi}\, g^2_{NN\pi}$
$V_{\Lambda\Sigma^-}$	$+2\sqrt{2}g_{\Lambda\Sigma\pi}g_{\Sigma\Sigma\pi}g^2_{NN\pi}$	$-2\sqrt{2}g_{\Lambda\Sigma\pi}g_{\Sigma\Sigma\pi}g^2_{NN\pi}$
$V_{\Sigma^o\Sigma^o}$	$(g^2_{\Lambda\Sigma\pi}+2g^2_{\Sigma\Sigma\pi})g^2_{NN\pi}$	$(g^2_{\Lambda\Sigma\pi}+2g^2_{\Sigma\Sigma\pi})g^2_{NN\pi}$
$V_{\Sigma^o\Sigma^-}$	$\sqrt{2}(g^2_{\Lambda\Sigma\pi}+g^2_{\Sigma\Sigma\pi})g^2_{NN\pi}$	$-\sqrt{2}(g^2_{\Lambda\Sigma\pi}+g^2_{\Sigma\Sigma\pi})g^2_{NN\pi}$
$V_{\Sigma^-\Sigma^-}$	$g^2_{\Sigma\Sigma\pi}\, g^2_{NN\pi}$	$(2g^2_{\Lambda\Sigma\pi}+3g^2_{\Sigma\Sigma\pi})g^2_{NN\pi}$
$V_{\Sigma^+\Sigma^+}$	$2g^2_{\Sigma\Lambda\pi}g^2_{NN\pi}$	$3g^2_{\Sigma\Sigma\pi}\, g^2_{NN\pi}$

(3.38)

We have included a factor $P = -P_x P_\sigma$ where P_x and P_σ are space and spin exchange operators. This factor is caused by the fact that the diagrams for

K-mesons (see Fig. 3.1) exchange the initial and final states [21].

The Hamiltonian (3.37) contains twelve independent coupling constants of which we have used eight in (3.38). In order to reduce the number of independent parameters we will require that the interaction Hamiltonian is invariant under SU(3) transformations.

In order to derive an SU(3) invariant Hamiltonian, we will consider briefly this theory [2]. After the success of the isospin formalism several higher symmetry schemes that treat isospin and hypercharge on an equal footing have been proposed. The most successful theory is the octet model, proposed independently by Gell-Mann [3] and Ne'eman [4]. In this model the irreducible representations (I.R.) of the unitary unimodular transformation group SU(3) in a three-dimensional complex linear vector space are considered. The strongly interacting particles are assigned to these I.R., in the same way as the isospin multiplets are assigned to I.R. of SU(2). In the octet model, unlike SU(2), not all possible I.R. of SU(3) are utilized, but only those I.R. that provide an integral charge and hypercharge. Hence only a one-dimensional representation (a singlet), an eight-dimensional representation (octet), a ten-dimensional representation (decuplet) etc. arise, but not the fundamental three-dimensional representation (triplet). The baryons N, Σ, Λ, and Ξ form an octet, and so do the mesons π, K, and η. The X^o is a unitary singlet.

Within a multiplet each particle is uniquely determined by its eigenvalues for the commuting operators T_z, Y, and T^2. Other properties like spin, parity and baryon number are the same for all particles within a multiplet. Also, for an exactly valid symmetry, the masses of the particles should be equal. Since this symmetry is broken not all the masses are equal (see e.g. Table 1.1 of Chapter 1), but, assuming octet-dominance, a relation between the masses of the particles in a multiplet exists [55]. The physical idea is that the strong interactions can be divided into two parts, namely a part which is invariant under SU(3) and a part which breaks SU(3) symmetry, but still commutes with $\underline{T}$ and Y. The Gell-Mann - Okubo mass formula then results:

$$M = M_o + M_1 Y + M_2 (T(T+1) - \tfrac{1}{4} Y^2) \quad , \tag{3.39}$$

where for fermions M is the mass of the particles and for bosons the mass squared. This gives for the baryon octet $M_N + M_\Xi = 3M_\Lambda/2 + M_\Sigma/2$ and for the pseudoscalar mesons $m_K^2 = 3m_\eta^2/4 + m_\pi^2/4$. Both formulae are satisfied to within a few MeV.

For the vector mesons there is another complication. If one assumes ρ, K^* and ω belonging to the same octet, the mass formula is not satisfied very well. The generally accepted explanation [56] for this feature is as follows. In the absence of the SU(3) breaking strong interaction one has an octet of vector mesons ρ, K^* , ϕ_o, and a unitary singlet ω_o. Due to the SU(3) breaking interaction the ω_o and ϕ_o mix with each other and the physical particles become

$$\omega = \omega_o \cos\theta + \phi_o \sin\theta \quad ,$$
$$\phi = -\phi \sin\theta + \omega_o \cos\theta \quad , \tag{3.40}$$

with a mixing angle $\theta \sim 35^o \sim \text{arctg}(1/\sqrt{2})$, obtained from the mass formula (3.39) and the masses of the physical particles.

An octet can be described by a 3 × 3 traceless matrix. Using the phase convention of De Swart [57], we can write

$$B = \begin{pmatrix} \frac{1}{\sqrt{2}}\Sigma^o + \frac{1}{\sqrt{6}}\Lambda & \Sigma^+ & -p \\ \Sigma^- & -\frac{1}{\sqrt{2}}\Sigma^o + \frac{1}{\sqrt{6}}\Lambda & -n \\ \Xi^- & -\Xi^o & -\sqrt{\frac{2}{3}}\Lambda \end{pmatrix} ,$$

$$\bar{B} = \begin{pmatrix} \frac{1}{\sqrt{2}}\bar{\Sigma}^o + \frac{1}{\sqrt{6}}\bar{\Lambda} & \bar{\Sigma}^+ & \bar{\Xi}^+ \\ \bar{\Sigma}^- & -\frac{1}{\sqrt{2}}\bar{\Sigma}^o + \frac{1}{\sqrt{6}}\Lambda & -\bar{\Xi}^o \\ -\bar{p} & -\bar{n} & -\sqrt{\frac{2}{3}}\bar{\Lambda} \end{pmatrix} ,$$

$$P = \begin{pmatrix} \frac{1}{\sqrt{2}}\pi^o + \frac{1}{\sqrt{6}}\eta & \pi^+ & -K^+ \\ \pi^- & -\frac{1}{\sqrt{2}}\pi^o + \frac{1}{\sqrt{6}}\eta & -K^o \\ -K^- & -\bar{K}^o & -\sqrt{\frac{2}{3}}\eta \end{pmatrix} ,$$

$$V = \begin{pmatrix} \frac{1}{\sqrt{2}}\rho^{o} + \frac{1}{\sqrt{2}}\omega & \rho^{+} & -K^{*+} \\ \rho^{-} & -\frac{1}{\sqrt{2}}\rho^{o} + \frac{1}{\sqrt{2}}\omega & -K^{*o} \\ -K^{*-} & -\bar{K}^{*o} & \phi \end{pmatrix} , \qquad (3.41)$$

where we define p as the wave function of an proton, etc. For the vector mesons we did not use a traceless matrix, but we included the ϕ-ω mixing approximately. This corresponds to the mixing angle given above.

An invariant Hamiltonian for Yukawa interactions $\bar{B}BM$ can be constructed by using the invariants $Tr(\bar{B}BM)$, $Tr(\bar{B}MB)$ and $Tr(\bar{B}B)Tr\ M$. The linear combination

$$\mathcal{H}_I = g\sqrt{2}\ \{\alpha[\bar{B}BP]_F + (1-\alpha)\ [\bar{B}BP]_D\} \quad , \qquad (3.42)$$

is usually taken, with

$$[\bar{B}BP]_F = Tr(\bar{B}PB) - Tr(\bar{B}BP) \quad ,$$

$$[\bar{B}BP]_D = Tr(\bar{B}BP) + Tr(\bar{B}PB) - \frac{2}{3}\,Tr(\bar{B}B)TrP \quad . \qquad (3.43)$$

Consequently, we have for $\bar{B}BP$ interactions only two independent parameters, the coupling constant $g = g_{NN\pi}$ and the parameter α, sometimes called the F/(F+D) ratio. SU(3) symmetry as such gives no predictions about the value of this parameter, but there are several reasons to assume that $\alpha \sim 0.4$ [58]. One of our aims is to see whether this value of α is consistent with the hyperon-nucleon interaction data.

Using this procedure, we can write the coupling constants as a function of g and α. We get

$$\begin{array}{lll} g_{NN\pi} = g & g_{NN\eta} = \frac{1}{3}\sqrt{3}\ g(4\alpha-1) & g_{N\Lambda K} = -\frac{1}{3}\sqrt{3}g(1+2\alpha) \\ g_{\Xi\Xi\pi} = -g(1-2\alpha) & g_{\Xi\Xi\eta} = -\frac{1}{3}\sqrt{3}g(1+2\alpha) & g_{\Xi\Lambda K} = \frac{1}{3}\sqrt{3}g(4\alpha-1) \\ g_{\Lambda\Sigma\pi} = \frac{2}{3}\sqrt{3}\ g(1-\alpha) & g_{\Sigma\Sigma\eta} = \frac{2}{3}\sqrt{3}\ g(1-\alpha) & g_{N\Sigma K} = g(1-2\alpha) \\ g_{\Sigma\Sigma\pi} = 2g\alpha & g_{\Lambda\Lambda\eta} = -\frac{2}{3}\sqrt{3}\ g(1-\alpha) & g_{\Xi\Sigma K} = -g \quad . \end{array} \qquad (3.44)$$

We have suppressed the space-time dependence in our Hamiltonian. In fact, for $\bar{B}BP$ interactions two Hamiltonians, a direct coupling $ig\bar{\psi}\ \gamma_5\phi$ and a derivative coupling $(f/m)\ \bar{\psi}\gamma_\mu\gamma_5\psi\partial_\mu\phi$ are possible. According to the equivalence theorem [59] they give the same result if one relates the coupling

constants by

$$g = \frac{M+M'}{m} f \tag{3.45}$$

If the masses of the particles were equal, it would make no difference which coupling constants one assumes to obey unitary symmetry. If the masses are broken, there is a difference, mainly because of the large difference between m_π and m_K or m_η. We have chosen unitary symmetry for the pseudoscalar coupling constants g.

When we use the second set of potentials, we will require SU(6) symmetry to find relations for the coupling constants. In order to derive these relations, we will suppose first SU(3) symmetry. An SU(3) invariant Hamiltonian can then be written as

$$\begin{aligned}\mathcal{H}_I = {} & g_P\sqrt{2}\{\alpha[\bar{B}BP]_F + (1-\alpha)[\bar{B}BP]_D\} + g_{P,S}[\bar{B}BP]_S + \\ & + g_V\sqrt{2}\{\alpha_V^e[\bar{B}BV]_F + (1-\alpha_V^e)[\bar{B}BV]_D\} + g_{V,S}[\bar{B}BV]_S + \\ & + f_V\sqrt{2}\{\alpha_V^m[\bar{B}BV]_F + (1-\alpha_V^m)[\bar{B}BV]_D\} + f_{V,S}[\bar{B}BV]_S \quad .\end{aligned} \tag{3.46}$$

We have included the pseudoscalar unitary singlet X^o (mass about 960 MeV) in P by redefining P as

$$P_\beta^\alpha = P_\beta^\alpha + \frac{1}{\sqrt{3}} X^o \delta_\beta^\alpha \quad . \tag{3.47}$$

This implies no η - X^o mixing, which is in fact very small [60]. Because of it $[\bar{B}BP]_S = Tr(\bar{B}B)TrP$ now gives a non-vanishing contribution. This Hamiltonian gives us as many as 9 parameters of which only a few are known experimentally.

An obvious generalization of SU(3) symmetry is the group SU(6), which contains the unitary spin group SU(3) and the ordinary spin group SU(2). One assumes that the static phenomena involving hadrons are described approximately by SU(6). This symmetry group is essentially a non-relativistic theory [61], since the Lorentz transformations would mix the intrinsic spin and the orbital angular momentum. In spite of many attempts, a satisfactory generalization of SU(6) to the relativistic domain has not been given. We will not discuss the properties of the SU(6) symmetry scheme nor its relativistic generalizations which are surveyed by many authors [5].

Although not all questions concerning SU(6) and its relativistic generalizations have been resolved, we will use some of its predictions. In the

SU(6) theory the 8 pseudoscalar mesons and the 3×9 vector mesons (3 for the spin) are assigned to a 35-plet, whereas the baryons of the SU(3) octet and decuplet are assigned to a 56-plet. In the relativistic generalizations the pseudoscalar X^o is usually included, giving a 36-plet for the mesons.

Given the symmetry group and the assignments for the particles, it is a rather trivial but laborious task to find the relations for the coupling constants. One of the earliest results [62] of SU(6) symmetry was the prediction that for $\bar{B}BP$ interactions $\alpha = 0.4$ and a relation between g_P and g_V, giving $g_V^2/(4\pi) \sim 0.5$. In fact, deriving these relations, one is already beyond the static SU(6) theory. The several approaches towards a relativistic generalization of the static SU(6) theory do not yield always the same results for the coupling constants, but neglecting terms of order $(m/M)^2$ with respect to 1, one generally finds the α's for the $\bar{B}BP$ and $\bar{B}BV$ vertices. Also the coupling constants for the unitary singlet mesons (X^o and ω_o) can be related to the other ones.

When we are considering potentials due both to pseudoscalar and vector mesons we will use the following interaction Hamiltonian, written in the same way as (3.22),

$$\mathcal{H}_I = g_P\sqrt{2}\left\{\frac{2}{5}\,[\bar{B}BP]_F + \frac{3}{5}\,[\bar{B}BP]_D + \frac{1}{5}[\bar{B}BP]_S\right\} + g_V\sqrt{2}\left\{[\bar{B}BV]_F + [\bar{B}BV]_S\right\} +$$
$$+ f_V\sqrt{2}\left\{\frac{2}{5}\,[\bar{B}BV]_F + \frac{3}{5}\,[\bar{B}BV]_D + \frac{1}{5}[\bar{B}BP]_S\right\} \quad . \tag{3.48}$$

Considering the electric type of coupling, we see that we have $\alpha_V^e = 1$. This is not only an implication of SU(6) symmetry, but it has been proposed before by Sakurai [11].

The coupling constants can now be expressed in terms of g_P, g_V, and f_V, using $\alpha = 0.4$, 1, and 0.4, respectively, in (3.44) and replacing the pseudoscalar indices by the vectorial ones for g_V and f_V. The coupling constants for the unitary singlets are given by

$$g_{NNX^o} = \frac{1}{5}\sqrt{6}\, g_{NN\pi} \quad ,$$
$$g_{NN\omega_o} = \sqrt{6}\quad g_{NN\rho} \quad ,$$
$$f_{NN\omega_o} = \frac{1}{5}\sqrt{6}\, f_{NN\rho} \quad . \tag{3.49}$$

Using (3.40) for the ω-ϕ mixing we obtain for the coupling constants of the physical particles

$$g_{NN\omega} = \sqrt{\frac{2}{3}}\, g_{NN\omega_o} + \sqrt{\frac{1}{3}}\, g_{NN\phi_o} \quad ,$$

$$g_{NN\phi} = -\sqrt{\frac{1}{3}}\, g_{NN\omega_o} + \sqrt{\frac{2}{3}}\, g_{NN\phi_o} \quad , \tag{3.50}$$

and an analogous relation is valid for the f.

The potential between the baryons B and B' can now be written as

$$V_{BB'} = \sum_i O_i \sum_\mu g^2_{BB'\mu}\, V_{i\mu} \quad . \tag{3.51}$$

In this formula i runs over the different terms given in (3.24), μ runs over the mesons whose exchange we assumed, and $g_{BB'\mu}$ is given by (3.38) and (3.44) for the octet of pseudoscalar mesons, and the analogous formulae for the vector mesons.

CHAPTER 4
THE SCATTERING FORMALISM

4.1. Introduction.

The main purpose of this chapter is the derivation of an expression for the scattering amplitude. From this amplitude all experimental quantities can be derived. We will first give the Schrödinger equation for the hyperon-nucleon interaction. By means of a partial wave expansion, the scattering amplitude will be found. We then will give expressions for the experimental quantities in terms of the scattering amplitude.

The scattering formalism of particles with non zero spin is well known. One defines the total spin of the system $\underline{S} = \frac{1}{2}(\underline{\sigma}_1+\underline{\sigma}_2)$ and the total angular momentum $\underline{J} = \underline{L}+\underline{S}$, where $\underline{L}$ is the orbital angular momentum. The eigenfunctions of S^2 and S_z, $\xi^{(s)}_m$, are composed from the spin wave functions of the separate particles with the help of the Clebsch-Gordan coefficients $C^{s_1 s_2 s}_{m_1 m_2 m}$,

$$\xi^{(s)}_m = \sum_{m_1,m_2} C^{s_1 s_2 s}_{m_1 m_2 m} \; \xi^{(s_1)}_{m_1} \; \xi^{(s_2)}_{m_2} \quad , \tag{4.1}$$

and the eigenfunctions of J^2 and J_z, $\mathcal{Y}^{\ell s j}_m$, are formed by using these functions and the spherical harmonics $Y^{(\ell)}_m(\theta, \phi)$:

$$\mathcal{Y}^{\ell s j}_m = \sum_{m_\ell m_s} C^{\ell\ s\ j}_{m_\ell m_s m} \; Y^{(\ell)}_{m_\ell}(\theta,\phi) \; \xi^{(s)}_{m_s} \quad . \tag{4.2}$$

Since the potential contains the tensor force (see Chapter 3), the Hamiltonian no longer commutes with L^2, but it does with J^2 and S^2, and also with the parity operator P, as we are dealing with strong interactions. Considering the eigenfunctions of L^2, S^2, J^2, J_z and P, we have:

$s = 0$	$\ell = j$	$p = (-)^j$
$s = 1$	$\ell = j$	$p = (-)^j$
$s = 1$	$\ell = j\pm1$	$p = (-)^{j+1}$

We call these states singlet, triplet-uncoupled, and triplet-coupled, respectively. In the last case the solutions of the Schrödinger equation will be a linear combination of $\mathcal{Y}^{j+1,1,j}_m$ and $\mathcal{Y}^{j-1,1,j}_m$, but of course there will be no coupling with states having opposite parity or different spin.

Using the spectroscopic notation $^{2s+1}\ell_j$, we have the following states.

s \ j	0	1	2
0	$^1S_0$	$^1P_1$	$^1D_1$
1		$^3P_1$	$^3D_2$
1	$^3P_0$	$^3S_1+^3D_1$	$^3P_2+^3F_2$

If we had not excluded terms containing $\underline{\sigma}_1-\underline{\sigma}_2$ in the potential (see the discussion following (3.21)), the Hamiltonian would not have commuted with S^2. In that case also the states with different spin would be coupled, hence, giving, for example, a coupling of the $^1P_1$ with the $^3P_1$ state.

Besides the coupling between states of different orbital angular momentum there is another type of coupling, namely for Σ^-p scattering the coupling with channels consisting of other particles. We have the reactions II^a, II^b and II^c (see Chapter 2).

Due to these couplings we will obtain from the Schrödinger equation a set of coupled differential equations.

4.2. The partial wave expansion.

In the c.m. system the Schrödinger equation, in units $\hbar = c = 1$, reads

$$-\frac{1}{2m}\nabla^2\psi + V\psi = E\psi \quad , \tag{4.3}$$

where m is the reduced mass operator. We will decouple this equation in a set of matrix differential equations.

The wave function ψ can be written as

$$\psi = \Sigma_\alpha \psi_\alpha \eta_\alpha \quad , \tag{4.4}$$

where η_α is the particle wave function for the different channels. These functions can be described by using the so called isospin basis, as has been done by De Swart et al [15-17,22,23]. One uses as a basis the T=1/2 and T=3/2 isospin wave functions and afterwards an orthogonal transformation to the particle basis is performed. We will use this particle basis directly, choosing as our basis states (Λn) $(\Sigma^o n)$, and $(\Sigma^- p)$ for Σ^-p interactions or $(\Sigma^+ p)$ for Σ^+p scattering. This has the advantage that we can take into account directly the breaking of isospin symmetry, caused by electromagnetic interactions and by the mass differences in the different

channels.

For $\Sigma^- p$ scattering we write ψ as a vector

$$\psi = \begin{pmatrix} \psi_{\Lambda n} \\ \psi_{\Sigma^0 n} \\ \psi_{\Sigma^- p} \end{pmatrix} \quad . \tag{4.5}$$

The action of the potential on this vector can be described by the real symmetric matrix V,

$$V = \begin{pmatrix} V_{\Lambda\Lambda} & V_{\Lambda\Sigma^0} & V_{\Lambda\Sigma^-} \\ V_{\Sigma^0\Lambda} & V_{\Sigma^0\Sigma^0} & V_{\Sigma^0\Sigma^-} \\ V_{\Sigma^-\Lambda} & V_{\Sigma^-\Sigma^0} & V_{\Sigma^-\Sigma^-} \end{pmatrix} \quad . \tag{4.6}$$

Consider for the moment a definite channel. We can expand ψ_α in partial waves

$$\psi_\alpha = \sum_{jm\ell s} R_\alpha^{\ell sjm}(r)\, \mathcal{Y}^{\ell sj}_m(\theta,\phi) \quad , \tag{4.7}$$

where R describes the radial dependence. We substitute (4.7) into the Schrödinger equation and by using the orthogonality of the $\mathcal{Y}^{\ell sj}_m$ we will separate off the angular dependence. Since $[S^2,H]=0$ we obtain two uncoupled equations for s=0 (singlet) and s=1 (triplet). Due to the presence of the tensor potential $V_T S_{12}$, we have

$$V\,\mathcal{Y}^{\ell 1j}_m = V_{\ell\ell}\,\mathcal{Y}^{\ell 1j}_m + V_{\ell'\ell}\,\mathcal{Y}^{\ell' 1j}_m \quad ,$$

where $\ell=j-1$ and $\ell'=j+1$, but when $\ell=j$ we have

$$V\,\mathcal{Y}^{j1j}_m = V_{jj}\,\mathcal{Y}^{j1j}_m \quad .$$

Hence, there is no coupling between states with $\ell=j$ and $\ell=j\pm1$.

In the triplet coupled case the general form of the solution of the Schrödinger equation for given j and m can therefore be written as

$$\psi^{(j)}_m = \frac{\chi_{j-1}(r)}{r}\,\mathcal{Y}^{j-1,1,j}_m + \frac{\chi_{j+1}(r)}{r}\,\mathcal{Y}^{j+1,1,j}_m \quad , \tag{4.8}$$

where $\chi_{j\pm1}(r)$ is a solution of the radial Schrödinger equation with $\ell=j\pm1$. When V acts on this wave function, we get

$$V\psi_m^{(j)} = \left[V_{\ell\ell}\frac{\chi_\ell(r)}{r} + V_{\ell\ell'}\frac{\chi_{\ell'}(r)}{r}\right]\mathcal{Y}_m^{\ell 1 j} + \left[V_{\ell'\ell}\frac{\chi_\ell(r)}{r} + V_{\ell'\ell'}\frac{\chi_{\ell'}(r)}{r}\right]\mathcal{Y}_m^{\ell' 1 j} \quad . \tag{4.9}$$

We will write this in matrix form by defining the vector

$$\chi = \begin{pmatrix}\chi_\ell \\ \chi_{\ell'}\end{pmatrix} \tag{4.10}$$

and the symmetric matrix

$$V = \begin{pmatrix}V_{\ell\ell} & V_{\ell\ell'} \\ V_{\ell'\ell} & V_{\ell'\ell'}\end{pmatrix} \quad . \tag{4.11}$$

Combining now the coupling between the different channels and between states of different orbital angular momentum, we can write the radial Schrödinger equation as

$$\left[\frac{d^2}{dr^2} - \frac{L^2}{r^2} + k^2 - U\right]\chi = 0 \quad . \tag{4.12}$$

For $\bar{\Sigma}p$ scattering χ is a vector with components χ_1, χ_2, and χ_3, and for the triplet-coupled case each component χ_α is again the vector (4.10), yielding for χ a vector with six components. The orbital angular momentum L^2 is the diagonal matrix

$$\begin{pmatrix}\ell(\ell+1) & 0 & 0 \\ 0 & \ell(\ell+1) & 0 \\ 0 & 0 & \ell(\ell+1)\end{pmatrix} \quad . \tag{4.13}$$

for singlet and triplet-uncoupled cases; for triplet-coupled states each diagonal element should be replaced by the 2×2 matrix

$$\begin{pmatrix}\ell(\ell+1) & 0 \\ 0 & \ell'(\ell'+1)\end{pmatrix} \quad . \tag{4.14}$$

The momenta k_i and k_j in channel i and j are related through

$$k_i^2/2m_i + M_i^{(1)} + M_i^{(2)} = k_j^2/2m_j + M_j^{(1)} + M_j^{(2)} \quad , \tag{4.15}$$

where m_i are the reduced masses in the different channels, and $M_i^{(n)}$ are the rest masses of the particles in each channel. Hence k^2 in (4.12) is a 3 × 3 or 6 × 6 matrix with the diagonal elements k_j^2 as the only non zero elements. The matrix U is defined by the relation U = 2mV, where V is given by (4.6) and m is the matrix

$$m = \begin{pmatrix} m_1 & 0 & 0 \\ 0 & m_2 & 0 \\ 0 & 0 & m_3 \end{pmatrix} \quad . \tag{4.16}$$

For triplet coupled states each element of V is again the matrix (4.11).

For $\Sigma^+ p$ scattering we have only the elastic channel, and equation (4.12) consists at most of 2 × 2 matrices, this being the case in the triplet coupled state.

The n × n matrix equation (4.12) has n independent solutions satisfying the required boundary condition $\chi(r)=0$ at $r=0$ or $r=r_c$, r_c being the hard core radius. We consider these solutions as the columns of a n × n matrix Ψ. Consequently, we have for the Schrödinger equation

$$\left[\frac{d^2}{dr^2} - \frac{L^2}{r^2} + k^2 - U\right]\Psi = 0 \quad . \tag{4.17}$$

Using the symmetry of V, we can derive from (4.17) a relation that we will need later. It is

$$\tilde{\Psi}\, m^{-1}\Psi' - \tilde{\Psi}'\, m^{-1}\Psi = 0 \quad , \tag{4.18}$$

where $\tilde{}$ means transposition and ' differentiation.

4.3. The scattering amplitude.

In order to describe the scattering process we consider a plane wave $e^{i\underline{k}.\underline{r}}\xi_m^{(s)}\eta_i$ of incoming particles in channel i. We suppose the particles to be in a definite eigenstate of the total spin. The z-axis is taken in the direction of motion of the incident hyperons. We require that after the scattering only the plane wave in the channel i and outgoing spherical waves in the channels f are present at large distances from the scattering

center. The scattering amplitude is then defined by requiring that, asymptotically, the solution of (4.3) is

$$\psi_{as} \sim e^{ik_i z}\, \xi^{(s)}_m \eta_i + \sum_{m',f} \left(\frac{v_i}{v_f}\right)^{\frac{1}{2}} M_{mm',if}(\theta,\phi)\, \frac{e^{ik_f r}}{r}\, \xi^{(s)}_{m'} \eta_f \quad . \tag{4.19}$$

We expand the incoming plane wave in partial waves, using the spherical Hankel functions

$$\begin{aligned} h^{(1)}_\ell(\rho) &= j_\ell(\rho) + i n_\ell(\rho) \\ h^{(2)}_\ell(\rho) &= j_\ell(\rho) - i n_\ell(\rho) \end{aligned} \quad , \tag{4.20}$$

where j_ℓ and n_ℓ are the spherical Bessel and Neumann functions. For $\rho \to \infty$ the asymptotic behaviour of the spherical Hankel functions is

$$\begin{aligned} h^{(1)}_\ell(\rho) &\sim -ie^{i(\rho-\frac{1}{2}\ell\pi)}/\rho \\ h^{(2)}_\ell(\rho) &\sim \; ie^{i(\rho-\frac{1}{2}\ell\pi)}/\rho \end{aligned} \quad . \tag{4.21}$$

This gives

$$e^{ik_i z} \xi^{(s)}_m \eta_i = \pi^{\frac{1}{2}} \sum_{j=0}^{\infty} \sum_\ell (2\ell+1)^{\frac{1}{2}} i^\ell \{h^{(1)}_\ell(k_i r) + h^{(2)}_\ell(k_i r)\} C^{\ell s j}_{0mm}\, \mathcal{Y}^{\ell s j}_m \eta_i \quad . \tag{4.22}$$

This will be transformed by the interaction into

$$\begin{aligned} &\pi^{\frac{1}{2}} \sum_{j\ell\ell',f} (2\ell+1)^{\frac{1}{2}} i^\ell C^{\ell s j}_{0mm} \{h^{(2)}_{\ell'}(k_f r)\delta_{\ell\ell'}\delta_{fi} + \\ &+ \langle f\ell' | S_j | \ell i \rangle (m_f k_f / m_i k_i)^{\frac{1}{2}}\, h^{(1)}_{\ell'}(k_f r)\}\, \mathcal{Y}^{\ell' s j}_m \eta_f \quad . \end{aligned} \tag{4.23}$$

We have to insert here the factor $(m_f k_f / m_i k_i)^{\frac{1}{2}}$ to be sure that when the coupling is such that the particles all go out via one definite channel, the flux in that channel equals the outgoing flux in the absence of coupling. This gives us a unitary S-matrix. Using the asymptotic behaviour (4.21) and the definition of the $\mathcal{Y}^{\ell s j}_m$ (4.2), we can subtract the plane wave, yielding

$$\psi_{as} = e^{ik_i z}\, \xi^{(s)}_m \eta_i + \pi^{\frac{1}{2}} \sum_{j\ell\ell',f} (2\ell+1)^{\frac{1}{2}}\, i^{\ell-\ell'}\, \frac{e^{ik_f r}}{ik_i r} \left(\frac{v_i}{v_f}\right)^{\frac{1}{2}}$$

$$C_{m-m',m'm}^{\ell' s j} C_{0mm}^{\ell s j} Y_{m-m'}^{\ell'}(\theta,\phi)\langle f\ell'|S_j-1|\ell i\rangle \xi_{m'}^{(s)} \eta_f \quad . \tag{4.24}$$

Using (4.19), we get for the scattering amplitude

$$M_{mm',if} = \frac{\pi^{\frac{1}{2}}}{ik_i} \sum_{j\ell\ell'} (2\ell+1)^{\frac{1}{2}} i^{\ell-\ell'} C_{m-m',m'm}^{\ell' s j} C_{0mm}^{\ell s j}$$

$$Y_{m-m'}^{(\ell')}(\theta,\phi)\langle f\ell'|S_j-1|\ell i\rangle \quad . \tag{4.25}$$

This formula can be simplified for singlet states:

$$M_{s,if} = \frac{\pi^{\frac{1}{2}}}{ik_i} \sum_{\ell}(2\ell+1)^{\frac{1}{2}} Y_o^{(\ell)}(\theta,\phi)\langle f|S_\ell-1|i\rangle \quad . \tag{4.26}$$

We have tabulated terms occuring in the scattering amplitude $M_{mm'}(\theta,0)$ for values of ℓ and j of interest for us, apart from the factor $\langle|S-1|\rangle/(2ik_i)$ (see Table 4.1).

4.4. The experimental quantities.

We will use the expression for the scattering amplitude, derived in the last section, to calculate the cross sections, angular distributions, and polarizations.

The angular distributions are given by

$$\left(\frac{d\sigma}{d\Omega}\right)_{singlet} = |M_{singlet}|^2 \quad ,$$

$$\left(\frac{d\sigma}{d\Omega}\right)_{triplet} = \frac{1}{3}\sum_{mm'} |M_{mm'}|^2 \quad . \tag{4.27}$$

In the last equation we sum over the different spin states of the final state and average over those of the incoming state, this last operation giving the factor 1/3. By integrating over $d\Omega$ and using the orthogonality of the spherical harmonies and the symmetry properties of the Clebsch-Gordan coefficients, we get for the total cross sections

$$\sigma_s(i \to f) = \frac{\pi}{k_i^2} \sum_{\ell=0}^{\infty} (2\ell+1)|\langle \ell f|S_\ell-1|i\ell\rangle|^2 \quad ,$$

$$\sigma_t(i \to f) = \frac{\pi}{3k_i^2} \sum_{j\ell\ell'}(2j+1)|\langle \ell' f|S_j-1|i\ell\rangle|^2 \quad , \tag{4.28}$$

$$\begin{pmatrix} 1 & 0 & 0 \\ 0 & 1 & 0 \\ 0 & 0 & 1 \end{pmatrix} \qquad \begin{pmatrix} -\frac{1}{4}\sqrt{2}(3\cos^2\theta-1) & -\frac{3}{2}\sin\theta\cos\theta & -\frac{3}{4}\sqrt{2}\sin^2\theta \\ -\frac{3}{2}\sin\theta\cos\theta & \frac{1}{2}\sqrt{2}(3\cos^2\theta-1) & \frac{3}{2}\sin\theta\cos\theta \\ -\frac{3}{4}\sqrt{2}\sin^2\theta & \frac{3}{2}\sin\theta\cos\theta & -\frac{1}{4}\sqrt{2}(3\cos^2\theta-1) \end{pmatrix}$$

$^3S_1 \to {}^3S_1$ $\qquad$ $^3S_1 \to {}^3D_1$

$$\begin{pmatrix} -\frac{1}{2}\sqrt{2} & 0 & 0 \\ 0 & \sqrt{2} & 0 \\ 0 & 0 & -\frac{1}{2}\sqrt{2} \end{pmatrix} \qquad \begin{pmatrix} 0 & 0 & 0 \\ -\frac{1}{2}\sqrt{2}\sin\theta & \cos\theta & \frac{1}{2}\sqrt{2}\sin\theta \\ 0 & 0 & 0 \end{pmatrix}$$

$^3D_1 \to {}^3S_1$ $\qquad$ $^3P_0 \to {}^3P_0$

$$\begin{pmatrix} \frac{3}{2}\cos\theta & \frac{3}{4}\sqrt{2}\sin\theta & 0 \\ 0 & 0 & 0 \\ 0 & -\frac{3}{4}\sqrt{2}\sin\theta & \frac{3}{2}\cos\theta \end{pmatrix} \qquad \begin{pmatrix} \frac{3}{2}\cos\theta & -\frac{3}{4}\sqrt{2}\sin\theta & 0 \\ \frac{1}{2}\sqrt{2}\sin\theta & 2\cos\theta & -\frac{1}{2}\sqrt{2}\sin\theta \\ 0 & \frac{3}{4}\sqrt{2}\sin\theta & \frac{3}{2}\cos\theta \end{pmatrix}$$

$^3P_1 \to {}^3P_1$ $\qquad$ $^3P_2 \to {}^3P_2$

$$\begin{pmatrix} -\frac{1}{4}\sqrt{6}(5\cos^3\theta-3\cos\theta) & -\frac{1}{2}\sqrt{3}(5\cos^2\theta-1)\sin\theta & -\frac{5}{4}\sqrt{6}(\cos\theta-\cos^3\theta) \\ -\frac{1}{2}\sqrt{3}(5\cos\theta-1)\sin\theta & \frac{1}{2}\sqrt{6}(5\cos^3\theta-3\cos\theta) & \frac{1}{2}\sqrt{3}(5\cos^2\theta-1)\sin\theta \\ -\frac{5}{4}\sqrt{6}(\cos\theta-\cos^3\theta) & \frac{1}{2}\sqrt{3}(5\cos^2\theta-1)\sin\theta & -\frac{1}{4}\sqrt{6}(5\cos^3\theta-3\cos\theta) \end{pmatrix}$$

$^3P_2 \to {}^3F_2$

(1) $\qquad$ $(3\cos\theta)$

$^1S_0 \to {}^1S_0$ $\qquad$ $^1P_1 \to {}^1P_1$

Table 4.1. Terms of the scattering amplitude for $\phi = 0$, apart from the factor $\langle i|S-1|i\rangle/(2ik_i)$. The form of the triplet matrices is $\begin{pmatrix} M_{11} & M_{10} & M_{1-1} \\ M_{01} & M_{00} & M_{0-1} \\ M_{-11} & M_{-10} & M_{-1-1} \end{pmatrix}$

and

$$\sigma_{tot}(i \to f) = \tfrac{1}{4}\,\sigma_s(i \to f) + \tfrac{3}{4}\,\sigma_t(i \to f) \quad . \tag{4.29}$$

The capture ratio r_C is defined in Chapter 2. Using the assumptions mentioned there, it is given by

$$r_C = \lim_{k_i \to 0} \left[\frac{1}{4}\, \frac{\sigma_s(\Sigma^- p \to \Sigma^0 n)}{\sigma_s(\Sigma^- p \to \Sigma^0 n) + \sigma_s(\Sigma^- p \to \Lambda n)} + \right.$$

$$\left. + \frac{3}{4}\, \frac{\sigma_t(\Sigma^- p \to \Sigma^0 n)}{\sigma_t(\Sigma^- p \to \Sigma^0 n) + \sigma_t(\Sigma^- p \to \Lambda n)} \right] \quad , \tag{4.30}$$

where σ_s and σ_t are the singlet and triplet cross sections for $\ell=0$. The ratio in flight r_F, however, is

$$r_F = \frac{\sigma_{tot}(\Sigma^- p \to \Sigma^0 n)}{\sigma_{tot}(\Sigma^- p \to \Sigma^0 n) + \sigma_{tot}(\Sigma^- p \to \Lambda n)} \quad . \tag{4.31}$$

In order to derive an expression for the polarization in terms of the scattering amplitudes, we will first give an outline of the treatment by Wolfenstein [63]. The spin state of the two particle system is described by a vector $\underline{a}(n)$ with four components, where n numbers the particle systems. Furthermore, we describe each operator by a linear combination of sixteen basis matrices S^μ, $\mu=1\ldots16$. Since we consider only hermitean operators, we can choose for the S^μ a hermitean set and we have to consider only real linear combinations. We assume the unit matrix being part of this set and we normalize our basis matrices such that

$$\mathrm{Tr}(S^\mu S^\nu) = 4\,\delta_{\mu\nu} \quad . \tag{4.32}$$

We define a density matrix $\rho_{jk} = \Sigma_n a_j(n) a_k^*(n)$, giving for the average of the expectation value of the operator S^μ

$$\overline{\langle S^\mu \rangle} = \mathrm{Tr}(\rho S^\mu)/\mathrm{Tr}(\rho) \quad . \tag{4.33}$$

Because of the interaction a plane wave in a definite spin state will be transformed into

$$\psi_j(n) = e^{ikz}\, a_j(n) + e^{ikr}\, \Sigma_\ell M_{j\ell}(\theta,\phi)\, a_\ell(n)/r \quad .$$

Defining now a density matrix for the final states ρ_f by $\rho_{f;jk} = \Sigma_n a_{f,j}(n) a^*_{f,k}(n)$, we have

$$\rho_f = M \rho_i M^\dagger \quad . \tag{4.34}$$

Consequently, with $\rho = \frac{1}{4}\Sigma_{\nu=1}^{16} \mathrm{Tr}(\rho S^\nu) S^\nu$,

$$\overline{\langle S^\mu \rangle}_f = \tfrac{1}{4} \mathrm{Tr}(\rho_i) \mathrm{Tr}(\Sigma_\nu M \overline{\langle S^\nu \rangle}_i S^\nu M^\dagger S^\mu)/\mathrm{Tr}(\rho_f) \quad . \tag{4.35}$$

When unpolarized particles are scattered on an unpolarized target, all $\overline{\langle S^\nu \rangle}_i$ are zero, except the unit matrix, so we get

$$\overline{\langle S^\mu \rangle}_f = \tfrac{1}{4} \mathrm{Tr}(\rho_i)\ \mathrm{Tr}(MM^\dagger S^\mu)/\mathrm{Tr}(\rho_f) \quad . \tag{4.36}$$

The polarization is defined as the vector $\underline{P}$ with direction $\underline{n}$ given by the direction of $\langle \underline{\sigma} \rangle$ and with size $P = (\overline{\langle \sigma_x \rangle^2} + \overline{\langle \sigma_y \rangle^2} + \overline{\langle \sigma_z \rangle^2})^{\frac{1}{2}}$. Using $\mathrm{Tr}(\rho_f)/\mathrm{Tr}(\rho_i) = \frac{1}{4}\mathrm{Tr}(M^\dagger M)$, we can write

$$P = \mathrm{Tr}(MM^\dagger\ \underline{S}^\mu \underline{n})/\mathrm{Tr}(M^\dagger M) \quad . \tag{4.37}$$

On the singlet-triplet basis, M has the form

$$M = \begin{pmatrix} M_{11} & M_{10} & M_{1-1} & 0 \\ M_{01} & M_{00} & M_{0-1} & 0 \\ M_{-11} & M_{-10} & M_{-1-1} & 0 \\ 0 & 0 & 0 & M_s \end{pmatrix} \tag{4.38}$$

The polarization is in the direction

$$\underline{n} = \underline{k}_i \times \underline{k}_f / |\underline{k}_i \times \underline{k}_f| \quad . \tag{4.39}$$

We take our coordinate axes such that $\underline{k}_i$ points to the direction of the positive z-axis and we take k_f in the x-z plane, which is no restriction. For the polarization of the scattered hyperon we then only have to know $\langle \sigma_{1_y} \rangle$ where $\underline{\sigma}_1$ is the spin operator for the hyperon. On the singlet-triplet basis σ_{1_y} is given by

$$\sigma_{1_y} = \frac{i}{\sqrt{2}} \begin{pmatrix} 0 & -1 & 0 & 1 \\ 1 & 0 & -1 & 0 \\ 0 & 1 & 0 & 1 \\ -1 & 0 & -1 & 0 \end{pmatrix} \quad . \tag{4.40}$$

Using $M_{m,m'}(\phi=0) = (-)^{m-m'} M_{-m,-m'}(\phi=0)$, we get finally

$$P = -2\sqrt{2}\ \mathrm{Im}(M^*_{01}M_{11}+M^*_{00}M_{10}+M^*_{-11}M_{01})/\mathrm{Tr}(M^\dagger M) \quad , \tag{4.41}$$

where all the matrix elements of M are taken at $\phi=0$.

When the total spin is not conserved, the elements in the last row and column of M (4.38) in general will be different from zero. This implies that the polarization of the outgoing hyperon and nucleon are no longer equal [17,64].

4.5. Some useful formulas.

The S-matrix element in (4.25) can be calculated if one knows the wave function and its derivative at some point outside the range of the potential. We can write the solution of the Schrödinger equation at distances so large that the potentials can be neglected, as follows:

$$\Psi(\underline{r}) = (m/k)^{\frac{1}{2}}(J_\ell(kr)K^{-1}-N_\ell(kr))k^\ell(m/k)^{-\frac{1}{2}} \quad , \tag{4.42}$$

where $J_\ell(kr)$ and $N_\ell(kr)$ are diagonal matrices with elements $k_i r\, j_{\ell_i}(k_i r)$ and $k_i r\, n_{\ell_i}(k_i r)$. The factor $(m/k)^{\frac{1}{2}}$ is needed to give a unitary S-matrix, the factor $k^\ell(m/k)^{-\frac{1}{2}}$ is a convenient normalization. The real matrix K is related to the S-matrix by

$$S = (1+iK)(1-iK)^{-1} \quad . \tag{4.43}$$

We actually find the K-matrix by numerical integration (see Chapter 6) of the Schrödinger equation from the hard core radius to a point r_a where the potentials can be neglected. We find then the wave function u(r) and its derivative u'(r) at r_a and join them to (4.42) by requiring

$$\begin{aligned} u\,B &= \Psi(r) \quad , \\ u'B &= \Psi'(r) \quad , \end{aligned} \tag{4.44}$$

where B is an arbitrary non-singular matrix. Multiplying from the left with $\tilde{u}'m^{-1}$ and $\tilde{u}m^{-1}$ respectively, we get, after subtraction and using (4.18),

$$K = (mk)^{\frac{1}{2}}(\tilde{u}'N'-\tilde{u}N)^{-1}(\tilde{u}'J'-\tilde{u}J)(mk)^{-\frac{1}{2}} \quad . \tag{4.45}$$

It is possible to give an effective range expansion for K [65]. Using the same assumptions as are used for the well known expansion $k \cot g\delta = (-1/a)+\frac{1}{2}r_o k^2$, De Swart and Dullemond [16] give the expression

$$k^{\ell+\frac{1}{2}}\, K^{-1}\, k^{\ell+\frac{1}{2}} = -A^{-1} + \tfrac{1}{2}(k^2-k_o^2)^{\frac{1}{2}}\, R(k^2-k_o^2)^{\frac{1}{2}} \quad . \tag{4.46}$$

Here R and A are matrices, $k^{\ell+\frac{1}{2}}$ is a diagonal matrix with elements $k_i^{\ell_i+\frac{1}{2}}$ and k_o is the momentum corresponding to the energy at which the expansion is performed. By writing the expansion in the form (4.46), we obtain for the scattering length A and effective range R symmetric matrices. For a discussion of A and R we refer to reference 16.

CHAPTER 5
COULOMB INTERACTIONS

5.1. The Coulomb wave functions.

Besides the short range strong interactions between the hyperon and the nucleon the Coulomb interaction for the $\Sigma^- p$ and $\Sigma^+ p$ channels should be included. Because of the long range of these potentials some changes in the foregoing treatment must be made. We will first give some properties of the Coulomb wave functions, after which we will outline the well known scattering of particles having Coulomb interactions with no coupling to other channels [66]. This is done to settle the notation and to clarify the main changes we need for the many channel formalism.

Consider two particles with charges $Z_1 e$ and $Z_2 e$, where e is the proton charge, having only Coulomb interactions. The Schrödinger equation is

$$\left[-\frac{1}{2m} \nabla^2 + \frac{Z_1 Z_2 e^2}{r} - E \right] \psi(\underline{r}) = 0 \quad . \tag{5.1}$$

We use the dimensionless constant $\eta = Z_1 Z_2 e^2 m/k$ and define

$$\psi(\underline{r}) = \Sigma_{\ell m} \frac{\chi_\ell(r)}{r} Y_m^{(\ell)}(\theta,\phi) \quad .$$

Using $\rho = kr$, we obtain for χ the equation

$$\chi_\ell'' + \left[1 - \frac{2\eta}{\rho} - \frac{\ell(\ell+1)}{\rho^2} \right] \chi_\ell = 0 \quad . \tag{5.2}$$

As two independent solutions of (5.2) one usually takes the so called Coulomb wave functions $F_\ell(\eta,\rho)$ and $G_\ell(\eta,\rho)$. The first one is regular at the origin. Their asymptotic behaviour for $\rho \to \infty$ is

$$\begin{aligned} F_\ell(\eta,\rho) &\simeq \sin(\rho - \eta \ell n\, 2\rho - \tfrac{1}{2}\ell\pi + \sigma_\ell) \quad , \\ G_\ell(\eta,\rho) &\simeq \cos(\rho - \eta \ell n\, 2\rho - \tfrac{1}{2}\ell\pi + \sigma_\ell) \quad , \end{aligned} \tag{5.3}$$

where the Coulomb phase shift σ_ℓ is defined by

$$\sigma_\ell = \arg \Gamma(\ell+1+i\eta) \quad . \tag{5.4}$$

For the regular Coulomb wave function the series expansion

$$F_\ell(\eta,\rho) = C_\ell(\eta) \sum_{n=\ell+1}^{\infty} A_n^\ell(\eta)\, \rho^n \tag{5.5}$$

can be derived [67,68], in which the coefficients $A_n^\ell(\eta)$ are defined by

$$\{n(n-1) - \ell(\ell+1)\}A_n^\ell(\eta) = 2\eta\, A_{n-1}^\ell(\eta) - A_{n-2}^\ell(\eta) \quad ,$$

$$A_{\ell+1}^\ell(\eta) = 1 \quad ,$$

$$A_{\ell+2}^\ell(\eta) = \frac{\eta}{\ell+1} \quad . \tag{5.6}$$

The constants $C_\ell(\eta)$ are given by

$$C_\ell(\eta) = C_o(\eta) \frac{1}{(2\ell+1)!!} \prod_{s=1}^{\ell} \left(1 + \frac{\eta^2}{s^2}\right)^{\frac{1}{2}} \tag{5.7}$$

for $\ell>0$ and

$$C_o(\eta) = \left(\frac{2\pi\eta}{e^{2\pi\eta}-1}\right)^{\frac{1}{2}} \quad . \tag{5.8}$$

The irregular function $G_\ell(\eta,\rho)$ has the expansion

$$G_\ell(\eta,\rho) = \frac{2\eta}{C_o^2(\eta)} F_\ell(\eta,\rho)\{\ell n 2\rho + \frac{q_\ell(\eta)}{p_\ell(\eta)}\} + D_\ell(\eta)\sum_{n=-\ell}^{\infty} a_n^\ell(\eta)\, \rho^n \tag{5.9}$$

with the definitions

$$\frac{q_\ell(\eta)}{p_\ell(\eta)} = \sum_{s=o}^{\ell} \frac{s}{s^2+\eta^2} - \sum_{s=1}^{2\ell+1} \frac{1}{s} + \mathrm{Re}\, \frac{\Gamma'(1+i\eta)}{\Gamma(1+i\eta)} + 2\gamma + \frac{r_\ell(\eta)}{p_\ell(\eta)} \quad ,$$

$$r_\ell(\eta) = \frac{(-1)^{\ell+1}}{(2\ell)!}\, \mathrm{Im} \sum_{n=o}^{2\ell} \left\{ \frac{2^n}{n!(2\ell+1-n)} \frac{\Gamma(i\eta-\ell+n)}{\Gamma(i\eta-\ell)} \right\} \quad ,$$

$$p_\ell(\eta) = \frac{2^{2\ell+1}\eta}{(2\ell+1)\{(2\ell)!\}^2} \prod_{n=1}^{\ell} (n^2+\eta^2) \quad \text{for} \quad \ell>0 \quad ,$$

$$p_o(\eta) = 2\eta \quad ,$$

$$D_\ell(\eta) = \frac{1}{(2\ell+1)C_\ell(\eta)} \quad , \tag{5.10}$$

where γ is Euler's constant. The coefficients $a_n^\ell(\eta)$ are found to be

$$(n-\ell-1)(n+\ell)a_n^\ell(\eta) = 2\eta a_{n-1}^\ell(\eta) - a_{n-2}^\ell(\eta) - (2n-1)p_\ell(\eta)A_n^\ell(\eta) \quad ,$$

$$a_{-\ell}^\ell(\eta) = 1 \quad ,$$

$$a_{\ell+1}^\ell(\eta) = 0 \quad ,$$

$$A_n^\ell(\eta) = 0 \quad \text{for} \quad n<\ell+1 \quad . \tag{5.11}$$

We will also use the linear combinations of the Coulomb wave functions

$$u_\ell^{(1)}(\eta,\rho) = \frac{F_\ell(\eta,\rho)-iG_\ell(\eta,\rho)}{\rho} \underset{\rho\to\infty}{\sim} -i\,\frac{e^{i(\rho-\eta\ell n2\rho-\frac{1}{2}\ell\pi+\sigma_\ell)}}{\rho} \quad ,$$

$$u_\ell^{(2)}(\eta,\rho) = \frac{F_\ell(\eta,\rho)+iG_\ell(\eta,\rho)}{\rho} \underset{\rho\to\infty}{\sim} i\,\frac{e^{-i(\rho-\eta\ell n2\rho-\frac{1}{2}\ell\pi+\sigma_\ell)}}{\rho} \quad , \tag{5.12}$$

which are analogous to the spherical Hankel functions used in the previous chapter.

5.2. Coulomb scattering.

In this section we will consider the scattering caused by a combination of a short range potential and the Coulomb potential. Because of the long range of the last potential it is useful to consider first the scattering by a Coulomb potential only.

A solution of the Schrödinger equation (5.1), which is regular at the origin and which approaches a plane wave in the z-direction when $\eta\to 0$, is

$$\psi_C = \pi^{\frac{1}{2}} \sum_{\ell=0}^{\infty} (2\ell+1)^{\frac{1}{2}}\, i^\ell\, e^{i\sigma_\ell}(u_\ell^{(1)}+u_\ell^{(2)})\, Y_0^{(\ell)}(\theta,\phi) \quad . \tag{5.13}$$

This ψ_C can be written as $\psi_C=\psi_i+\psi_s$ with asymptotic behaviour for $\rho\to\infty$

$$\psi_i \sim e^{i\{kz+\eta\ell n(2kr\,\sin^2\frac{1}{2}\theta)\}} \quad ,$$

$$\psi_s \sim -\frac{\eta}{2kr\,\sin^2\frac{1}{2}\theta}\, e^{i\{kr-\eta\ell n(2kr\,\sin^2\frac{1}{2}\theta)+2\sigma_o\}} \quad . \tag{5.14}$$

Because of the long range of the Coulomb potential ψ_i does not behave for large r like a plane wave e^{ikz}, but has the asymptotic behaviour given by $\psi_i \sim \exp\left[i\{kz+\eta\ell nk(r-z)\}\right]$. Since for large negative values of z the flux of ψ_i is $v=k/m$, in the direction of the positive z-axis, one interpretes ψ_i

as an incident plane wave. For large values of r, ψ_s can be written as $\psi_s \simeq M_C(\theta)\exp[i(kr-\eta\ell n2kr)]/r$, hence

$$M_C(\theta) = -\frac{\eta}{2k\sin^2\frac{1}{2}\theta}\, e^{-i\eta\ell n(\sin^2\frac{1}{2}\theta)+2i\sigma_o} \quad . \tag{5.15}$$

The factor $e^{-i\eta\ell n2kr}$ is also caused by the long range of the potential. To lowest order in 1/r the flux is directed outward along the radius and has the value $(k/m)|M_C(\theta)|^2/r^2$, so we have $(d\sigma/d\Omega)_C=|M_C(\theta)|^2$.

When also a short range potential is present, the solution of the Schrödinger equation outside the range of that potential will be a linear combination of the u_ℓ defined in (5.12):

$$\psi = \Sigma_\ell a_\ell (u_\ell^{(2)}+e^{2i\delta_\ell}u_\ell^{(1)})\, Y_0^{(\ell)} \quad . \tag{5.16}$$

Subtracting now instead of the plane wave, as we have done in Chapter 4, the Coulomb wave ψ_C and fixing the constants a_ℓ by requiring that in $\psi-\psi_C$ only an outgoing wave is present, we obtain

$$\psi-\psi_C = \pi^{\frac{1}{2}}\, \Sigma_\ell (2\ell+1)^{\frac{1}{2}}\, i^\ell\, e^{2i\sigma_\ell}(e^{2i\delta_\ell}-1)u_\ell^{(1)}\, Y_0^{(\ell)} \quad .$$

From this it follows that the total scattering amplitude $M(\theta)$ can be written as $M(\theta) = M_C(\theta)+M_N(\theta)$, where $M_C(\theta)$ is given by (5.15) and

$$M_N(\theta) = \frac{\pi^{\frac{1}{2}}}{ik}\, \Sigma_\ell (2\ell+1)^{\frac{1}{2}}\, e^{2i\sigma_\ell}(e^{2i\delta_\ell}-1)\, Y_0^{(\ell)} \quad . \tag{5.17}$$

This division of the scattering amplitude into two parts amounts to the subtraction of the Coulomb contribution, which can be summed directly, from the slowly converging series

$$M(\theta) = \frac{\pi^{\frac{1}{2}}}{ik}\, \Sigma_\ell (2\ell+1)^{\frac{1}{2}}\, (e^{2i(\sigma_\ell+\delta_\ell)}-1)\, Y_0^{(\ell)} \quad ,$$

yielding the much faster converging series (5.17).

It should be noted that the phase angle δ_ℓ is not equal to the angle δ_ℓ^N that one would obtain if the same short range potentials but no Coulomb potential were present.

The differential cross section $d\sigma/d\Omega$ consists of three parts:

$$\frac{d\sigma}{d\Omega} = |M_C(\theta)|^2 + |M_N(\theta)|^2 + 2\mathrm{Re}(M_C(\theta)M_N(\theta)) \quad . \tag{5.18}$$

The first part is the well known Coulomb scattering cross section (Rutherford cross section)

$$|M_C(\theta)|^2 = \frac{\eta^2}{4k^2\sin^4 \frac{1}{2}\theta} \quad , \tag{5.19}$$

which is only important for very small values of θ , where it causes a sharp peaking in the forward direction. The "nuclear" cross section has essentially the same behaviour as the cross section that one would obtain when no Coulomb forces were present, but it has a slightly different value. Finally, the interference term, although also only important at small angles, is greater at larger angles than the Coulomb cross section.

The values of θ for which the interference term becomes important or for which the Rutherford cross section is the most important contribution, depend in addition to the strength of the Coulomb potential also on the energy. Roughly speaking, $(d\sigma/d\Omega)_C \propto 1/k^4$ and $(d\sigma/d\Omega)_{IF} \propto 1/k^2$. We shall see later that for $\Sigma^{\pm}p$ scattering the Coulomb contribution is important at $\cos\theta \gtrsim 0.8$ for a laboratory energy of 10 MeV.

The sign of the interference term is determined by the overall properties of the short range potential and the sign of the charges. If for the nuclear potential only S-wave scattering is important, the interference term is given by

$$-\frac{\eta}{2k^2\sin^2\frac{1}{2}\theta} \sin 2\delta_o \{\cos(\eta \ell n \sin^2\tfrac{1}{2}\theta) - \sin(\eta \ell n \sin^2\tfrac{1}{2}\theta)\tan\delta_o\} \quad . \tag{5.20}$$

So we have a constructive interference when the nuclear and the Coulomb potential are both attractive or both repulsive, provided that no bound state is present.

5.3. Coupled channels and Coulomb effects.

The generalization of Section 4.3 is now simple. Since we are considering scattering of incident charged particles, we have an incident Coulomb wave

$$\psi_C=\pi^{\frac{1}{2}}\Sigma_{j\ell}(2\ell+1)^{\frac{1}{2}}i^{\ell}e^{i\sigma_\ell}\{u_\ell^{(1)}(k_3r)+u_\ell^{(2)}(k_3r)\}\ C^{\ell\ s\ j}_{0\ m\ m}\ \mathcal{Y}^{\ell\ s\ j}_{0\ m\ m}\ \eta_3 \qquad (5.21)$$

for Σ^-p scattering. For Σ^+p scattering we have only one η. This case we will not consider separately, because the generalization is straightforward.

Due to the interaction ψ_C will be transformed into a wave that outside the range of the nuclear potential can be written as

$$\psi=\pi^{\frac{1}{2}}\Sigma_{j\ell\ell'f}(2\ell+1)^{\frac{1}{2}}\ i^{\ell}e^{i\sigma_\ell}\{w_{\ell'}^{(2)}(k_fr)\delta_{\ell\ell'}\delta_{f,3}+$$

$$+\ \langle f\ell'|S_j|\ell 3\rangle(m_fk_f/m_ik_i)^{\frac{1}{2}}w_{\ell'}^{(1)}(k_fr)\}\mathcal{Y}^{\ell'\ s\ j}_{m\ \ C^{\ell\ s\ j}_{0\ m\ m}}\ \eta_f\ , \qquad (5.22)$$

where $w_\ell(\rho)=u_\ell(\rho)$ for channels with a Coulomb potential and $w_\ell(\rho)=h_\ell(\rho)$ for the other channels.

We subtract the incident Coulomb wave from (5.22) and use the asymptotic behaviour of the w_ℓ, given by (4.21) or (5.12). We then get

$$\psi-\psi_C=\pi^{\frac{1}{2}}\Sigma_{j\ell\ell'f}(2\ell+1)^{\frac{1}{2}}\ i^{\ell-\ell'}\langle f\ell'|e^{i\sigma_\ell}(S_j-1)e^{i\sigma_\ell}|\ell 3\rangle C^{\ell\ s\ j}_{0\ m\ m}\ C^{\ell'\ \ s\ j}_{m-m'\ m\ m'}$$

$$Y^{(\ell')}_{m-m'}(\theta,\phi)\ \xi^{(s)}_{m'}\left|\frac{v_3}{v_f}\right|^{\frac{1}{2}}\ \frac{e^{ik_fr+\eta\delta_{f,3}\ell n2k_fr}}{r}\ \eta_f\ . \qquad (5.23)$$

Consequently we can write for the scattering amplitude

$$M_{m,m';3,f}=M_C\ \delta_{m,m'}\ \delta_{3,f}+M^N_{m,m';3,f}\ , \qquad (5.24)$$

with

$$M^N_{m,m';3,f}=\frac{\pi^{\frac{1}{2}}}{ik_i}\Sigma_{j\ell\ell'm'}\ (2\ell+1)^{\frac{1}{2}}\ i^{\ell-\ell'}\langle f\ell'|e^{i\sigma_\ell}(S_j-1)e^{i\sigma_\ell}|\ell 3\rangle\ C^{\ell\ s\ j}_{0\ m\ m}$$

$$C^{\ell'\ \ s\ j}_{m-m'\ m'\ m}\ Y^{(\ell')}_{m-m'}(\theta,\phi)\ . \qquad (5.25)$$

The cross section consists of three parts, namely the pure Coulomb cross section

$$\left(\frac{d\sigma}{d\Omega}\right)_C = |M_C(\theta)|^2 = \frac{\eta^2}{4k^2\sin^4\frac{1}{2}\theta} \quad , \tag{5.26}$$

an interference part, and a nuclear part. For spin singlet one has

$$\left(\frac{d\sigma}{d\Omega}\right)_{\text{singlet}} = |M_C(\theta)|^2 + 2\mathrm{Re}(M_C\, M_s^N) + |M_s^N|^2 \quad , \tag{5.27}$$

and for triplet scattering

$$\left(\frac{d\sigma}{d\Omega}\right)_{\text{triplet}} = |M_C(\theta)|^2 + \frac{2}{3}\,\Sigma_m \mathrm{Re}(M_C\, M_{mm}^N) + \frac{1}{3}\,\Sigma_{mm'}|M_{mm'}^N|^2 \quad . \tag{5.28}$$

We can compute the S-matrix on the same manner as has been shown in Chapter 4, Section 5. The only change we have to make is that for channels with a Coulomb potential we should replace the spherical Bessel and Neumann functions $j_\ell(kr)$ and $n_\ell(kr)$ by the regular and irregular Coulomb wave functions $kr\,F_\ell(\eta,kr)$ and $-kr\,G_\ell(\eta,kr)$.

5.4. Effective range expansion.

We will derive an effective range expansion for multiple channel scattering, including Coulomb effects. This derivation follows quite closely the treatment given by De Swart and Dullemond [16] for the cases that no Coulomb forces are present or for the case that they are only present in channels with $\ell=0$.

In the Schrödinger equation,

$$-\frac{1}{2m}\,\psi'' + \left(V - \frac{1}{2m}\,\frac{L^2}{r^2}\right)\psi = E\psi \quad , \tag{5.29}$$

V contains besides the short range potential V_N the Coulomb potential, thus

$$V = V_N + \frac{\eta k}{m}\,\frac{1}{r} \quad , \tag{5.30}$$

with $\eta=0$ for channels where no Coulomb forces are present. This means that we add to the matrix V_N the diagonal matrix $\eta k/mr$ which has only nonzero elements for channels with charged particles. Using (5.29) for two different energies, we get

$$-\frac{d}{dr}\left(\tilde{\psi}_2\,\frac{1}{2m}\,\psi_1' - \tilde{\psi}_2'\,\frac{1}{2m}\,\psi_1\right) = \tilde{\psi}_2(E_1-E_2)\psi_1 \quad . \tag{5.31}$$

We will also consider the solutions ϕ of (5.29) with $V_N \equiv 0$. They satisfy also (5.31).

We choose for ϕ the specific solution

$$\phi = (m/k)^{\frac{1}{2}} (FK^{-1}+G)k^{\ell+\frac{1}{2}}/m^{\frac{1}{2}} \quad , \tag{5.32}$$

in which $F=F_\ell(\eta,kr)$ and $G=G_\ell(\eta,kr)$ for channels with Coulomb forces, but in channels without Coulomb forces we have $F=J_\ell(kr)$ and $G=-N_\ell(kr)$. We normalize ψ such that for large r $\psi(r)=\phi(r)$, so there (5.32) is identical to (4.42).

Using these solutions, we subtract (5.31) from the analogous equation for ϕ. Integration yields

$$\left[-\tilde{\phi}_2 m^{-1}\phi_1'+\tilde{\phi}_2' m^{-1}\phi_1\right]_\varepsilon = 2\int_\varepsilon^\infty dr\{\tilde{\psi}_2(E_1-E_2)\psi_1-\tilde{\phi}_2(E_1-E_2)\phi_1\} \quad . \tag{5.33}$$

Both sides of the equal sign in (5.33) are singular for $\varepsilon\to 0$. To be able to take the limit for $\varepsilon\to 0$, we will substitute (5.32) on the left hand side and subtract the singularities from both sides. Since (5.33) is an identity also the right hand side behaves properly at r=0 when the left hand side does, so we can then take the limit.

For the left hand side of (5.33) we can write

$$-k_2^{\ell+\frac{1}{2}}/m^{\frac{1}{2}}\left[K_2^{-1}(F_2F_1'-F_2'F_1)(k_1k_2)^{-\frac{1}{2}}K_1^{-1}+K_2^{-1}(F_2G_1'-F_2'G_1)(k_1k_2)^{-\frac{1}{2}}+\right.$$

$$\left.+(G_2F_1'-G_2'F_1)(k_1k_2)^{-\frac{1}{2}}K_1^{-1}+(G_2G_1'-G_2'G_1)(k_1k_2)^{-\frac{1}{2}}\right]k_1^{\ell+\frac{1}{2}}/m^{\frac{1}{2}} \quad . \tag{5.34}$$

We use now the series expansions (5.5) and (5.9) for the Coulomb wave functions. We do not have to consider here the expansions of the spherical Bessel and Neumann functions, for the series (5.5) and (5.9) reduce to those for the spherical Bessel and Neumann functions when $\eta\to 0$.

It is clear that the first term of (5.34) gives no contribution when $\varepsilon\to 0$. The other terms give different kinds of contributions. Firstly, they give a contribution that is singular for $\varepsilon\to 0$. In the same manner as can be done for the effective range expansion without Coulomb forces, we transpose these terms to the right hand side to remove the singularities. We will not consider these terms in detail, since we are not interested in giving an explicit formula for the effective range. It is indeed very hard to give such a formula because of the complexity of the series for the Coulomb wave functions. The terms that disappear for $\varepsilon\to 0$ we do not have to consider, so we have only to retain the terms independent of ε. For these terms we

have only to take the first term of each series, except for the product of the second series of G_ℓ. We obtain then for (5.34)

$$\frac{m^{-\frac{1}{2}}}{C_\ell(\eta_2)}\Big[C_\ell(\eta_2)k_2^{\ell+\frac{1}{2}}K_2^{-1}k_2^{\ell+\frac{1}{2}}C_\ell(\eta_2)-C_\ell(\eta_1)k_1^{\ell+\frac{1}{2}}K_1^{-1}k_1^{\ell+\frac{1}{2}}C_\ell(\eta_1) +$$

$$+2\eta_2\frac{C_\ell^2(\eta_2)}{C_o^2(\eta_2)}k_2^{2\ell+1}\left(\ell n 2k_2+\frac{q_\ell(\eta_2)}{p_\ell(\eta_2)}+\frac{1}{2\ell+1}\right)+$$

$$-2\eta_1\frac{C_\ell^2(\eta_1)}{C_o^2(\eta_1)}k_1^{2\ell+1}\left(\ell n 2k_1+\frac{q_\ell(\eta_1)}{p_\ell(\eta_1)}+\frac{1}{2\ell+1}\right)\Big]\frac{m^{-\frac{1}{2}}}{C_\ell(\eta_1)} +$$

$$+\frac{1}{m}\Big[\sum_{n=-\ell}^{o}(2n-1)\{k_1^{n+\ell}k_2^{1-n+\ell}a_{1-n}^{\ell}(\eta_2)a_n^{\ell}(\eta_1)+$$

$$-k_1^{1-n+\ell}k_2^{n+\ell}a_n^{\ell}(\eta_2)a_{1-n}^{\ell}(\eta_1)\}\Big]\frac{1}{(2\ell+1)^2C_\ell(\eta_1)C_\ell(\eta_2)} \quad . \tag{5.35}$$

We can now take the limit $\varepsilon\to 0$. Then we take the limit $k_2\to k_1$. Since the last term of (5.35) gives no contribution for $n=-\ell$, it has at least the energy dependence $\mathcal{O}(k^2)$, and for $\ell=0$ it disappears. Therefore

$$\frac{d}{dE}\{C_\ell(\eta)k^{\ell+\frac{1}{2}}K^{-1}k^{\ell+\frac{1}{2}}C_\ell(\eta)+2\eta k\left(\frac{C_\ell(\eta)}{C_o(\eta)}\right)^2k^{2\ell}(\ell n|2k\eta|-\tfrac{1}{2}\ell n^2+\frac{q_\ell(\eta)}{p_\ell(\eta)}+\frac{1}{2\ell+1})\}$$

is independent of the energy in lowest order. So we can write

$$(2\ell+1)!!\;C_\ell(\eta)k^{\ell+\frac{1}{2}}K^{-1}k^{\ell+\frac{1}{2}}C_\ell(\eta)(2\ell+1)!! +$$

$$+2\eta k\left[(2\ell+1)!!\frac{C_\ell(\eta)}{C_o(\eta)}\right]^2k^{2\ell}(\ell n|2k\eta|-\tfrac{1}{2}\ell n\eta^2+\frac{q_\ell(\eta)}{p_\ell(\eta)}+\frac{1}{2\ell+1}) =$$

$$=-\frac{1}{A}+\frac{1}{2}(k^2-k_o^2)^{\frac{1}{2}}R\,(k^2-k_o^2)^{\frac{1}{2}} \quad . \tag{5.36}$$

We have included the factor $(2\ell+1)!!$ so that for $\eta\to 0$ this formula reduces to the effective range expansion (4.46), neglecting the second term on the left hand side of (5.36).

This term in (5.36) is well known from the effective range expansion for one channel and $\ell=0$ [16,69]. In that case it reads

$$2\eta k(\ell n|2\eta k|-\tfrac{1}{2}\ell n\eta^2+\mathrm{Re}\,\frac{\Gamma'(1+i\eta)}{\Gamma(1+i\eta)}+2\gamma) \quad . \tag{5.37}$$

Including the energy independent term $2\eta k(\ell n|2\eta k|+2\gamma)$ in the scattering length gives back the well known formula

$$C_o^2(\eta)k \cot g\delta + 2\eta k h(\eta) = -\frac{1}{A} + \frac{1}{2}(k^2-k_o^2)R \quad , \tag{5.38}$$

with $h(\eta) = \mathrm{Re}\,\frac{\Gamma'(1+i\eta)}{\Gamma(1+i\eta)} - \frac{1}{2}\ell n\eta^2$.

For higher ℓ the equivalent expression of (5.37) is somewhat more complicated. We remark that the leading term has the energy dependence $k^{2\ell}$. Therefore it gives no contribution to the scattering length and only for $\ell=1$ to the effective range. This implies that the effective range expansion is correct in principle also when the second term of the left hand side of (5.36) for $\ell>0$ is neglected. Moreover, we have calculated that for Σ^+p scattering its contribution for $\ell=1$ is -0.007 at 0.1 MeV and -0.04 at 20 MeV laboratory energy (in units $\hbar=c=m_\pi=1$), so its effect can be only important for small effective ranges, but even then its influence can be neglected since the scattering length will dominate, at least at the energies we are considering.

CHAPTER 6
NUMERICAL PROCEDURES

6.1. Introduction.

In order to obtain a solution of the coupled Schrödinger equations, we have to make use of a computer. Computations have been carried out, using the IBM 7090 at Düsseldorf, the IBM 7094/II at the IBM computer center in Rijswijk, and the IBM System/360 model 40 at the computing center of the Catholic University of Nijmegen.

We have employed a program that calculates the potentials and integrates the Schrödinger equation point by point, for each partial wave separately. In the same program the cross sections can be calculated.

Also the matrix

$$B = k^{-(\ell+\frac{1}{2})}\, K\, k^{-(\ell+\frac{1}{2})} \tag{6.1}$$

can be punched on cards to be input for other programs, e.g., for computing the angular distributions and polarizations. Since for these computations the amplitudes of several partial waves are to be combined, it is more economical to do this in separate programs.

For convenience we have used different programs for $\Sigma^- p$ and $\Sigma^+ p$ scattering.

Before we will outline the organization of the computer programs, we will first consider some numerical methods. Most of the methods employed have also been used for ΛN scattering and are considered by Fast [27]. We therefore will restrict ourselves to a short discussion of the numerical integration. Also we will consider the computation of the Coulomb wave functions and some related quantities, used only for Σp scattering.

6.2. Numerical methods.

The numerical integration of the differential equation (4.17), which we write as

$$u''(r) = A(r)u(r) \quad , \tag{6.2}$$

where u and A are matrices, is done by means of a generalization of Numerov's

method [70,15], which is very convenient for handling matrix differential equations on a digital computer.

One defines the matrix $w(r)=u(r)-h^2u''(r)/12$, where h is the integration step length. Then the relation $w(r+h)-2w(r)+w(r-h)=h^2u''(r) + -h^6u^{VI}(r)/240 + \ldots$ holds, so for small intervals h one is able to compute w in the point r+h from the two foregoing points by

$$w(r+h) = h^2A(r)u(r) + 2w(r) - w(r-h) \quad , \tag{6.3}$$

and u(r+h) can be obtained by inversion of $w(r)=(1-h^2A(r)/12)u(r)$.

Since we are starting the integration from the hard core radius r_c, we have as boundary condition $u(r_c)=0$. We choose $u'(r_c)=I$, where I is the unit matrix, giving us a set of independent solutions of (6.2). All solutions with $u(r_c)=0$ can be obtained by multiplying u(r) with an arbitrary non singular matrix from the right. From these boundary conditions we get the wave function in the first two points.

The errors in the integration are mainly determined by two factors, namely the accuracy of (6.3), and the rounding off errors in each step of the computation. For these reasons we have chosen a small step size in the region where the potentials are strong and a larger step size farther away, where the potentials are much weaker. A good choice appeared to be h=0.005 (m_π^{-1}) for the first 50 points, h=0.01 for the following 100 points and h=0.02 for the last 150 points. All these calculations are performed in double precision arithmetic.

We have integrated to about 6 fm, where the short range potentials can be neglected. The solutions of the Schrödinger equation are then linear combinations of the spherical Bessel and Neumann functions or of the regular and irregular Coulomb wave functions.

Since we have to join the wave function and its derivative, we have to know $u'(r_a)$, where r_a is the point where the joining is performed. This derivative is computed by fitting u(r) in the last 7 points to a polynomial of degree 6, from which $u'(r_a)$ is calculated easily.

As r_a is varying, since it depends on the hard core radius, and also because the momenta k and the value of η are dependent on the energy, we have to compute again the spherical Bessel and Neumann functions and the Coulomb wave functions for every integration. The computation of the spherical Bessel and Neumann functions, having a closed expression in terms of the goniometric functions, is performed easily, but this is not so simple for the Coulomb wave functions.

The regular and irregular Coulomb wave functions and their derivatives with respect to ρ are computed for $\ell=0$, using the series (5.5) and (5.9). These series are very convenient for the small values of η and the rather small values of $\rho = kr_a$ we need. For higher values of ℓ we have used the recurrency relations [71]

$$\ell v_\ell = (\ell^2+\eta^2)^{\frac{1}{2}} v_{\ell-1} - \left(\frac{\ell^2}{\rho}+\eta\right) v_\ell \quad ,$$

$$(\ell+1) v'_\ell = \left\{\frac{(\ell+1)^2}{\rho} + \eta\right\} v_\ell - \{(\ell+1)^2+\eta^2\}^{\frac{1}{2}} v_{\ell+1} \quad ,$$

$$\ell\{(\ell+1)^2+\eta^2\}^{\frac{1}{2}} v_{\ell+1} = (2\ell+1)\left\{\frac{\ell(\ell+1)}{\rho}+\eta\right\} v_\ell - (\ell+1)(\ell^2+\eta^2)^{\frac{1}{2}} v_{\ell-1} \quad , \qquad (6.4)$$

where v_ℓ is F_ℓ or G_ℓ. The Wronskian condition $F'_\ell G_\ell - F_\ell G'_\ell = 1$ can be used as a test on the computations.

In Eq. (5.10) the logarithmic derivative of the Γ-function appears. It can be calculated, using

$$\mathrm{Re}\,\frac{\Gamma'(1+i\eta)}{\Gamma(1+i\eta)} = \eta^2 \sum_{h=1}^{\infty} \frac{1}{h(h^2+\eta^2)} - \gamma \quad , \qquad (6.5)$$

where γ is Euler's constant. Instead of (6.5) it is better to use a much faster converging series that can easily be derived from (6.5). It is

$$\mathrm{Re}\,\frac{\Gamma'(1+i\eta)}{\Gamma(1+i\eta)} = 1-\gamma - \frac{1}{1+\eta^2} + \sum_{k=1}^{\infty} (-1)^{k+1} \{\zeta(2k+1)-1\} \eta^{2k} \quad , \qquad (6.6)$$

in which $\zeta(2k+1)$ is the Riemann Zeta function. This function is not computed in the program, but we have used tabulated values [72] for k=1(1)10, which always gave enough accuracy.

We can also compute the Coulomb phase angle σ_ℓ in the same manner. This angle is defined by $\sigma_\ell = \arg\Gamma(\ell+1+i\eta)$, so

$$\sigma_\ell = \sigma_o + \sum_{s=1}^{\ell} \mathrm{arctg}(\eta/s) \qquad (6.7)$$

and

$$\sigma_o = -\eta\gamma + \sum_{s=1}^{\infty} \left(\frac{\eta}{s} - \mathrm{arctg}\,\frac{\eta}{s}\right) \quad .$$

Here one can also use the more convenient series

$$\sigma_o = -\eta\gamma + \sum_{n=1}^{\infty} (-1)^{n+1}\, \eta^{2n+1} \zeta(2n+1)/(2n+1) \quad . \qquad (6.8)$$

6.3. The organization of the computer programs.

The program that integrates the Schrödinger equation for $\Sigma^- p$ scattering is organized as follows (Fig. 6.1). In INPUTM one or more data cards are read in, containing parameters like the SU(3) parameter α, the hard core radii etc., and some control data. Then SMP is called, which performs the control proper and does some simple calculations.

In a loop enclosing the whole routine SMP the Schrödinger equation is integrated and the matrix B (6.1) is computed. These calculations are usually done for all partial waves having the same ℓ in the incoming channel, for example $^1S_0$ and $^3S_1+^3D_1$. Then the cross sections are calculated. This has the advantage that for $\ell=0$ we obtain directly the most important contributions to the ratios and total cross sections, hence avoiding calculations by hand afterwards.

In this loop first the potentials are calculated in POTENM, using the formulae of Section 3.3. The modified Bessel functions K_0 and K_1 (3.35) are computed in BESKV, using a numerical series [73]. In AMAT these potentials are multiplied with the appropriate coupling constants and isospin factors. Also the other contributions to A (6.2), like centrifugal barrier and momenta are included. For convenience these computations are done for all 300 integration points at the same time, so when returning from AMAT we have the matrix A for all points.

We are then ready to integrate Eq. (6.2). This is done in subroutine DIFEQM by means of the method described in the foregoing section. The matrix

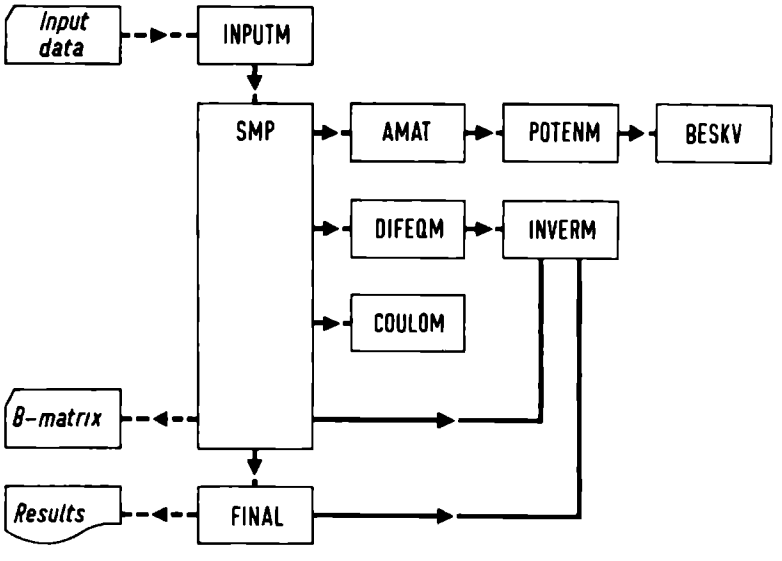

Fig 6 1 The organization of the computer program for the computation of Σ p scattering
⟶ — is a linkage between subroutines, ---▸--- is input/output data flow

inversions needed herefore, are done in INVERM. After performing the joining of the wave functions (see Eq. (4.45)) to the spherical Bessel and Neumann functions or to the Coulomb wave functions, calculated in COULOM, we obtain the matrix B (Eq. (6.1)). This matrix can be punched on cards and is stored to be input for subroutine FINAL. In this routine finally the cross sections and ratios are calculated and printed out.

The intermediate output is used as input for other programs. The data flow is sketched in Fig. 6.2. Besides the calculation of the cross sections by FINAL directly from the results of the computation in SMP, our program gives the matrix B on punched cards. From these matrices for different partial waves the angular distributions and polarizations are calculated by DIFM, an essentially straightforward program. Its results are printed out, both numerically and graphically. The last is done very conveniently with the routine GRAVEL, that makes graphics, interpolating on a "physical" manner [74].

In order to study the correction method for the Coulomb effects discussed in the next chapter, we have the possibility to incorporate this correction starting from the B-matrix using COUCOR and calculating then the cross sections by CROSS. For completeness this less important possibility is also shown.

An important use of the intermediate output is the calculation with the isospin T=1/2 or T=3/2 potentials separately, as described in Chapter 8. The two B-matrices are combined in TT, Coulomb corrections are applied and the total cross sections are calculated by FINALT, which is essentially

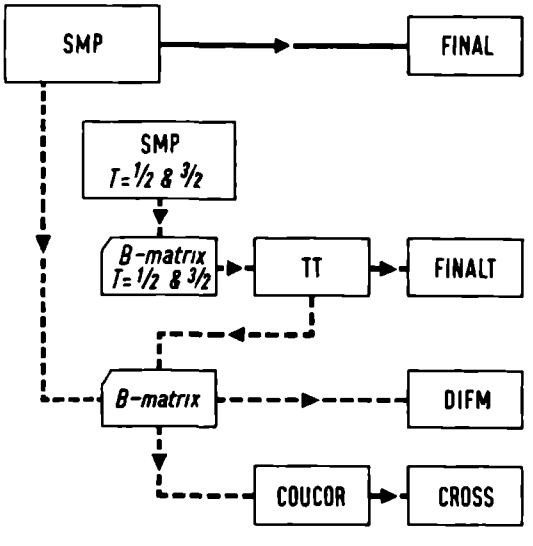

Fig 6 2 The data flow for the computation of Σ^-p scattering ——►—— is a linkage between subroutines, ---►--- are connections via intermediate output on punched cards

the same routine as FINAL. The TT program also gives the combined B-matrix as input for DIFM.

The organization of the programs for the computation of Σ^+p scattering is essentially the same as for Σ^-p scattering. Also for this scattering the matrix B is punched to be input for a program that calculates the Σ^+p angular distributions.

All the programs are written in Fortran, except the subroutine INVERM, which is written in assembler language. Since the matrix inversions use most of the computing time, one could expect to save a relatively large amount of computing time by writing this subroutine as economically as possible. Actually, the time saved was about 10-20%. This rather slight improvement is caused by the fact that the double precision arithmetic in this subroutine uses a large part of the total time needed. This arithmetic cannot be done faster by using the assembler language instead of Fortran. Consequently, the substantial improvement in fixed point arithmetic for index handling and things like that has less influence on the whole computing time.

The Σ^-p program and its subroutines use approximately 27 K words. A large part of this storage space is occupied by $6 \times 6 \times 300$ words, which serves first as location for the potentials in the 300 integration points and which is used next to contain the matrix A defined in (6.1).

The computation times for one singlet and one triplet case, a frequently occurring situation, were approximately 4 minutes on the 7090, 1 minute on the 7094/II and 4 minutes on the 360/40. The program runned faster on the 7094/II than on the 7090, because in the first computer the double precision arithmetic uses hardware instructions, whereas the 7090 has to use macros for this. Likewise due to the more adapted hardware for the double precision arithmetic, the 360/40 is not so much slower than the 7094/II. Other programs were running a factor 10-15 slower on the 360/40 than on the 7094/II, depending heavily on the amount of input-output operations at the time the computations were performed.

CHAPTER 7
CALCULATIONS WITH POTENTIALS DUE TO THE EXCHANGE OF PSEUDOSCALAR MESONS

7.1. Introduction.

In this chapter we will give the results of calculations done with the model described in the foregoing chapters. For the calculations described in this chapter we have taken the potentials due to the exchange of one and two pions, the exchange of one K meson and of one η meson. These potentials are given by the equations (3.32), (3.34), and (3.35).

We relate the pseudoscalar coupling constants by assuming SU(3) symmetry for them, so they are given by (3.44). The $NN\pi$ coupling constant is well known. We have used the value $f_{NN\pi}/(4\pi)^{\frac{1}{2}}=0.283$. The SU(3) ratio, α, remains still as a free parameter.

To these potentials we have to add the repulsive hard cores. In principle the radii of these cores can be different for different quantum numbers. In the first calculations we have taken only two different radii, namely one for singlet states, X_s, and one for triplet states, X_t. Doing so, we make the essential assumption that these radii are independent of the total isospin, which is different for the different states. The ΛN system is a pure isospin T=1/2 state, but the $\Sigma^- p$ system is a mixture of T=1/2 and T=3/2 states, whereas $\Sigma^+ p$ forms a pure T=3/2 state. The assumption of isospin independence for the cores implies that the core radii should be equal for Λp, $\Sigma^- p$ and $\Sigma^+ p$ scattering. If this is true, we can use the information from the ΛN interaction for which the singlet and triplet scattering lengths are known. For a given value of α and assuming no ΛN bound state this determines uniquely the values for X_s and X_t. These core radii have been calculated by Fast [27], using the scattering lengths obtained from the hyperfragment data (2.1), and for the values obtained from the Λp scattering experiments (2.3). In these computations the same potentials have been used as in our calculations, but of course with the appropriate coupling constants and isospin factors. The core radii have been adjusted such that they give the correct scattering lengths.

Since we have the two different sets of scattering lengths (2.1) and (2.3), we also have two possibilities for the hard core radii. We will call the core radii that are adjusted to the ΛN scattering lengths derived from the hyperfragment data the Hf cores, whereas we denote with Lp cores the

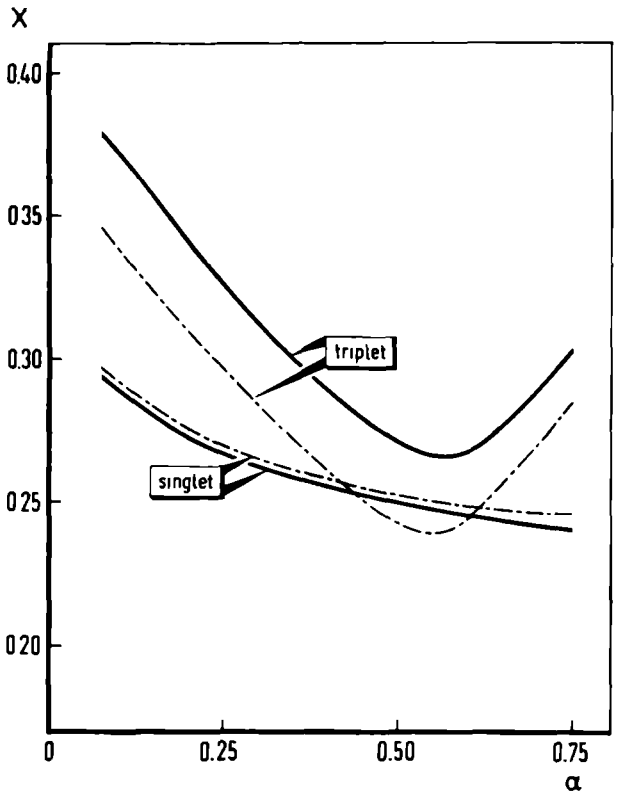

Fig. 7 1. The singlet and triplet hard core radii as a function of α. ——— are the radii that fitted the hyperfragment data (2 1) (Hf cores), —·—·— are the radii that fitted the Λp scattering data (2.3) (Lp cores).

core radii that are fitted to the scattering lengths obtained from Λp scattering. Both sets of radii are given in Fig. 7.1. We see from this figure that the singlet Hf and Lp cores are almost equal, but that the triplet radii are much more different. Especially for the Hf radii the difference between singlet and triplet radius is sizable, caused by the large difference between the singlet and triplet scattering length.

We will first study the influence of the Coulomb potential at the energies we are considering. We will also derive a possible approximation to include the effects of this potential and compare it with the results of the exact calculations.

Then we will compare our results for $\Sigma^{\pm}$p scattering with the experimental data, using the assumptions mentioned above. Hence, we have used potentials due to the exchange of the SU(3) octet of pseudoscalar mesons, the coupling constants are related by SU(3) symmetry and the hard core radii are fitted to the ΛN scattering lengths.

We will investigate whether our results are in agreement with the experimental data for values of α in the neighbourhood of α=0.4, the SU(6) prediction. We will show that we can obtain a good fit with the Σ^{-}p experimental data for $\alpha \sim 0.5$ [75]. The slight difference of this α with the SU(6) prediction is not too bad, since the uncertainties in the potentials are quite large. Also the fact that the breaking of SU(3) symmetry has only been taken into account in the masses of the particles involved, but not in the coupling constants, can be responsible for this difference.

The agreement with the Σ^{+}p data is not as good. This can be explained by the fact that we assumed that the T=1/2 and T=3/2 cores are equal.

7.2. The influence of the Coulomb potential.

In order to study the influence of the Coulomb potential, we have compared some calculations for $\Sigma^{\pm}p$ scattering performed with and without the presence of the Coulomb potential, leaving all other things unchanged.

The Coulomb potential gives rise to two effects. First, the angular distribution will show a strong forward peaking in the channels where charged particles are present. This is caused by the term $M_C(\theta)$ in the expression for the scattering amplitude $M(\theta)$, given in (5.28). In the experiments one usually leaves aside the forward scattering events. We will define a total cross section by using $|M_N(\theta)|^2$ instead of $|M(\theta)|^2$. This cross section will be almost equal to the total cross section that one would obtain if one neglects the angular region $\cos\theta \lesssim 1$. The second consequence of the Coulomb potential is that $M_N(\theta)$ will be different from $M'_N(\theta)$, where $M'_N(\theta)$ is the scattering amplitude obtained without taking into account the Coulomb potential. Hence, the total cross section will not be equal to the cross section obtained without the presence of the Coulomb force.

It will be clear that the importance of the Coulomb effects increases for low energy and that these effects are more important for the elastic channels, where charged particles are present, than for the inelastic channels, where the Coulomb potential acts only indirectly. Therefore, it is not surprising that the influence on the ratios r_F and even on r_C can be neglected, although the cross sections from which the latter ratio is calculated, are quite different.

The columns I and II of Table 7.1 give an example of the total cross sections for Σ^-p and Σ^+p scattering as a function of the energy, resulting from calculations without and with the presence of the Coulomb potential. The influence of the Coulomb potential can be neglected totally for energies higher than 20 MeV. For higher ℓ its influence is larger, as can be seen from Table 7.2, but since the total cross sections for higher ℓ are small, the larger relative difference is less important.

Since at 10 MeV the Coulomb potential gives a not unimportant change, we will give an approximation to take into account this effect without the necessity of doing an exact calculation with the inclusion of the Coulomb potential.

Although we are able to take the Coulomb potential into account exactly, an approximation is useful for two reasons. First, it enables us to incorporate its influence in cases where we are not able to do such an exact

$\Sigma^- p \to \Lambda n$

	$^1S_0$			$^3S_1$		
E_{lab}	I	II	III	I	II	III
0.1	83.3	227.2	231.8	3997.9	15762.2	17083.2
1	22.6	28.7	29.2	797.8	1085.7	1126.9
5	9.4	10.0	10.1	219.8	237.8	243.1
10	6.4	6.7	6.7	112.4	116.2	117.8
20	4.4	4.5	4.5	53.3	53.8	54.1

$\Sigma^- p \to \Sigma^0 n$

	$^1S_0$			$^3S_1$		
E_{lab}	I	II	III	I	II	III
0.1	474.1	1300.0	1318.9	1189.7	4611.7	5053.7
1	126.1	161.0	162.9	244.4	328.9	345.2
5	48.6	52.1	52.3	73.4	78.5	81.2
10	30.6	31.8	31.9	39.7	40.6	41.7
20	18.2	18.6	18.7	19.6	19.5	20.0

$\Sigma^- p \to \Sigma^- p$

	$^1S_0$			$^3S_1$		
E_{lab}	I	II	III	I	II	III
1	80.7	163.7	163.6	276.3	587.0	640.4
5	58.1	75.5	79.7	172.7	222.8	242.8
10	43.7	51.4	54.1	125.8	145.0	156.6
20	29.1	32.1	33.7	84.0	96.2	89.9

$\Sigma^+ p \to \Sigma^+ p$

	$^1S_0$			$^3S_1$		
E_{lab}	I	II	III	I	II	III
0.1	623.9	23.8	19.8	52.9	0.5	0.5
1	536.2	352.7	310.0	52.5	15.1	14.4
5	326.2	311.4	294.2	50.6	31.3	29.5
10	215.2	212.1	206.5	47.6	35.6	33.3
20	124.0	123.5	122.7	40.6	34.9	32.4

Table 7 1 The total cross sections (in mb) for $\Sigma^- p$ and $\Sigma^+ p$ scattering as a function of the laboratory energy (in MeV) for singlet and triplet scattering The statistical factors 1/4 and 3/4 are included The meaning of the columns is as follows In Columns I and II are the results obtained without and with inclusion of the Coulomb potential In Column III are the results of the approximation described in section 7 2

	$\Sigma^- p \to \Lambda n$			$\Sigma^- p \to \Sigma^0 n$		
	I	II	III	I	II	III
$^1P_1$	0.9	1.0	1.0	1.2	1.2	1.3
$^3P_0$	0.2	0.2	0.2	4.5	3.1	3.8
$^3P_1$	12.5	14.0	13.8	10.3	11.3	11.4
$^3P_2$	3.3	3.6	3.7	0.2	0.3	0.3

	$\Sigma^- p \to \Sigma^- p$			$\Sigma^+ p \to \Sigma^+ p$		
	I	II	III	I	II	III
$^1P_1$	0.1	0.1	0.1	1.1	0.9	0.8
$^3P_0$	0.5	0.2	0.4	4.6	3.8	3.6
$^3P_1$	8.1	9.7	10.2	1.2	1.1	1.0
$^3P_2$	0.3	0.3	0.3	0.2	0.2	0.2

Table 7.2. The total cross sections for $\Sigma^- p$ and $\Sigma^+ p$ scattering for P-waves at $E_{lab} = 20$ MeV. See for the meaning of the columns the caption of Table 7.1.

computation, as is described in Chapter 8. The approximation is also useful for an effective range analysis of the experiments, where it enables one to separate off the Coulomb effects [69].

The simple approximation, $M=M_C+M'_N$, where M'_N is the scattering amplitude obtained without taking into account the Coulomb potential, describes the behaviour of the angular distribution very well, but the total cross sections, calculated from M'_N, remain unchanged. A much better approximation for the latter is the following one. We use the effective range expansion (4.46) for the K-matrix K, calculated without the presence of a Coulomb potential and the corresponding expansion (5.36) for the K-matrix K_C, where the Coulomb potential is taken into account exactly. By relating the scattering length and effective range matrices for both cases, we can express K_C in terms of K.

We will take as a crude approximation $R_C=R$ and $A_C=A$, except that for those elements of A that connect channels with charged particles and $\ell=0$, we will use a correction.

For pp scattering Jackson and Blatt [69] give the formula

$$\frac{1}{a_C} = \frac{1}{a} + \frac{1}{\Delta a} \tag{7.1}$$

with

$$\frac{1}{\Delta a} = 2\eta k\{\ell n(2\eta k r_o) + 2\gamma - 0.824\} \quad . \tag{7.2}$$

For r_o one has to take the range of the nuclear potential. The term $\ell n(r_o)-0.824$ results from a rough calculation, the other terms we have already seen in the derivation of the effective range expansion. For one channel scattering the relation (7.2) is an exact one for a square well potential with a depth such that $1/a=0$, i.e. a bound state with zero binding energy. We will use this correction. Taking $r_o=1$, we obtain for $\Sigma^{\pm}p$ scattering $1/\Delta a=\mp 0.14$.

We have checked this correction for an attractive square well potential with different widths and depths to which a repulsive Coulomb potential has been added. The results are given in Table 7.3. We see that when

V_o	X	$-1/a$	$-1/a_C$	$1/\Delta a$	r^o	r_C^o
5	1	9.71	9.46	0.25	4.95	4.74
10	1	4.25	4.22	0.03	2.74	2.63
20	1	1.52	1.60	-0.08	1.63	1.57
50	1	-0.13	0.02	-0.15	0.96	0.93
100	1	-0.69	-0.55	-0.14	0.72	0.70
5	4	-0.14	-0.04	-0.10	3.46	3.08
10	4	-0.24	-0.12	-0.11	2.51	2.32
20	4	-0.43	-0.26	-0.17	-1.67	-0.53
50	4	-0.27	-0.15	-0.11	2.68	2.40
100	4	-0.25	-0.14	-0.11	3.04	2.67

Table 7 3 The scattering length and effective range for a square well potential with depth V_o (in MeV) and width X (m_π^{-1}), without and with the presence of a repulsive Coulomb potential

$1/a$ is small, the correction has the right order of magnitude, whereas for larger $1/a$ the correction is not as good as could be expected. For these scattering lengths the correction is less important. We have also given the effective ranges r^o and r_C^o in this table. Although they are not exactly equal, the influence of the difference will be small for energies up to about 10 MeV. For $\ell=1$ the effective ranges and scattering lengths are equal within a few percents.

Using this correction we expect that a reasonably good approximation for coupled channels will be

$$(2\ell+1)!!C_\ell(\eta)k^{\ell+\frac{1}{2}}K_C k^{\ell+\frac{1}{2}}C_\ell(\eta)(2\ell+1)!! = k^{\ell+\frac{1}{2}}Kk^{\ell+\frac{1}{2}} - 2k\eta h(\eta) - 1/\Delta a \quad , \tag{7.3}$$

where $C_\ell(\eta)$ and $h(\eta)$ are defined as in Chapter 5 and where $1/\Delta a$ is a diagonal matrix with only non zero elements for the channels connecting charged particles with $\ell=0$.

We have verified this formula for $\Sigma^{\pm}p$ scattering. The results as a function of the energy are given in Table 7.1 and 7.2. The Coulomb interference is shown in Table 7.4. The shape of the angular distribution is perfectly represented by the correction (Table 7.5).

It appeared also that our results are only slightly dependent on the specific example we have chosen. This could be seen by taking a set of different potentials and therefore different values of A and R by using different values of α. The approximation gave the best results when $1/a=0$, but even for other values of the scattering length the difference did not become too large.

	E_{lab} = 5 MeV			E_{lab} = 10 MeV			E_{lab} = 20 MeV		
cosθ	I	II	III	I	II	III	I	II	III
-1.0	-2	-2	2	-1	-1	0	0	0	0
-0.6	-4	-4	3	-2	-2	1	-1	-1	0
-0.2	-7	-7	5	-3	-3	1	-2	-2	0
0.2	-14	-14	10	-7	-7	3	-4	-4	1
0.6	-38	-38	41	-19	-19	10	-10	-10	3
0.8	-94	-95	162	-45	-45	40	-23	-24	10
0.9	-220	-224	648	-101	-102	162	-52	-52	40
0.95	-501	-511	2590	-221	-225	648	-111	-112	62

Table 7.4. The Coulomb interference computed exactly (Column I) and employing the approximation (Column II). Column III shows the pure Rutherford scattering cross section.

	$\Sigma^-p \to \Lambda n$			$\Sigma^-p \to \Sigma^0 n$			$\Sigma^-p \to \Sigma^-p$		
cosθ	I	II	III	I	II	III	I	II	III
-1.0	79	83	83	46	47	48	69	78	83
-0.6	75	79	80	42	43	44	75	86	92
-0.2	71	74	75	40	41	42	82	95	102
0.2	64	67	68	38	40	40	90	105	112
0.6	56	58	59	38	40	40	98	115	123
1.0	45	47	47	38	41	42	106	126	134

Table 7.5. The angular distributions $d\sigma/d\cos\theta$ in mb for Σ^-p scattering at 10 MeV laboratory energy. The meaning of the columns is the same as for Table 7.1.

7.3. Results for $\Sigma^- p$ scattering.

For $\Sigma^- p$ scattering we have calculated first the total cross sections for the reactions II, and the ratios r_C and r_F. The Coulomb potential has been taken into account exactly. The cross sections and r_F are calculated at 10 MeV laboratory energy, corresponding to about 155 MeV/c laboratory momentum, being about the middle of the momentum interval considered in the experiments. The ratio r_C is calculated at 0.1 MeV. At this energy this ratio is almost equal to its limit for $E_{lab} \to 0$.

Although the energy at which the calculations are performed is rather small, so that the main contribution comes from $^1S_0$ and $^3S_1$ waves, it could be expected that there is also a contribution from P-waves, especially in the channel $\Sigma^- p \to \Lambda n$, where because of the mass difference a rather large energy is available.

The experiments indicate indeed the presence of P-waves. Considering the experimental inelastic cross section, we notice that this cross section almost reaches the unitarity limit for S-waves π/k^2, which is 254 mb at 10 MeV. Also the experimental angular distributions show a slight anisotropy. Both can be explained by assuming a contribution of waves with higher angular momentum.

From our calculations it followed that for almost all cases the P-waves are negligible, except for the $^3P_1$ ones. There was a very large $^3P_1$ contribution in the neighbourhood of α=0.6, but also for other values of α this partial wave is the most important contribution for ℓ=1.

The cross sections and ratios are given in Fig. 7.2 and 7.3, and in Table 7.6 and 7.7. In the figures we have also given the experimental data. We see from these data that we obtain a reasonable good fit for $\alpha \sim 0.5$, being close to the SU(6) prediction, α=0.4. This result should be contrasted with earlier calculations [23], using only pion exchange potentials. A comparison of these calculations with the then existing data, namely only the capture ratio r_C [76] and the deuterium capture ratio [77], which has not been used by us, predicted a much lower value of α.

Although the experimental angular distributions show large uncertainties, it is interesting to compare them with the distributions we can calculate. Clearly it is much more difficult to fit an angular distribution, since it depends not only on the magnitude of the S-matrix, but also on the sign of the matrix elements. Also, large cancellations between different terms can give unexpected results.

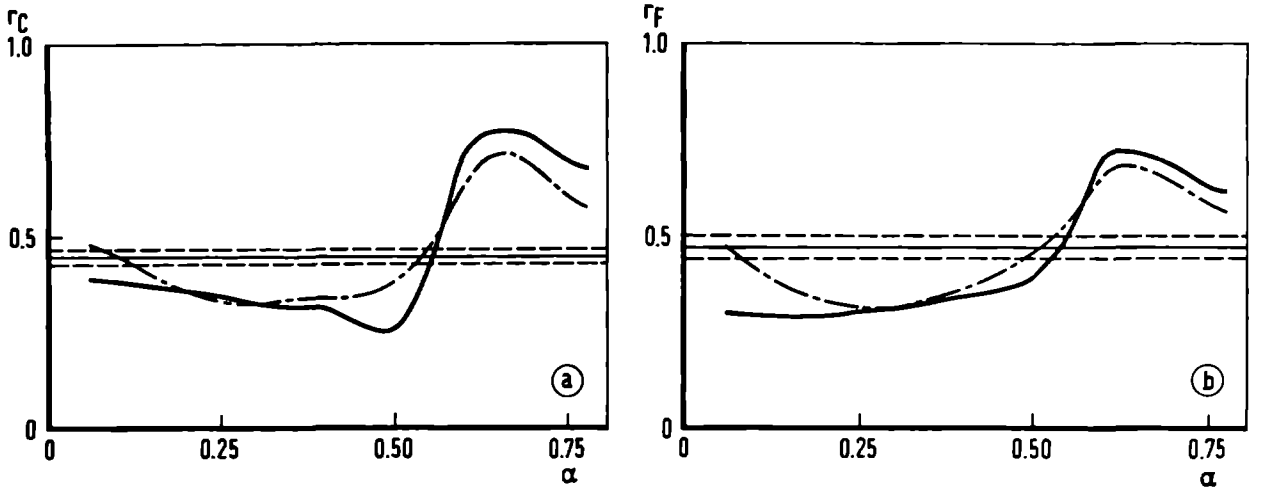

Fig. 7.2. The capture ratio at rest (a) and in flight (b) as a function of α. The experimental values are $r_C = 0.45 \pm 0.02$, $r_F = 0.47 \pm 0.03$, shown by ═══. ——— are the results for Hf cores, — · — · — for Lp cores.

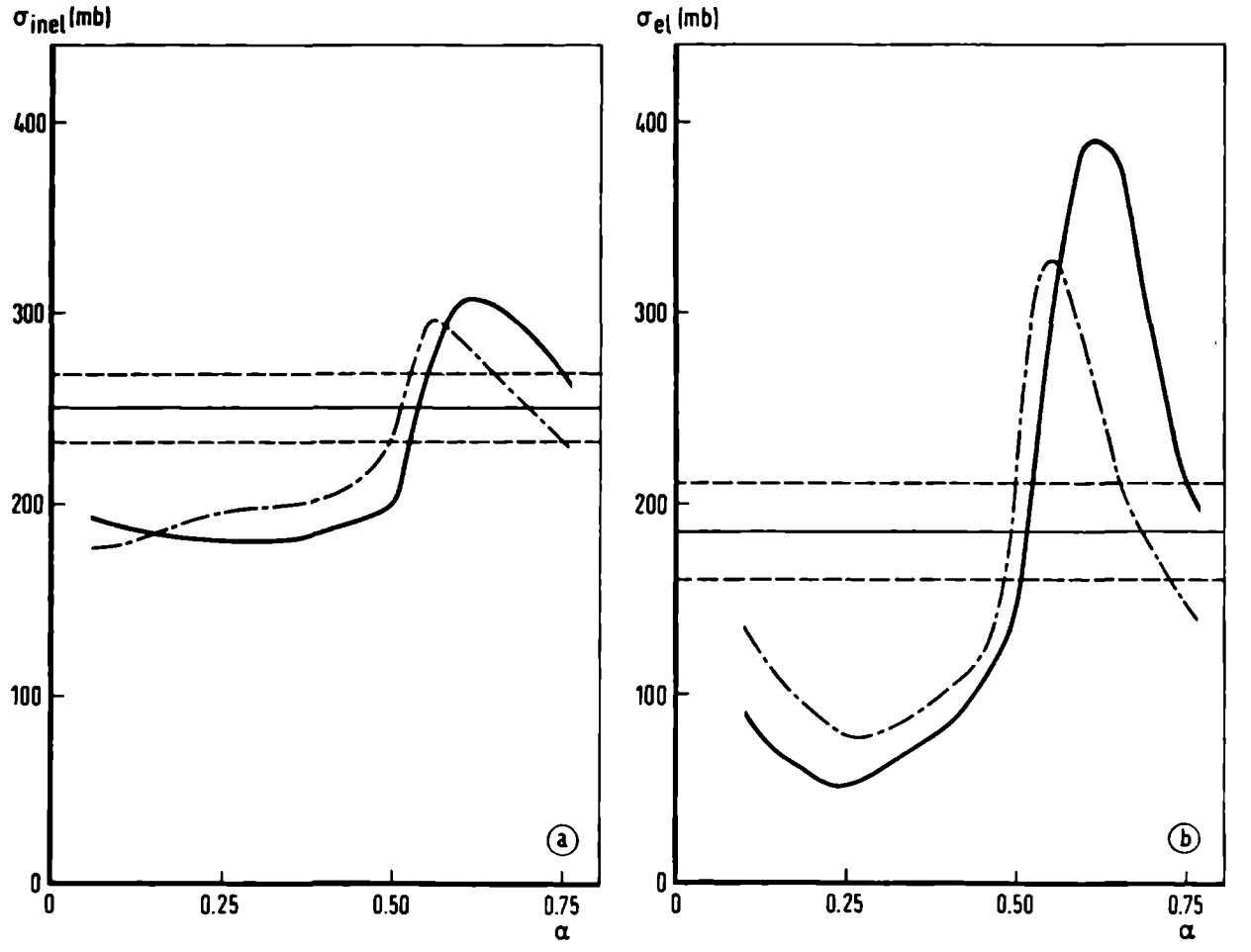

Fig. 7.3. The inelastic (a) and elastic (b) cross section as a function of α. The experimental values $\sigma_{inel} = 250 \pm 17$ mb and $\sigma_{el} = 185 \pm 25$ mb are indicated by ═══. ——— are the results for Hf cores, — · — · — for Lp cores.

$\Sigma^- p \to \Lambda n$

α	$^1S_0$	$^3S_1$	$^1P_1$	$^3P_1$	$^3P_2$	$^3P_0$	total
0.1	0.0	116.5	0.9	4.5	6.5	1.5	130
0.25	2.1	110.0	1.1	4.7	4.3	0.3	123
0.4	6.7	103.6	0.8	6.4	2.9	0.4	121
0.5	8.3	99.5	0.4	12.6	2.2	0.2	123
0.6	9.2	5.0	0.2	68.7	1.8	0.1	85
0.75	8.6	65.5	0.0	27.1	0.2	0.1	103

$\Sigma^- p \to \Sigma^0 n$

α	$^1S_0$	$^3S_1$	$^1P_1$	$^3P_1$	$^3P_2$	$^3P_0$	total
0.1	16.9	39.6	0.0	0.3	0.0	0.4	57
0.25	27.0	25.2	0.3	1.5	0.0	1.2	55
0.4	31.5	23.7	0.8	4.8	0.1	2.6	64
0.5	1.3	52.5	2.2	11.4	0.1	4.6	74
0.6	1.0	166.1	0.1	43.5	0.2	9.5	220
0.75	12.9	107.2	1.7	3.8	0.3	42.2	168

$\Sigma^- p \to \Sigma^- p$

α	$^1S_0$	$^3S_1$	$^1P_1$	$^3P_1$	$^3P_2$	$^3P_0$	total
0.1	4.1	86.4	0.0	0.1	0.0	0.1	91
0.25	5.9	44.0	0.1	0.5	0.0	0.2	51
0.4	51.5	34.3	0.1	2.3	0.1	0.3	89
0.5	37.4	102.9	0.0	6.9	0.1	0.3	148
0.6	26.9	320.5	0.7	38.7	0.3	0.4	387
0.75	16.6	171.4	0.4	9.5	0.9	12.9	212

α	$r_C(^1S_0)$	$r_C(^3S_1)$	r_C	r_F
0.1	0.25	0.14	0.39	0.30
0.25	0.23	0.10	0.34	0.31
0.4	0.21	0.10	0.32	0.35
0.5	0.02	0.22	0.24	0.38
0.6	0.04	0.72	0.75	0.72
0.75	0.17	0.42	0.59	0.62

Table 7.6. The total cross sections (in mb) for $\Sigma^- p$ scattering for S- and P-waves at E_{lab} = 10 MeV and the ratios for different values of α using the Hf cores The statistical factors are included. The Coulomb potential is taken into account exactly

$\Sigma^- p \to \Lambda n$

α	$^1S_0$	$^3S_1$	$^1P_1$	$^3P_1$	$^3P_2$	$^3P_0$	total
0.1	0.0	88.8	0.9	5.1	6.6	1.5	103
0.25	2.0	118.2	1.0	5.3	4.4	0.8	132
0.4	6.6	112.3	0.7	7.5	2.9	0.4	130
0.5	8.2	100.5	0.4	19.0	2.3	0.2	130
0.6	9.1	12.9	0.2	75.2	1.9	0.1	99
0.75	8.2	69.8	0.0	9.9	1.7	0.1	90

$\Sigma^- p \to \Sigma^0 n$

α	$^1S_0$	$^3S_1$	$^1P_1$	$^3P_1$	$^3P_2$	$^3P_0$	total
0.1	15.0	59.3	0.0	0.3	0.0	0.5	75
0.25	24.2	35.9	0.3	1.6	0.0	1.2	63
0.4	38.9	25.6	0.8	5.2	0.1	2.8	73
0.5	3.1	81.9	1.9	14.6	0.1	5.0	107
0.6	0.6	150.0	0.0	25.9	0.2	12.0	189
0.75	8.3	93.9	1.5	0.1	0.4	24.4	129

$\Sigma^- p \to \Sigma^- p$

α	$^1S_0$	$^3S_1$	$^1P_1$	$^3P_1$	$^3P_2$	$^3P_0$	total
0.1	4.3	133.1	0.0	0.1	0.0	0.1	138
0.25	5.3	69.3	0.1	0.6	0.0	0.2	75
0.4	49.0	42.9	0.1	2.7	0.1	0.3	95
0.5	39.6	181.6	0.0	9.8	0.1	0.3	231
0.6	27.8	198.6	1.0	32.5	0.4	0.6	261
0.75	19.1	113.6	0.4	1.5	1.1	16.3	152

α	$r_C(^1S_0)$	$r_C(^3S_1)$	r_C	r_F
0.1	0.25	0.24	0.49	0.42
0.25	0.23	0.13	0.36	0.32
0.4	0.22	0.10	0.33	0.36
0.5	0.04	0.29	0.33	0.45
0.6	0.03	0.69	0.72	0.66
0.75	0.14	0.39	0.53	0.59

Table 7.7. The same table as Table 7.6, but now using the Lp cores.

We have calculated the angular distributions, using incoming waves with $\ell=0$ and $\ell=1$, for waves with higher angular momenta are unimportant at these low energies. The angular distributions have in general the following behaviour. The $\Sigma^- p \to \Lambda n$ distribution has an enhancement in the forward direction for $\alpha \lesssim 0.5$, but for larger values of α it becomes isotropic and even enhanced in the backward directions. Except in the neighbourhood of $\alpha=0.25$ and $\alpha=0.6$ the $\Sigma^- p \to \Sigma^0 n$ angular distribution is almost isotropic. The $\Sigma^- p \to \Sigma^- p$ angular distribution is enhanced in the forward directions, also when the Coulomb interference and the Rutherford scattering are omitted. These results are valid both for Lp and Hf cores. We have shown the $\Sigma^- p \to \Lambda n$ and $\Sigma^- p \to \Sigma^- p$ angular distributions in Fig. 7.4. It should be noted that the Λn angular distribution for Lp cores becomes more enhanced in the forward directions for values of α slightly smaller than 0.5. The total $\Sigma^- p$ elastic cross section increases for values of α a little above 0.5, so for Hf cores the agreement with the experiments can be made better by taking a slightly larger value of α.

The occurrence of P-waves can give rise to polarization of the scattered particles. The polarization of the Λ is the most interesting one, for it can be measured from the angular distribution of the proton into which it

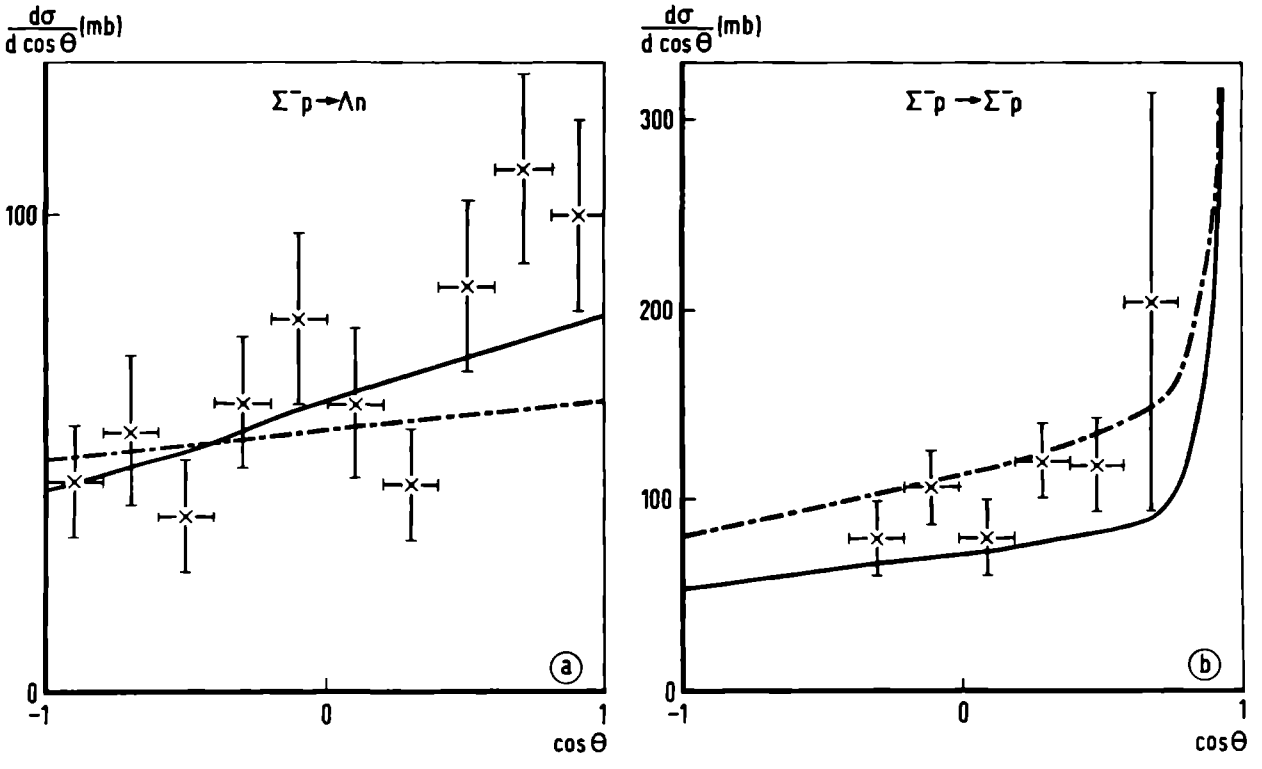

Fig 7 4 The angular distribution for the reaction $\Sigma^- p \to \Lambda n$ (a) and for the reaction $\Sigma^- p \to \Sigma^- p$ (b) at 10 MeV laboratory energy ——— are the results for Hf cores, — · — · — for Lp cores The experimental points and the error bands are also given

decays. We have therefore calculated the polarization in the reaction $\Sigma^- p \to \Lambda n$.

It turned out, however, that for $\alpha \sim 0.5$ this polarization was very small, $|P| \lesssim 0.05$. This was due to cancellations in the different terms of (4.41) that contribute to the polarization.

7.4. Results for $\Sigma^+ p$ scattering.

Using the same potentials as in the foregoing section, we have done calculations for $\Sigma^+ p$ scattering. The coupling constants have also been taken from (3.44).

For the $\Sigma^+ p$ interaction the experimental data are the total cross section and the angular distribution at about 10 MeV laboratory energy. In addition, a $\Sigma^+ p$ bound state probably does not exist.

We will investigate first whether a bound state may exist for these potentials. This can be done most easily by considering the behaviour of the scattering length. It is well known that the scattering length is negative for very weak attractive potentials, for more attractive potentials its modulus becomes larger and it goes to $-\infty$ when the attraction is strong enough to give a bound state. Therefore, the scattering length as a function of the hard core radius will be as sketched in Fig. 7.5.

We first need to calculate this scattering length as a function of the hard core radius X. For simplicity we have not calculated a, but we have used the matrix B at 0.1 MeV, where this matrix is only slightly different from the scattering length matrix A. For singlet states B is of course a number, for triplet states we have to consider the (1,1) element of B, describing the scattering for $\ell=j-1 \to \ell=j-1$. Calculations have been done for several values of α. The core radius at which a bound state occurs for the first time is called a bound state radius and is given in Fig. 7.6, both for singlet and triplet states.

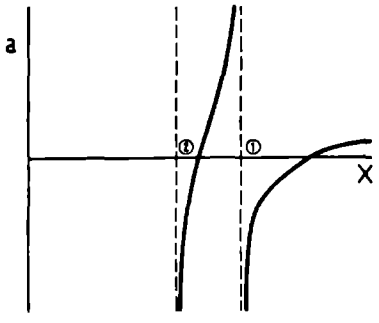

Fig. 7.5. The scattering length a as a function of the hard core radius X. At ① the first bound state appears, followed by a second one at ②.

Comparing these cores with the values obtained from the ΛN data (also given in Fig. 7.6), we see that a singlet bound state occurs for values of $\alpha \gtrsim 0.4$.

The experimental evidence for a $\Sigma^+ p$ bound state is ambiguous. A search for a Σ^- hyperfragment by means of the study of K^- capture

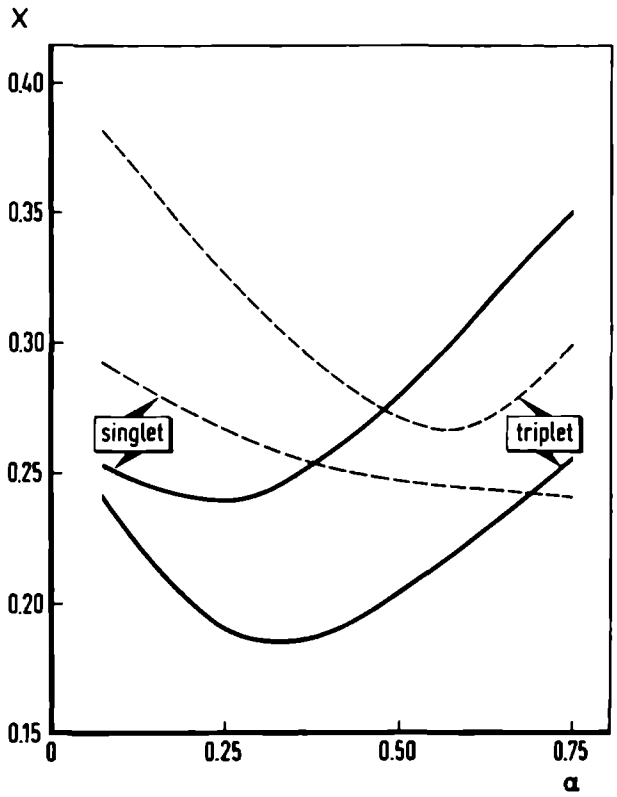

Fig. 7.6. The bound state core radius as a function of α.– – – – – are the core radii obtained from the hyperfragment data, shown for comparison.

in nuclear emulsion [78] give some events which could be interpreted as a $\Sigma^- n$ hyperfragment, but in no case is the interpretation unequivocal. Therefore, the existence of the charge symmetric $\Sigma^+ p$ hyperfragment is also probably excluded.

The experimental $\Sigma^+ p$ angular distribution (Fig. 2.1) shows a forward peaking. The most reasonable explanation is that it is only a statistical fluctuation, but if the effect is real, it can be caused by strong contributions of P-waves or by assuming a constructive Coulomb interference. The latter can be obtained by assuming a repulsive potential or an attractive potential admitting a $\Sigma^+ p$ bound state.

If one assumes such a bound state, it is reasonable to suppose that it is a singlet one, since the total $\Sigma^+ p$ cross section is rather small. Therefore, only a singlet bound state having a low binding energy will give a not too large contribution to the cross section owing to the statistical factor 1/4. This assumption is in accordance with experiments of K^- scattering on deuterium [79], giving rise to the reaction $K^- d \to \Sigma^- n \pi^+$ from which it has been concluded that a triplet bound state can have only a binding energy of a few keV.

Assuming a singlet bound state we have made a rough calculation with an attractive square well potential and a repulsive hard core to estimate the binding energy of the bound state. For cores and wells fitting the total cross section we have obtained the rather large binding energy of about 4 MeV, only slightly dependent on the well and core parameters.

For the hard core radii that fit the experimental total cross section and the experimental angular distribution, we can say the following. Since the P-wave contributions are very small, we have to consider the effects of the Coulomb potential. Using α=0.4, we have calculated the total cross sections, the Coulomb interference and the Coulomb scattering contributions to

the angular distribution. In Fig. 7.7 we have given the total cross section and the Coulomb interference term at $\cos\theta=0.7$ as a function of the radius X. At $\cos\theta=0.7$ the Coulomb scattering has the value 11.7 mb. We conclude that if we want to obtain a sizable constructive Coulomb interference assuming no Σ^+p bound state we need very large core radii (see Fig. 7.7[a]).

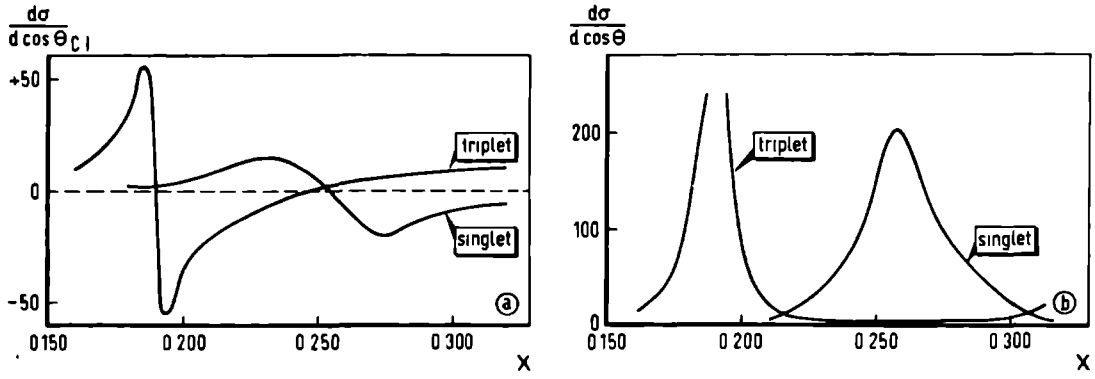

Fig 7 7 The Coulomb interference at $\cos\theta = 0\ 7$ (a) and the total Σ^+p cross section (b) as a function of the hard core radii at $E_{lab} = 12\ 5$ MeV

Assuming a singlet bound state, we obtain a positive contribution to the angular distribution due to Coulomb effects for $X_t \geq 0.205$ and $X_s \geq 0.245$, but this contribution remains small. Finally, a triplet bound state is able to give a larger contribution, but then X_t should be smaller than 0.180, implying not only a Σ^+p bound state, but also a (non stable) Σ^-p and a Λp bound state.

It appears therefore that it is very difficult to obtain a sizable forward peaking by assuming a constructive Coulomb interference. It seems to be more realistic to reject the possibility of a Σ^+p bound state.

The Σ^+p cross section as a function of α (Table 7.8) for cores fitted to the ΛN data reflect the presence of the Σ^+p bound state. At $\alpha=0.4$ the singlet core radius is near the bound state radius, so there the cross section is large. In order to avoid a Σ^+p bound state for $\alpha \geq 0.4$ and to fit the experimental cross section, we have to take a larger singlet core than the one determined by the ΛN data. For the Σ^-p scattering this will not change our results drastically due to the statistical factor 1/4. Since the cross section in the neighbourhood of a bound state is large, and since the triplet Σ^+p scattering is small for almost all values of α, it is always possible to fit the total Σ^+p cross section. The angular distribution we obtain for Σ^+p scattering is almost isotropic, besides a very small des-

tructive interference and, for somewhat smaller angles ($\cos\theta \geq 0.8$), the Coulomb peaking. In the following chapter we will come back to the Σ^+p scattering in more detail.

	Hf cores			Lp cores		
α	$^1S_0$	$^3S_1$	total	$^1S_0$	$^3S_1$	total
0.1	14.2	10.2	24	10.9	5.4	16
0.25	38.6	11.3	50	30.6	7.4	38
0.4	197.6	4.5	202	233.4	1.7	225
0.5	42.7	1.5	44	52.1	11.6	64
0.6	9.7	18.1	28	12.1	99.8	112
0.75	2.6	13.0	16	0.0	39.1	39

Table 7.8. The total Σ^+p cross sections (in mb) for S-waves at $E_{lab} = 11$ MeV. The statistical factors 1/4 and 3/4 are included.

CHAPTER 8
THE ISOSPIN DEPENDENCE OF THE HARD CORE RADII

8.1. Introduction.

The calculations of Chapter 7 were based on the assumption that the T=1/2 and T=3/2 core radii are equal. We have seen that the core radii derived from the ΛN data imply a singlet Σ^+p bound state for values of $\alpha \geq 0.4$. The occurrence of this T=3/2 bound state explains some features of our results. When we have a value of α with the appropriate core radius such that this radius is in the neighbourhood of a bound state radius, this will result in a large T=3/2 cross section (Table 7.8). This effect can be seen also in the behaviour of the singlet $\Sigma^-p \to \Sigma^-p$ and $\Sigma^-p \to \Sigma^0n$ cross sections (Table 7.6 and 7.7), which show a large value at α=0.4, this being about the point of intersection of the bound state radius with the singlet radius (Fig. 7.6). Of course one could argue that since a Σ^+p bound state has not been found experimentally, values of $\alpha \geq 0.4$ are therefore excluded.

The fact remains, however, that our results are strongly dependent on the core radii, since we are so close to a bound state. Moreover, we do not obtain a reasonable fit for Σ^+p scattering at the same value of α as for the Σ^-p scattering without changing our singlet radius. Therefore, it is reasonable to drop the assumption that the cores are equal for T=1/2 and T=3/2, and to investigate whether we can improve our results by using different cores in these states.

In this chapter we will therefore determine the T=3/2 cores such that they fit the Σ^+p total cross sections but do not give a bound state. The T=1/2 cores are chosen as before i.e., so that they fit the ΛN scattering lengths. Since the Σ^-p system is a mixture of T=1/2 and T=3/2 states, we will first describe a method of calculation which handles different cores in these different states. We will investigate into what extend our earlier results have been affected by this bound state.

8.2. The separation of the T=1/2 and T=3/2 calculations.

Since the Σ^-p system is a mixture of T=1/2 and T=3/2 states, an exact calculation with different cores is extremely difficult, if one wants to take into account the breaking of isospin symmetry by the mass differences. Nevertheless, it is possible to do an approximate one by the following procedure.

We can easily split the potential matrix in a T=1/2 and a T=3/2 part, using the transformation formula for an operator on the isospin basis into an operator on the particle basis.

Recalling that we have chosen for the particle basis the states Λn, $\Sigma^o n$, and $\Sigma^- p$, respectively, an operator O on the particle basis can be written as [16]

$$O = \begin{pmatrix} O_{\Lambda\Lambda} & \frac{1}{\sqrt{3}} O_{\Lambda\Sigma} & -\sqrt{\frac{2}{3}}\, O_{\Lambda\Sigma} \\ \frac{1}{\sqrt{3}} O_{\Sigma\Lambda} & \frac{2}{3} O_D + \frac{1}{3} O_{\Sigma\Sigma} & \frac{1}{3}\sqrt{2}(O_D - O_{\Sigma\Sigma}) \\ -\sqrt{\frac{2}{3}}\, O_{\Sigma\Lambda} & \frac{1}{3}\sqrt{2}(O_D - O_{\Sigma\Sigma}) & \frac{1}{3} O_D + \frac{2}{3} O_{\Sigma\Sigma} \end{pmatrix} , \qquad (8.1)$$

where O_D is the operator in the T=3/2 states, and the operator in the T=1/2 states is

$$\begin{pmatrix} O_{\Lambda\Lambda} & O_{\Lambda\Sigma} \\ O_{\Sigma\Lambda} & O_{\Sigma\Sigma} \end{pmatrix} .$$

For s=0 all the matrix elements are numbers, but if s=1 they are 2×2 matrices.

Using the potential V_D, we can perform the one channel calculation to obtain the T=3/2 amplitude (or the two channel calculation for spin triplet). The T=1/2 amplitude can be obtained in the same way using the potential matrix

$$\begin{pmatrix} V_{\Lambda\Lambda} & V_{\Lambda\Sigma} \\ V_{\Sigma\Lambda} & V_{\Sigma\Sigma} \end{pmatrix} .$$

These amplitudes can be combined by means of (8.1). Doing so the amplitudes for the different channels can be obtained, but the mass differences between Σ^-p and $\Sigma^o n$ cannot be taken into account. They give a large effect at these low energies.

In order to take into account this breaking of isospin symmetry, we will use the particle basis. Using (8.1) we define a potential V_1 in the T=1/2 states and a potential V_3 in the T=3/2 states by

$$V_1 = \begin{pmatrix} V_{\Lambda\Lambda} & \frac{1}{\sqrt{3}} V_{\Lambda\Sigma} & -\sqrt{\frac{2}{3}} V_{\Lambda\Sigma} \\ \frac{1}{\sqrt{3}} V_{\Sigma\Lambda} & \frac{1}{3} V_{\Sigma\Sigma} & -\frac{1}{3}\sqrt{2} V_{\Sigma\Sigma} \\ -\sqrt{\frac{2}{3}} V_{\Sigma\Lambda} & -\frac{1}{3}\sqrt{2} V_{\Sigma\Sigma} & \frac{2}{3} V_{\Sigma\Sigma} \end{pmatrix}, \quad V_3 = \begin{pmatrix} 0 & 0 & 0 \\ 0 & \frac{2}{3} V_D & \frac{1}{3}\sqrt{2} V_D \\ 0 & \frac{1}{3}\sqrt{2} V_D & \frac{1}{3} V_D \end{pmatrix} \tag{8.2}$$

The matrix elements are defined according to the order of the particle basis. For example, the (3,2) element of V_1 denoted the T=1/2 part of the potential between $\Sigma^o n$ and $\Sigma^- p$.

We can now solve the Schrödinger equation with the exact masses in the different channels. From this we obtain the scattering parameters, e.g., the A-matrices, which can be combined to give the A-matrix for the combination of T=1/2 and T=3/2 states.

We have first to decide which scattering parameter we will actually use. It is reasonable to do the combination as early in the calculations as possible. We have taken the matrix B (6.1) for the following reasons. According to the effective range expansion (4.46),

$$B^{-1} = -A^{-1} + \tfrac{1}{2}(k^2-k_o^2)^{\frac{1}{2}} R (k^2-k_o^2)^{\frac{1}{2}} \quad ,$$

B has a finite limit if $E_{lab} \to 0$, also for the inelastic channels. Next, we have used B and not B^{-1}. This can be seen as follows. It is well known that for one channel the S-wave phase shift δ is given by [16]

$$\tan\delta \propto \int_o^\infty \sin kr \; V(r) \; \psi(r) dr \tag{8.3}$$

where $\psi(r)$ is the solution of the Schrödinger equation with asymptotic behaviour for $r \to \infty$ $\psi(r) \to \sin(kr) + \tan\delta \cos(kr)$. Since the scattering length a is defined by

$$-a = \lim_{k \to 0} \frac{\tan\delta}{k} \quad ,$$

we can conclude that if we add two potentials, according to (8.3) this will result in lowest order to the addition of the separate $\tan\delta$, so we have to add the scattering lengths. This result is correct in lowest order Born

approximation and it is approximately valid in a better approximation given by De Swart and Dullemond [16]. Generalizing this result for matrices, we should use B rather than B^{-1}.

We define the matrix B_1 by the 3×3 (or 6×6) B-matrix, obtained from calculations with T=1/2 potentials. With $B_1(1,2)$ we denote the element on the first row and second column in the spin singlet case. The numbering of rows and columns is of course according to the channels Λn, $\Sigma^o n$, and $\Sigma^- p$. For triplet coupled states we use the same notation, but now each element is a 2×2 matrix, of which the elements correspond with the different values of ℓ. The matrix B_3 is the B matrix obtained from calculations with T=3/2 potentials. The elements in the first row and column of B_3 have no significance, since the Λn is purely T=1/2.

The simplest way to obtain the matrix B from B_1 and B_3 is the addition $B=B_1+B_3$. This prescription gives reasonable results. It appeared, however, that we could reduce the errors considerably by another prescription, which is purely heuristic. Writing B in the form (8.1), we can find B_D and $B_{\Sigma\Sigma}$ from the diagonal elements:

$$\begin{aligned} B_D &= 2B(2,2) - B(3,3) \\ B_{\Sigma\Sigma} &= -B(2,2) + 2B(3,3) \quad . \end{aligned}$$

Analogous equations can be obtained using B(2,2) and B(2,3) or B(3,3) and B(2,3). When the masses were equal, the three solutions should be identical, but now, due to the mass differences, they are different. We take the arithmetic mean of these solutions and we define

$$\begin{aligned} B_D &= B_3(2,2) + \tfrac{1}{2}\sqrt{2}\, B_3(2,3) \\ B_{\Sigma\Sigma} &= B_1(3,3) - \tfrac{1}{2}\sqrt{2}\, B_1(2,3) \quad . \end{aligned} \tag{8.4}$$

The B-matrix that we will use in our calculations is defined by

$$B = \begin{pmatrix} B_1(1,1) & B_1(1,2) & B_1(1,3) \\ B_1(2,1) & \frac{1}{3}B_{\Sigma\Sigma} + \frac{2}{3}B_D & \frac{1}{3}\sqrt{2}(B_D - B_{\Sigma\Sigma}) \\ B_1(3,1) & \frac{1}{3}\sqrt{2}(B_D - B_{\Sigma\Sigma}) & \frac{1}{3}B_D + \frac{2}{3}B_{\Sigma\Sigma} \end{pmatrix} \tag{8.5}$$

This prescription, which is intermediate between the use of the isospin basis and the calculation of B with $B=B_1+B_3$, gives better results than the other ones. We could compare the results of different prescription by performing calculations with equal T=1/2 and T=3/2 cores. In this case we

can also calculate the result directly. It turned out that the errors for equal cores are about 5%, not too bad considering the experimental errors.

Finally, the Coulomb effects are taken into account by using the method described in Chapter 7.

8.3. Results with different T=1/2 and T=3/2 cores.

Employing the prescription of the foregoing section we have performed calculations, using the same potentials and coupling constants as in Chapter 7, but with different cores for the T=1/2 and T=3/2 states.

Consider a fixed value of α. We take for the T=1/2 radii the Hf and Lp radii given in Fig. 7.1. The T=3/2 radii are then chosen larger than the bound state radius at this value of α such that they fit the Σ^+p total cross section. This determines the singlet T=3/2 radius as a function of the triplet T=3/2 radius. For the two sets of T=1/2 radii we have tried to fit the Σ^-p cross sections and ratios, using the possible T=3/2 radii. This has been repeated for several values of α.

The T=3/2 radii that fitted the Σ^+p cross sections are given in Fig. 8.1. The general behaviour of the singlet radius as a function of the triplet radius is simple to understand. For a value of X_s we obtain a certain singlet cross section and we should determine the triplet core which gives such a contribution that the sum of the singlet and triplet cross sections just yields the experimental value. As for larger radii the cross sections are small (see e.g. Fig. 7.7[b]), the curves in Fig. 8.1 become straight vertical or horizontal lines, until the scattering due to the hard core becomes so large that it gives a sizable contribution. Then the lines will bend over. This is not shown in the figure since this happens at much larger radii (X > 0.5). The P-wave contributions are small, about 2-4mb. The singlet core radii deviate much from the T=1/2 radii, which could be expected since we have avoided a bound state (cf. Fig. 7.6). The cal-

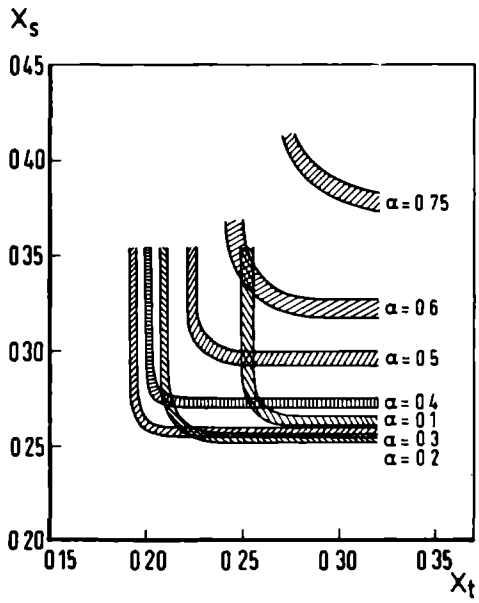

Fig 8.1 The T = 3/2 cores that fit the Σ^+p total cross section within the experimental errors for several values of α

culations are performed at three energies, namely 9.8, 11.0, and 12.5 MeV, which corresponds to Σ^+ laboratory momenta of 153, 162, and 173 MeV/c, respectively, hence corresponding to the middle of the experimental intervals.

Having obtained in this way a set of T=3/2 cores, we will study now the Σ^-p scattering. Before we will consider these calculations in detail, we will make some general remarks. The cross section for the reaction $\Sigma^-p \to \Lambda n$ does not depend very much on the T=3/2 radii, but it does on the T=1/2 ones. This could be expected since the Λn system has isospin T=1/2. Furthermore, the P-wave contributions for all reactions are practically independent of the T=3/2 radii. Variations in the T=1/2 radii have only a slight influence on the P-wave contributions. Apparently the centrifugal barrier, $\ell(\ell+1)/r^2$, is more important than the hard core. There is one exception, namely at α=0.6 the strong $^3P_1$ contribution reappears, being strongly dependent on the T=1/2 radius.

This implies that the cross sections for the reaction $\Sigma^-p \to \Lambda n$ are to within a few percent equal to the values given in Table 7.6 and 7.7. For most values of α they are within one standard deviation of the experimental value (135 $\pm$ 12mb at this energy), except for $\alpha \gtrsim 0.6$ and $\alpha \sim 0.1$ and Lp cores, where they are smaller.

We will investigate first what happens when we take for the triplet T=3/2 radius the same value as for the T=1/2 one, but we allow the T=3/2 singlet radius to be different from the T=1/2 one. This enables us to avoid the singlet Σ^+p bound state.

The general behaviour of the singlet cross sections and capture ratio as a function of the T=3/2 core is as follows. Close to the bound state radius the inelastic cross section reaches the $^1S_0$ unitarity limit $\frac{1}{4}\pi/k^2$ *, which is 65 mb at 10 MeV. Since the $\Sigma^-p \to \Lambda n$ singlet cross section is small, the inelastic cross section is mainly generated by the reaction $\Sigma^-p \to \Sigma^0 n$. Therefore, the $\Sigma^-p \to \Sigma^0 n$ cross section can reach values up to about 50 mb, and it decreases for larger T=3/2 cores. The $\Sigma^-p \to \Sigma^-p$ cross section increases also when the T=3/2 core approaches the bound state radius. It remains smaller than the $\Sigma^-p \to \Sigma^0 n$ cross section and only for cores very close to the bound state radius does it reach the elastic unitarity limit when maximal absorption is present, which is also $\frac{1}{4}\pi/k^2$ for singlet scattering. Since the singlet $\Sigma^-p \to \Lambda n$ scattering is small, also for very low energies,

* We will include in this chapter the statistical factors 1/4 and 3/4, not only for the cross sections, but also for the capture ratio r_c. For the in flight ratio r_F this is of course not possible (see (4.31)).

the singlet capture ratio is almost maximal (0.25) and decreases slowly when we enlarge the T=3/2 cores.

Since the triplet Σ^+p cross section in general is small at the cores we are considering now, we have to choose singlet T=3/2 cores rather close to the bound state radius. In this context we remark that the unitarity limit for singlet Σ^+p scattering, which is π/k^2, is not too much larger than the total Σ^+p cross section. We obtain then for singlet Σ^-p scattering, practically independent of α,

$$\begin{aligned} \tfrac{1}{4}\,\sigma(\Sigma^-p \to \Sigma^0 n) &\sim 45 \pm 5 \text{ mb} \\ \tfrac{1}{4}\,\sigma(\Sigma^-p \to \Sigma^-p) &\sim 25 \pm 5 \text{ mb} \\ \tfrac{1}{4}\,r_C(^1S_0) &\sim 0.23 \pm 0.02 \quad . \end{aligned}$$

Considering first the capture ratio r_C, which is known experimentally with rather high accuracy, we can rule out most values of α. Adding the singlet contribution we have given above to the value of the triplet ratio (see Table 7.6 and 7.7), we have as remaining possibilities $\alpha \sim 0.5$ and $\alpha \sim 0.1$. It should be noted that $\alpha=0.4$ is ruled out since we obtain then $r_C \sim 0.35$, deviating too much from the experimental value $r_C=0.45 \pm 0.02$.

Continuing with $\alpha=0.1$ and $\alpha=0.5$ we have tried next to determine the $\Sigma^-p \to \Sigma^0 n$ cross section such that we obtained the best value for the ratio r_F. Doing so we also have fixed the $\Sigma^\pm p \to \Sigma^\pm p$ elastic cross sections. The results are given in Table 8.1. It appears that $\alpha=0.1$ gives a rather bad fit, whereas the data for $\alpha \sim 0.5$ are much better. Keeping in mind the behaviour of the cross sections and ratios as a function of α for equal cores (Fig. 7.2 and 7.3) we may conclude that the Hf cores can give a fit for

	α=0.1;Hf	α=0.1;Lp	α=0.5;Hf	α=0.5;Lp
$\sigma(\Sigma^-p \to \Lambda n)$	130	104	123	130
$\sigma(\Sigma^-p \to \Sigma^0 n)$	95	97	113	135
$\sigma(\Sigma^-p \to \Sigma^-p)$	115	140	135	202
r_F	0.42	0.48	0.48	0.51
r_C	0.39	0.49	0.43	0.50
$\sigma(\Sigma^+p \to \Sigma^+p)$	140	85	115	75

Table 8.1 The Σ^-p cross sections and r_F at 10 MeV laboratory energy, the capture ratio r_C, and the Σ^+p cross section at 11 MeV laboratory energy. The singlet T = 3/2 core is changed such that a Σ^-p bound state is avoided

values of α slightly above α=0.5 and that the Lp cores give a fit slightly below α=0.5. The results of Chapter 7 are therefore not affected by avoiding the Σ^+p singlet bound state. The angular distributions and Λ polarization are not changed in comparison with the results of Chapter 7, so we refer to Fig. 7.4 for the angular distributions.

The Σ^+p angular distribution does not give a very good fit to the experiments. There is indeed a small enhancement in the forward direction, except of course for very small angles where the Rutherford scattering becomes infinite, but it is smaller than the experimental results (see Fig. 8.2).

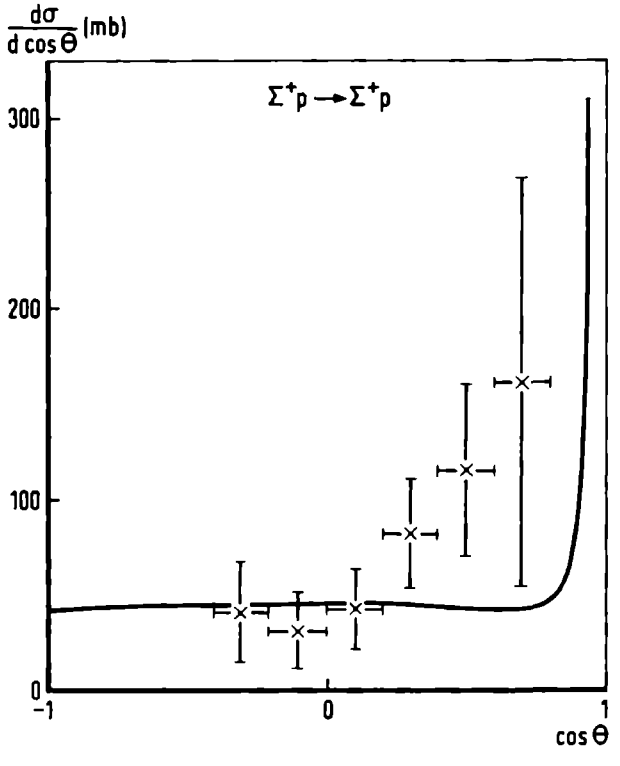

Fig. 8.2. An angular distribution for Σ^+p scattering at E_{lab} = 11 MeV.

There is no a priori reason why we should not vary also the triplet T=3/2 cores as we have varied the singlet ones. Allowing both cores to be varied, it will be clear that we obtain much more freedom, making it easier to obtain a fit, the more so as the Σ^+p scattering data, having large experimental uncertainties, do not yield a serious constraint on the cores.

We have first investigated the capture ratio r_C. The best fit we could obtain without deviating to much from the T=3/2 cores given in Fig. 8.1, is shown in Fig. 8.3[a]. Values of $\alpha \geq 0.6$ are clearly excluded, and for $0.3 \lesssim \alpha \lesssim 0.4$ the results are rather bad. For $\alpha \leq 0.5$ also the cross sections and r_F are determined, paying again special attention to the $\Sigma^-p \to \Sigma^0n$ cross section, since this cross section together with the $\Sigma^-p \to \Lambda n$ one determines the ratio r_F. The results are given in Fig. 8.3 - 8.5. Comparing these data with those from Chapter 7 (Fig. 7.2 and 7.3), we notice that our results are not changed much. We have been able to bring the results a little closer to the experimental values. Also the angular distributions which we will not show again, and the polarization of the Λ-hyperon,

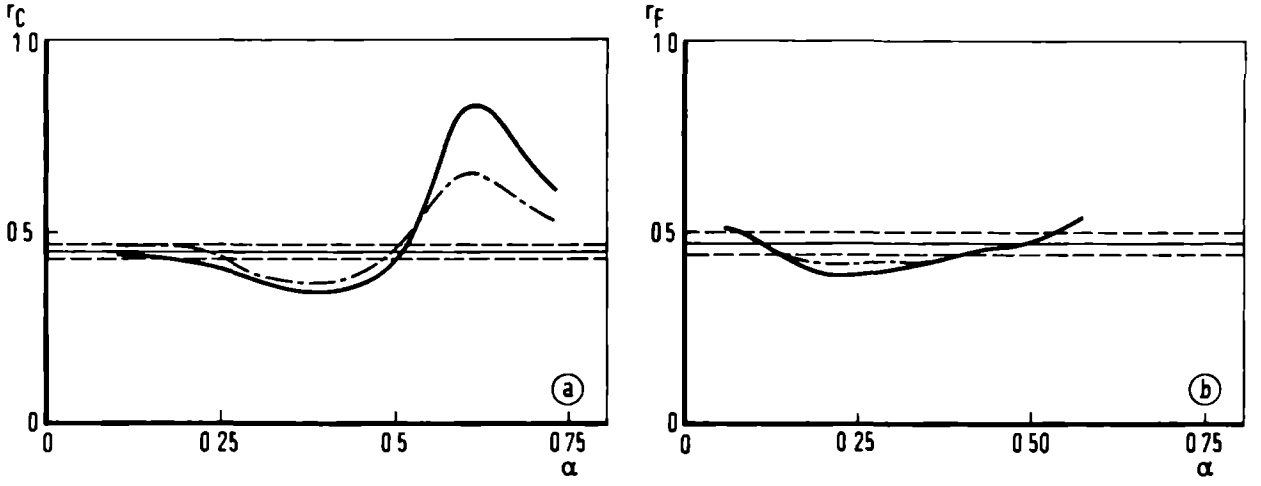

Fig 8 3 The capture ratio at rest (a) and in flight (b) as a function of α, calculated with different T = 1/2 and T = 3/2 cores The experimental values, $r_C = 0\ 45 \pm 0\ 02$ and $r_F = 0\ 47 \pm 0\ 03$, are indicated by ═══ ——— are the results for Hf cores, —·—·— for Lp cores

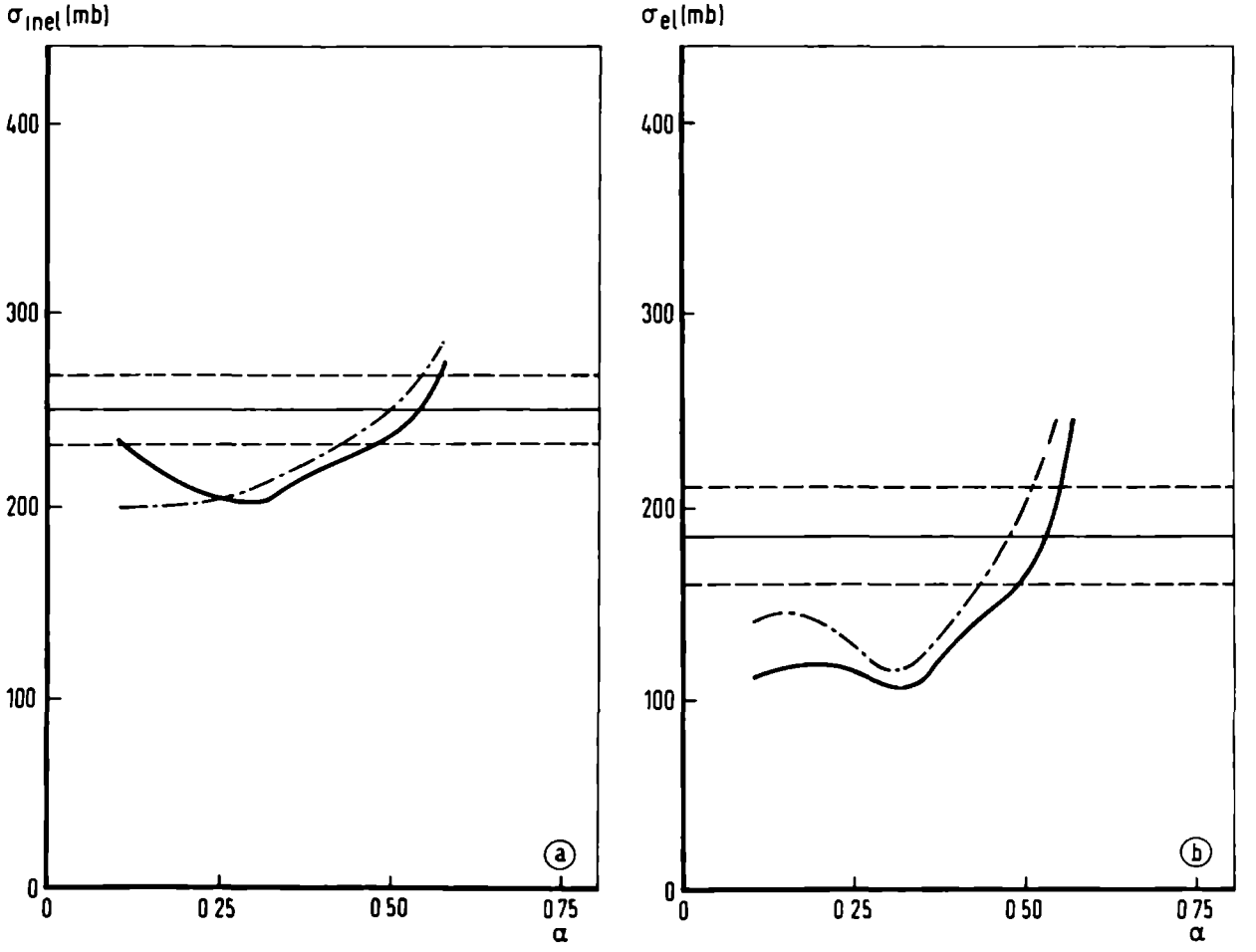

Fig 8 4 The inelastic (a) and elastic (b) Σ^-p cross section as a function of α at 10 MeV laboratory energy, calculated with different T – 1/2 and T – 3/2 cores The experimental values, $\sigma_{inel} = 250 \pm 17$ mb and $\sigma_{el} = 185 \pm 25$ mb are indicated by ═══ ——— are the results for Hf cores, —·—·— for Lp cores

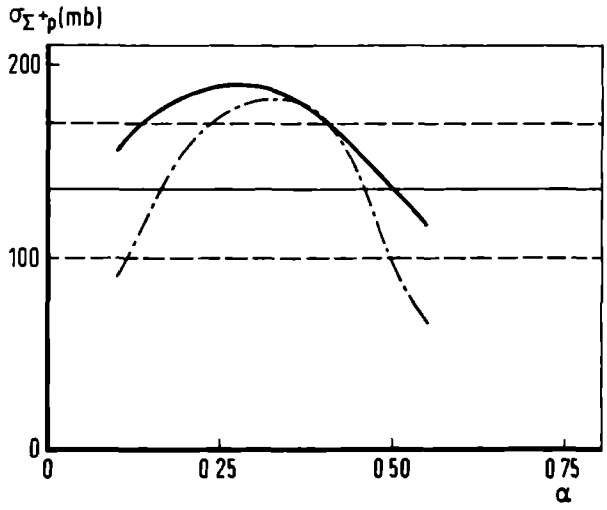

Fig 8 5 The Σ^+p cross section as a function of a at 11 MeV laboratory energy The experimental result, $\sigma = 135 \pm 35$ mb is indicated by ═══ ——— are the results for Hf cores, —·—·— for Lp cores

are essentially unchanged for $\alpha=0.5$. Concluding, only at $\alpha=0.5$ can we obtain a good agreement with the experimental results. The T=3/2 cores, finally, are a little larger than the bound state radii given in Fig. 7.6. They deviate therefore much from the T=1/2 ones, except in the neighbourhood of $\alpha=0.5$.

The reason why our results are rather independent of the T=3/2 cores, is clear. From the experiments it follows that the Σ^+p scattering, which is purely T=3/2, is weak. Moreover, in our calculations this interaction is a relatively stronger one for singlet scattering and in this case the changes in the Σ^-p scattering are less important. The main variations in the Σ^-p cross sections and ratios are in fact caused by the triplet scattering, what can be seen very clearly in Table 7.6 and 7.7. This is the more distinct when we avoid a singlet T=3/2 bound state. Therefore, the Σ^-p results are mainly determined by the T=1/2 potentials.

CHAPTER 9
CALCULATIONS WITH POTENTIALS DUE TO THE EXCHANGE OF PSEUDOSCALAR AND VECTOR MESONS

9.1. Introduction.

Untill now we have only considered potentials due to the exchange of the least massive strongly interacting particles that can be exchanged between baryons. One could hope to describe the baryon-baryon potential better by considering also the exchange of heavier particles. Therefore, we will consider in this chapter the $\Sigma^{\pm}$p interaction, using potentials due to the exchange of the pseudoscalar mesons π, K, η, and X^o, and of the vector mesons ρ, K^*, ω, and ϕ.

The potentials have been derived in Chapter 3. In the same chapter we have discussed the symmetry properties one might assume for the coupling constants. In our calculations we will use (3.48), so $\alpha_{PS}=0.4$, $\alpha_V^e=1.0$ and $\alpha_V^m=0.4$. Since we have found that we could obtain a fit at $\alpha_{PS}=0.5$ but not at $\alpha_{PS}=0.4$, when using only pseudoscalar mesons, we have also done calculations for $\alpha_{PS}=0.5$, leaving α_V^e and α_V^m unchanged.

Using these symmetry relations, we still must choose three coupling constants, namely $f_{NN\pi}$, $g_{NN\rho}$, and $f_{NN\rho}$. As before we have taken $f_{NN\pi}/(4\pi)^{\frac{1}{2}}=0.283$. The values of the other constants are less well known experimentally. Fairly reliable values exist for $g_{NN\rho}$ which has been determined in eight different ways [80,81], all yielding about the same results, $g^2_{NN\rho}/4\pi\sim 0.5\text{-}0.8$.

The methods usually used to determine the vector meson-nucleon coupling constants are based on fitting nucleon form factor data in terms of vector meson poles [82]. The theoretical foundation of such a single pole fit is uncertain, and the results of these analyses are not very convincing. Trying to fit the isovector form factors with the ρ meson, a much smaller ρ mass is needed [83], or a second heavier isovector meson with a mass of about 875 MeV has to be added [84]. Another analysis [85] gives a very small value of $g_{NN\rho}$, namely $g^2_{NN\rho}/4\pi\sim 0.14$, much lower than is generally expected. Only the latest result [31] gives a reasonable value, namely $g^2_{NN\rho}/4\pi\sim 0.7$.

Another way of obtaining information about these coupling constants is the analysis of the nucleon-nucleon scattering data in terms of one boson exchange potentials and other "pole" models [12]. The results of these investigations generally agree about the value of $g_{NN\rho}$, giving $g^2_{NN\rho}/4\pi\sim 0.9\text{-}1.4$, and a value of about 2 for the ratio $f_{NN\rho}/g_{NN\rho}$. This value of $g_{NN\rho}$ somewhat

exceeds the value obtained from the width of the ρ meson through universal coupling of the ρ to the isospin current [11], which yields $g^2_{NN\rho}/4\pi \sim 0.5$-$0.6$. This value agrees also with the SU(6) prediction [62], $g^2_{NN\pi}/4\pi \sim 0.5$. The $f_{NN\rho}$ is less well known. The result of the nucleon-nucleon analyses, $f_{NN\rho}/g_{NN\rho} \sim 2$ does not seem to be in contradiction with the nuclear form factor data.

We have used in our calculation $g_{NN\rho}/(4\pi)^{\frac{1}{2}}=0.71$ and $f_{NN\rho}/(4\pi)^{\frac{1}{2}}=1.5$. We have also done calculations with $f_{NN\rho}/(4\pi)^{\frac{1}{2}}=3$. This larger value is chosen since from the NN analyses [36] it follows that a larger value for $f_{NN\rho}$ can give a value for $g_{NN\rho}$ which is in better agreement with the other determinations of this coupling constant.

We do not want to suggest that this choice is necessarily the most accurate one. We are quite aware that we cannot merely transfer the NN results to our calculations. Not only did we not include the exchange of hypothetical scalar mesons (instead we have used two pion exchange potentials), but also other results of the NN investigations differ from ours. Especially the $g_{NN\omega}$ is sometimes substantially larger than the value we have used. However, we feel that the choice we have made is the best one could do at the moment.

Although the range of the vector meson potentials is much shorter than the range of the pion exchange potential, its strength is comparable at not too large distances, due to the fact that the vector meson coupling constants are much larger than $f_{NN\pi}$. We will see, therefore, that the inclusion of these potentials gives a sizable change in our calculations, which can be seen most clearly in the ΛN results by the change in the hard core radii that fit the scattering lengths.

9.2. The results of the calculations.

In this section we will give the results of our calculations, along the same lines as in Chapter 7 and 8.

Firstly, the hard core radii have been determined [27] for both sets of ΛN scattering lengths. The results for the cases we will consider are given in Table 9.1. It appears that these radii increase for larger values of the magnetic vector meson coupling constants. This is caused by the attraction of the K*, which for larger values of $f_{NN\rho}$ cannot be compensated by the repulsion due to ω exchange. It is remarkable that the singlet radius is not diminished by including vector meson exchange. A sizable decrease of this radius can only be obtained by taking a much smaller value for $f_{NN\rho}/g_{NN\rho}$ [27],

Nr	f_V	α_{PS}	core	X_s	X_t	X_s^B	X_t^B
1	1.5	0.4	Hf	0.280	0.248	0.295	0.175
2	1.5	0.4	Lp	0.283	0.224		
3	1.5	0.5	Hf	0.276	0.243	0.314	0.182
4	1.5	0.5	Lp	0.280	0.233		
5	3.0	0.4	Hf	0.370	0.388	0.400	0.198
6	3.0	0.4	Lp	0.374	0.386		
7	3.0	0.5	Hf	0.380	0.392	0.411	0.204
8	3.0	0.5	Lp	0.383	0.389		

Table 9 1 The singlet (X_s) and triplet (X_t) hard core radii that fit the ΛN scattering lengths for the cases we will consider, namely $f_{NN\rho}/(4\pi)^{1/2} = 1\,5$ or $3\,0$, $\alpha_{PS} = 0\,4$ or $0\,5$ Also, the radii are given for which a Σ^+p bound state is possible (X_s^B and X_t^B)

in contradiction to other evidence, or by choosing a much larger $g_{NN\omega}$, not in agreement with the symmetry relations we imposed.

We have also determined the bound state radii for Σ^+p scattering. Considering these radii, also given in Table 9.1, we see that we have a singlet bound state like we had when using only the exchange of pseudoscalar mesons. The triplet bound state radius is much smaller, and even at the cores we are considering, the triplet Σ^+p potential is repulsive. This has important consequences as we will see in the following.

In the first calculations for Σ^-p interactions we have assumed equal cores for T=1/2 and T=3/2 states, although we know that for singlet scattering this cannot be true since we already have a Σ^+p bound state. However, we have seen in the foregoing chapter that the main features of our results using the same cores in T=1/2 and T=3/2 states have not been affected by dropping this assumption.

The results of the calculations with the same T=1/2 and T=3/2 cores are given in Table 9.2. We have obtained a good fit with the experimental data for α_{PS}=0.4, $f_{NN\rho}/(4\pi)^{\frac{1}{2}}$=1.5 and Lp cores (No. 2), whereas the result with Hf cores is rather bad. It is remarkable that α_{PS}=0.5 does not yield good results. The inclusion of the exchange of vector mesons now gives a fit exactly at the value of α_{PS} predicted by SU(6) symmetry.

It should be noted, however, that the singlet $\Sigma^-p \to \Sigma^-p$ cross sections are larger due to the T=3/2 bound state. As in the calculations of Chapter 7, we will have to drop the assumption that the T=1/2 and T=3/2 cores are equal, at least for singlet scattering. Therefore, the next step is the calculation with different cores for T=1/2 and T=3/2 states, following the method described in Chapter 8. The Σ^+p cross sections are first determined

$\Sigma^- p \to \Lambda n$

Nr	$^1S_0$	$^3S_1$	$^1P_1$	$^3P_1$	$^3P_2$	$^3P_0$	total
1	5.5	92.1	1.1	7.7	2.7	0.1	109
2	5.6	110.7	1.1	3.5	2.8	0.3	129
3	6.1	42.7	0.7	15.5	2.1	0.1	67
4	6.2	26.0	0.7	17.6	2.1	0.5	53
5	4.9	104.6	1.7	3.5	2.5	0.5	118
6	5.0	95.7	1.6	3.6	2.5	1.0	109
7	5.3	104.6	1.2	4.2	1.9	0.1	117
8	5.3	91.3	1.2	4.2	1.9	0.1	104

$\Sigma^- p \to \Sigma^0 n$

Nr	$^1S_0$	$^3S_1$	$^1P_1$	$^3P_1$	$^3P_2$	$^3P_0$	total
1	28.2	40.7	1.2	5.4	0.1	1.5	77
2	33.7	67.3	1.1	5.7	0.1	1.6	110
3	4.1	139.1	2.9	13.0	0.2	2.3	162
4	6.6	131.3	2.5	14.0	0.2	2.5	157
5	20.5	21.2	2.4	3.9	0.2	0.6	49
6	24.9	15.8	2.3	3.9	0.2	0.4	48
7	20.6	23.6	3.3	7.0	0.2	1.5	56
8	23.8	14.8	3.2	7.0	0.2	1.5	51

$\Sigma^- p \to \Sigma^- p$

Nr	$^1S_0$	$^3S_1$	$^1P_1$	$^3P_1$	$^3P_2$	$^3P_0$	total
1	59.1	39.0	0.1	2.6	0.0	0.4	101
2	57.7	134.8	0.1	2.9	0.0	0.4	197
3	51.1	198.7	0.0	8.0	0.1	0.5	258
4	53.9	285.6	0.0	9.0	0.1	0.6	349
5	69.9	68.2	0.0	1.5	0.0	0.1	140
6	69.7	72.7	0.0	1.5	0.0	0.1	144
7	72.6	60.0	0.0	3.1	0.0	0.5	136
8	72.4	60.0	0.0	3.2	0.0	0.4	136

Nr	$r_C(^1S_0)$	$r_C(^3S_1)$	r_C	r_F
1	0.21	0.17	0.39	0.41
2	0.22	0.21	0.43	0.46
3	0.08	0.50	0.58	0.71
4	0.11	0.57	0.67	0.75
5	0.20	0.09	0.30	0.29
6	0.21	0.08	0.29	0.30
7	0.20	0.10	0.30	0.32
8	0.21	0.07	0.28	0.33

Table 9 2 The total cross sections (in mb) for $\Sigma^- p$ scattering at E_{lab} 10 MeV, and the ratios r_C and r_F The numbering corresponds with Table 9 1

as a function of the T=3/2 radius. For values of X_t slightly larger than the bound state radius, the triplet cross section is rather independent of the radius, due to the fact that the potential is then repulsive. The singlet cross section decreases rather fast for cores above the bound state radius. Therefore, the singlet radius is rather restricted, whereas the triplet radius can be chosen more freely.

Considering Table 9.2 again, we see that we do not have to investigate Nos. 3 and 4 (α_{PS}=0.5, $f_{NN\rho}/(4\pi)^2$=1.5), since the $\Sigma^-p \to \Lambda n$ cross section is much too small. This cross section will not change for calculations with different T=1/2 and T=3/2 cores as we have seen in Chapter 8.

When we use only different cores in singlet states and taking equal triplet cores for T=1/2 and T=3/2 states, it follows also from Table 9.2 (especially from the triplet capture ratio) that the only case in which we can expect to obtain fit, is No. 2. No. 1 is excluded since the elastic Σ^-p cross section remains too small. The results for No. 2 are given in Table 9.3.

Σ^-p data		Σ^+p data	
$\sigma(\Sigma^-p \to \Lambda n)$	129	$\sigma(\Sigma^+p)$ at 10 MeV	158
$\sigma(\Sigma^-p \to \Sigma^0 n)$	120	$\sigma(\Sigma^+p)$ at 11 MeV	148
$\sigma(\Sigma^-p \to \Sigma^-p)$	165	$\sigma(\Sigma^+p)$ at 12.5 MeV	135
r_F	0.48		
r_C	0.45		

Table 9.3. The Σ^-p cross sections and r_F at $E_{lab} = 10$ MeV, the capture ratio r_C, and the Σ^+p cross section at different laboratory energies, using $\alpha_{PS} = 0.4$, $f_{NN\rho}/(4\pi)^{1/2} = 1.5$. The triplet and singlet T = 1/2 cores are the Lp ones, whereas the singlet T = 3/2 core has been chosen a little larger ($X_s(T = 3/2) = 0.305$) to avoid a Σ^+p singlet bound state.

Allowing the triplet core radius to be varied also did not improve the foregoing results, nor could a fit be obtained for the other cases. This is caused also by the fact that the triplet T=3/2 potential becomes repulsive at distances slightly above the bound state radius. A variation of the radius of the repulsive core has then much less influence than it has when the potential is attractive. The only change in the triplet cross section could be obtained for values of the T=3/2 core very close to the bound state radius but then the Σ^+p cross section becomes already too large.

The angular distributions for the $\Sigma^- p$ reactions are much the same as those given in Chapter 7. We refer for them to Fig. 7.4. The polarization of the Λ-hyperon remains small, $P \sim -0.05$.

There is some change in the $\Sigma^+ p$ angular distribution. This is caused by the Coulomb interference which is now constructive for triplet scattering, and so large that it cancels the singlet destructive interference. The resulting angular distribution is therefore more comparable to the experimental one than the distribution we have calculated in Chapter 8, but there is still some discrepancy. We have shown the $\Sigma^+ p$ angular distribution in Fig. 9.1, where we have also shown the distribution from Fig. 8.2 for comparison.

For the values of the cores and the coupling constants described in Table 9.3, we have done an effective range expansion for $\Sigma^+ p$ scattering. We have found the following results:

$$\begin{aligned} a_s &= -6.9 \text{ fm} & r_s &= 2.5 \text{ fm} \\ a_t &= 0.63 \text{ fm} & r_s &= -0.45 \text{ fm} \end{aligned} \quad . \qquad (9.1)$$

They are in good agreement with the results of Dosch and Müller [26].

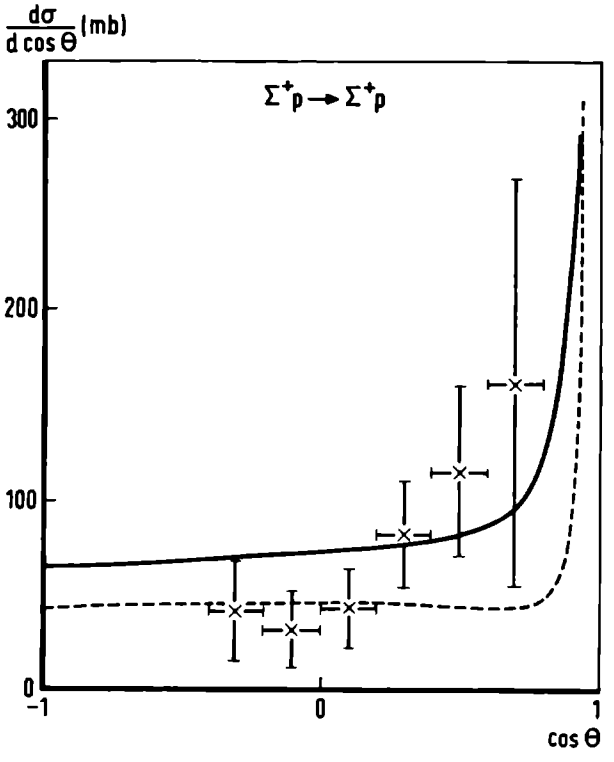

Fig. 9.1. The $\Sigma^+ p$ angular distribution at $E_{lab} = 11$ MeV, using the same cores and coupling constants as in Table 9.3. ——— are the results of this calculation, – – – – – is the distribution of Fig. 8.2, shown for comparison.

CHAPTER 10
DISCUSSION

Although the model we have used yields rather good results, we are aware that there are serious theoretical uncertainties. The derivation of potentials describing the baryon-baryon interactions has been criticized on several grounds. We will mention only two points that are unsatisfactory: the derivation of the two-pion-exchange potential, and the use of hard cores. The latter could not be avoided in our case, even when including the exchange of vector mesons.

It is well known that the SU(3) symmetry is badly broken. We could take into account this breaking only in the masses of the particles involved. There is also some evidence that the coupling constants can be different from the symmetry predictions. There are indications [87] that the $N\Lambda K$ coupling constant is smaller than the value we have used. This is not necessarily in contradiction with unitary symmetry. Due to the large K mass, the application of SU(3) symmetry on the derivative coupling constants will result in smaller K coupling constants than we obtained by requiring unitary symmetry for the direct coupling constants, as can be seen from (3.45). There is also some evidence [88] that perhaps the $\Sigma\Sigma\pi$ coupling constant is smaller than the one predicted by SU(3) symmetry for values of α generally assumed.

Nevertheless, it is satisfying that we can obtain with so few parameters a such relatively good agreement with experimental data. The only other data we have used are in fact only the ΛN scattering lengths. The particle masses and coupling constants ($f_{NN\pi}$ and $f_{NN\rho}$) are much more fundamental quantities, and the Σ^+p total cross section does not have much influence on the Σ^-p results. Hence, using the ΛN scattering lengths, we could obtain a good agreement with the three Σ^-p cross sections, the capture ratio, and the $\Sigma^-p \to \Lambda n$ angular distribution. The results for the elastic $\Sigma^\pm p$ angular distributions are also reasonable. The polarization of the Λ, however, differs one standard deviation from the experimental result.

With the exception of the ratios, the experimental errors are rather large, and it is not easy to obtain a fit with the experiments. This can be seen very clearly when we compare the experimental cross sections with the maximal possible values determined by the unitarity limit. The Σ^-p cross sections are then almost maximal and it appeared that such large values

could be obtained in our calculations for a few cases only. However, when the T=1/2 radii were adjusted to give the experimental ΛN scattering lengths, the $\Sigma^- p \to \Lambda n$ cross section was almost always within a few standard deviations of the experimental value. In many cases also the angular distribution showed an enhancement in the forward direction. It seems, therefore, that at least for S-waves this reaction is mainly determined as soon as the ΛN scattering lengths are fitted. This was clearly not true for the reactions $\Sigma^- p \to \Sigma^0 n$ and $\Sigma^- p \to \Sigma^- p$. The occurring variations in these cross sections were not caused by the T=3/2 potential, which has only a small influence.

The fact that the polarization shows a rather large discrepancy with the experimental result may be caused by the following. The ΛN scattering lengths, which are used to find the core radii, are mainly determined by the potential for $\ell=0$. We have used these cores also for higher values of ℓ, but it is not certain that they should be equal for different values of ℓ. If they are not, this will not influence the total cross sections, but it does change the angular distributions and the polarizations.

The experiments show a small $\Sigma^+ p$ cross section and hence, some experimentalists argue that the triplet $\Sigma^+ p$ interaction is weak [38,40]. Earlier calculations [14,15,89] have indeed indicated that the singlet $\Sigma^+ p$ interaction is stronger than the triplet one. We have even obtained a weakly bound $\Sigma^+ p$ singlet state, forcing us to enlarge slightly the T=3/2 singlet core radius. The singlet contribution, however, remained the stronger. The angular distribution for $\Sigma^+ p \to \Sigma^+ p$ shows a small enhancement in the forward direction. We could not obtain such a large enhancement, either by P-wave contributions, which were small, or by a constructive Coulomb interference. We mention that our triplet angular distribution shows a constructive Coulomb interference due to a repulsive potential, but the singlet interference remains a destructive one. We have the impression that it will never be possible to obtain this angular distribution by Coulomb effects only, since that would require a maximal Coulomb interference [35]. It would be worth studying the Σ^+ polarization to see if there are large P-wave contributions already at these low energy. Also a comparison of the $\Sigma^+ p$ angular distributions at different energies is useful to decide between a P-wave contribution or a Coulomb interference.

After the proposal of SU(3) and SU(6), several authors [19,20] have predicted various relations among the parameters describing baryon-baryon interactions. By adopting a unitary symmetric interaction, they compare the NN interaction with the YN and YY ones. Some qualitative considerations [19] seem to be correct. To mention a few: a ΛN or ΣN bound state may

not exist, although, e.g., the ΛN singlet state is quite close to binding, hence resulting in a stronger ΛN scattering in the $^1S_0$ than in the $^3S_1$ state. The more quantitative statements [20] are very badly fulfilled. Among the predicted relations for the baryon-baryon scattering lengths, the required equality for $a_s(np)$ and $a_t(np)$ is certainly not correct. Also, the relations for the total cross sections give a very poor agreement with the experimental data. It is clear that the symmetry-breaking effects in the interaction due to the mass differences [18] are so large that no reasonable results can be expected. We will therefore not consider these investigations in detail.

On the other hand, in our calculations we have used these symmetries in our calculations also. However, instead of deriving relations for the scattering amplitudes, we have employed relations for the coupling constants only, enabling us to take into account the mass breaking in a dynamical way by using the experimental particle masses in the potential. In doing so, we have found that the predictions of SU(6) are not in conflict with the experiments on YN scattering.

This was true, in particular, when we included the exchange of vector mesons. This has a large influence, as can be seen from the change in the hard core radii, obtained with and without the exchange of vector mesons. Other conclusions from the calculations with vector mesons are that a ratio $f_{NN\rho}/g_{NN\rho} > 4$ is very unlikely, since the hard core radii become then very large [27]. From our results we may even suppose that $f_{NN\rho}/g_{NN\rho} \leq 2$. However, because the 2π-exchange potentials are at least as important as the vector meson exchange potentials, it is unreasonable to study the latter in great detail without knowing more about the 2π exchange potentials.

We have seen in Chapter 9 that we could only obtain agreement with the experiments when the cores were adjusted to the scattering lengths derived from Λp scattering. When we considered only potentials due to the exchange of pseudoscalar mesons, we did not find this result, since the change of the T=1/2 core had a smaller influence in that case. Of course, we cannot conclude from the few calculations we did in Chapter 9 that the hyperfragment scattering lengths are excluded, but it is satisfying that we find the expected result, namely that the scattering lengths derived directly from Λp scattering are to be preferred [43]. The fact that SU(6) and $\tilde{U}(12)$ predict [20] that $a_s(\Lambda p)=a_t(\Lambda p)$, seems to be a happy coincidence.

SAMENVATTING

In dit proefschrift beschrijven we enige onderzoekingen aan Σp wisselwerkingen bij lage energie. Na een overzicht van de experimentele gegevens in hoofdstuk 2, beschouwen we in hoofdstuk 3, 4 en 5 het model dat voor deze berekeningen gebruikt is. Dit bestaat in wezen in het gebruik van de Schrödingervergelijking waarin een potentiaal geplaatst is die afgeleid kan worden met meson-theoretische methoden. Hetzelfde model wordt gebruikt voor nucleon-nucleon (NN) wisselwerkingen en is ook gebruikt voor hyperon-nucleon (YN) interacties.

Wij veronderstellen dat de potentiaal die de YN wisselwerking beschrijft, afgeleid kan worden met behulp van Born termen voor de uitwisseling van één meson. Aan deze potentiaal zijn toegevoegd de bijdragen ten gevolge van de uitwisseling van twee pionen, berekend volgens het voorschrift van Brueckner en Watson. Dit is gedaan omdat in de Λp → Λp wisselwerking de uitwisseling van één pion verboden is wegens isospinbehoud en omdat wegens de geringe pionmassa ook voor potentialen ten gevolge van de uitwisseling van twee pionen de dracht tamelijk groot is. Deze potentialen zijn in hoofdstuk 3 afgeleid voor de uitwisseling van pseudoscalaire en vectormesonen. In dit hoofdstuk zijn eveneens de symmetrieeigenschappen (SU(2), SU(3), SU(6)) besproken, waarmee relaties voor de koppelingsconstanten gevonden kunnen worden.

Het bekende formalisme voor verstrooiing in meerdere kanalen is toegepast op Σp verstrooiing in hoofdstuk 4. Voor deze wisselwerking heeft men koppeling tussen toestanden met verschillend baanimpulsmoment wegens het voorkomen van een tensorpotentiaal. Bovendien is er koppeling mogelijk met kanalen waarin andere deeltjes aanwezig zijn. Dit betekent dat de Schrödingervergelijking niet verder gereduceerd kan worden dan tot een stelsel van gekoppelde differentiaalvergelijkingen, maximaal zes in het meest gecompliceerde geval.

De Coulombpotentiaal heeft een belangrijke invloed bij deze lage energieën. De gevolgen van deze potentiaal met lange dracht worden beschouwd in hoofdstuk 5. Een effectieve-drachtontwikkeling voor verstrooiing in meerdere kanalen is afgeleid voor algemene baanimpulsmomenten voor het geval dat er ook een Coulomb potentiaal aanwezig is.

Hoofdstuk 6 is een intermezzo tussen de beschrijving van het model en de feitelijke berekeningen. Daarin worden de numerieke methodes en de struktuur van de rekenmachineprogramma's beschreven, die nodig waren om de Schrö-

dingervergelijking numeriek te integreren en de experimentele grootheden te berekenen.

De volgende hoofdstukken geven het resultaat van de berekeningen. In hoofdstuk 7 leiden we eerst een benadering af voor het meenemen van de Coulombeffecten en vergelijken dan de resultaten daarvan met de exacte berekeningen. Daarna wordt de Σ^-p verstrooiing bestudeerd, gebruik makend van potentialen uitsluitend ten gevolge van de uitwisseling van pseudoscalaire mesonen. Er moet een harde pit aan deze potentialen toegevoegd worden. De straal hiervan was berekend door de ΛN verstrooiingslengten aan te passen aan de experimentele waarden. Als men de bekende $NN\pi$ koppelingsconstante gebruikt, worden de overige koppelingsconstanten gegeven in termen van één parameter, de F/(F+D) verhouding α. Het bleek dat een goede aanpassing aan de experimenten verkregen kon worden voor $\alpha \sim 0.5$, dus bijna gelijk aan de SU(6) voorspelling: $\alpha = 0.4$. Ook klopten de hoekverdelingen met de experimenten.

Er is één punt in onze berekeningen dat nadere bestudering vraagt. Als men deze potentialen met dezelfde straal van de harde pit ook gebruikt voor Σ^+p wisselwerking, die zuiver isospin T=3/2 heeft, terwijl het ΛN systeem een zuivere T=1/2 toestand is, dan is er in veel gevallen een Σ^+p gebonden singlet toestand. Zo'n gebonden toestand is experimenteel niet gevonden. De enige experimentele aanwijzing hiervoor is een sterkere Σ^+p verstrooiing in voorwaartse richting. Dit kan eventueel verklaard worden door een gebonden toestand aan te nemen die aanleiding geeft tot een constructieve Coulomb interferentie. We hebben aangetoond dat deze verklaring leidt tot een te grote bindingsenergie voor zo'n gebonden toestand.

Wanneer we nu de mogelijkheid van een Σ^+p gebonden toestand verwerpen, dan moeten we ook de veronderstelling loslaten dat de T=1/2 en T=3/2 pitten gelijk zijn. In hoofdstuk 8 is daarom een benadering afgeleid die het mogelijk maakt voor Σ^-p verstrooiing, een mengsel van T=1/2 en T=3/2 toestanden, berekeningen te doen met verschillende pitstralen in deze toestanden. Het bleek dat de resultaten van de berekeningen in het vorige hoofdstuk niet essentiëel veranderden.

Tenslotte zijn in hoofdstuk 9 de berekeningen uit hoofdstuk 7 en 8 herhaald, nu met een potentiaal ten gevolge van de uitwisseling van pseudoscalaire en vectormesonen. Indien we voorspellingen van SU(6) en de uit de NN wisselwerking bepaalde waarde voor de magnetische $NN\rho$ koppelingsconstante gebruikten, verkregen we een goede overeenkomst met de experimenten.

REFERENCES

1) A.H. Rosenfeld, A. Barbaro-Galtieri, W.H. Barkas, P.L. Bastien, J. Kirz, M. Roos, Rev. Mod. Phys. 36, 977 (1964).
2) M. Gell-Mann and Y. Ne'eman, The Eightfold Way, New York 1964.
3) M. Gell-Mann, Phys. Rev. 125, 1067 (1962).
4) Y. Ne'eman, Nucl. Phys. 26, 222 (1961).
5) Surveys of SU(6) and its relativistic generalizations have been given by: A. Pais, Rev. Mod. Phys. 38, 215 (1966); H. Ruegg, W. Rühl, and T.S. Santhanam, Helv. Phys. Acta 40, 9 (1967).
6) A review can be found in: M.J. Moravcsik, The Two-Nucleon Interaction, Oxford 1963.
7) Reviews can be found in: R.J.N. Phillips, Reports on Progress in Physics, 22, 562 (1959); R. Cirelli and G. Stabilini, Suppl. N. Cim. 20, 157 (1961).
8) P.S. Signell and R.E. Marshak, Phys. Rev. 106, 832 (1957); Phys. Rev. 109, 1229 (1958); J.L. Gammel and R.M. Thaler, Phys. Rev. 107, 291 (1957); Phys. Rev. 107, 1337 (1957).
9) R. Jastrow, Phys. Rev. 81, 165 (1951).
10) W. Heisenberg, Progr. Theor. Phys. 5, 523 (1950); Y. Nambu, Phys. Rev. 106, 1366 (1957); Y. Fujii, Progr. Theor. Phys. (Kyoto) 21, 232 (1959); G. Breit, Proc. Natl. Acad. Sci. U.S. 46, 746 (1960); Phys. Rev. 120, 287 (1960); J.J. Sakurai, Phys. Rev. 119, 1784 (1960).
11) J.J. Sakurai, Ann. Phys. (New York) 11, 1 (1960).
12) References can be found in: R.A. Bryan, "Nucleon-Nucleon Scattering", International Nuclear Physics Conference, Gatlinburg 1966, New York 1967 (in press).
13) E.P. Wigner, Proc. Natl. Acad. Sci. U.S. 38, 449 (1952); J. Schwinger, Ann. Phys. (New York) 2, 407 (1957); M. Gell-Mann, Phys. Rev. 106, 1296 (1957).
14) R.A. Bryan, J.J. de Swart, R.E. Marshak, and P.S. Signell, Phys. Rev. Letters 1, 70 (1958); F. Ferrari and L. Fonda, Phys. Rev. 114, 874 (1959).
15) J.J. de Swart and C. Dullemond, Ann. Phys. (New York) 16, 263 (1961).
16) J.J. de Swart and C. Dullemond, Ann. Phys. (New York) 19, 458 (1962).
17) C. Dullemond, Thesis, University of Rochester 1961 (unpublished).
18) R.J. Oakes and C.N. Yang, Phys. Rev. Letters 11, 174 (1963); see also: R.H. Dalitz in Proceedings of the Oxford International Conference on Elementary Particles 1965, Oxford 1966.
19) R.J. Oakes, Phys. Rev. 131, 2239 (1963); A. Deloff and H.W. Wyld, Physics Letters 12, 245 (1964); S. Iwao, N. Cim. 34, 1167 (1964).
20) P.D. DeSouza, G.A. Snow, and S. Meshkov, Phys. Rev. 135, B565 (1964); D. Cline and N. Olsson, Physics Letters 17, 340 (1965); D.A. Akyeampong and R. Delbourgo, Phys. Rev. 140, B1013 (1965); V. Barger and M.H. Rubin, Phys. Rev. 140, B1366 (1965).
21) F. Ferrari and L. Fonda, N. Cim. 9, 842 (1958); D.B. Lichtenberg and M. Ross, Phys. Rev. 109, 2163 (1958).
22) J.J. de Swart and C.K. Iddings, Phys. Rev. 128, 2810 (1962).
23) J.J. de Swart and C.K. Iddings, Phys. Rev. 130, 319 (1963).
24) K.A. Brueckner and K.M. Watson, Phys. Rev. 92, 1023 (1953).
25) D.B. Lichtenberg and M.H. Ross, Phys. Rev. 107, 1714 (1957); N. Dallaparta and F. Ferrari, N. Cim. 5, 111 (1957).
26) H.G. Dosch and V.F. Müller, Physics Letters 19, 320 (1965).
27) G. Fast, private communication.
28) See e.g. J.M. Blatt and V.F. Weisskopf, Theoretical Nuclear Physics, New York 1952.
29) A review has been given by R.H. Dalitz, Nuclear Interactions of the Hyperons, Oxford 1965.
30) R.R. Ross, Bull. Am. Phys. Soc. 3, 335 (1958); F.S. Crawford, M. Cresti, M.L. Good, F.T. Solmitz, M.L. Stevenson, and H.K. Tycho, Phys. Rev. Letters 2, 174 (1959); L.W. Alvarez, Ninth International Annual Conference on High Energy Physics, Kiev, 1959, Moscow 1960.
31) N. Horwitz, D. Miller, and J. Murray, Bull. Am. Phys. Soc. 4, 289 (1959); O. Dahl, N. Horwitz, D. Miller and J. Murray, Phys. Rev. Letters 4, 77 (1960).
32) F.R. Stannard, Phys. Rev. 121, 1513 (1961).
33) H.G. Dosch, R. Engelmann, H. Filthuth, V. Hepp, E. Kluge, and A. Minguzzi-Ranzi, Physics Letters 14, 162 (1965); XII International Conference on High Energy Physics, Dubna 1964, Moscow 1966.
34) H.G. Dosch, R. Engelmann, H. Filthuth, V. Hepp, E. Kluge, Physics Letters 21, 236 (1966).
35) R. Engelmann, H. Filthuth, V. Hepp, E. Kluge, Physics Letters 21, 587 (1966).
36) V. Hepp, Thesis, Universität Heidelberg, Juni 1966 (unpublished).
37) R.A. Burnstein, T.B. Day, B. Kehoe, H.A. Rubin, B. Sechi-Zorn, and G.A. Snow, XII International Conference on High Energy Physics, Dubna 1964, Moscow 1966.
38) R.A. Burnstein, University of Maryland, Technical Report No. 469 (1965).
39) H.A. Rubin, Bull. Am. Phys. Soc. 11, 37 (1966) and private communication.
40) H.A. Rubin, and R.A. Burnstein, University of Maryland, Technical Report No. 655 (1967).
41) R. Carrara, M. Cresti, A. Grigoletto, S. Limentani, L. Peruzzo, R. Santangelo, and R.B. Willmann, N. Cim. 38, 724 (1965).
42) G. Alexander, O. Benary, U. Karshon, A. Shapiro, G. Yekutieli, R. Engelmann, H. Filthuth, A. Fridman, and B. Schiby, Physics Letters 19, 715 (1966).

43) A.R. Bodmer, Phys. Rev. 141, 1387 (1966); A. Gal, Phys. Rev. Letters 18, 568 (1967).
44) See e.g. D.E. Neville, Phys. Rev. 130, 327 (1963).
45) R.A. Burnstein, G.A. Snow, and H. Whiteside, Phys. Rev. Letters 15, 639 (1965).
46) T.B. Day, J. Sucher, and G.A. Snow, Phys. Rev. Letters 3, 61 (1959); Phys. Rev. 118, 864 (1960); M. Leon and H.A. Bethe, Phys. Rev. 127, 636 (1960); A.S. Wightman, Phys. Rev. 77, 521 (1950).
47) G.C. Wick, Nature 142, 994 (1938).
48) M. Taketani, Suppl. Progr. Theor. Phys. (Kyoto) 3, 1 (1956).
49) R.A. Bryan and B.L. Scott, preprint (March 1967).
50) N. Hoshizaki, I. Lin, and S. Machida, Progr. Theor. Phys. 26, 680 (1961).
51) P.A. Protopapadakis, Thesis, London 1963 (unpublished).
52) N. Hoshizaki and S. Machida, Progr. Theor. Phys. (Kyoto) 24, 1325 (1960).
53) L. Eisenbud and E.P. Wigner, Proc. Nat. Acad. Sci. U.S. 27, 281 (1941); S. Okubo and R.E. Marshak, Ann. Phys. (New York) 4, 166 (1958).
54) B. d'Espagnat and J. Prentki, Nucl. Phys. 1, 33 (1956); Progress on Elementary Particles and Cosmic Ray Physics 4, 1 (1958).
55) S. Okubo, Progr. Theor. Phys. (Kyoto) 27, 949 (1962).
56) J.J. Sakurai, Phys. Rev. Letters 9, 472 (1962).
57) J.J. de Swart, Rev. Mod. Phys. 35, 916 (1963).
58) Several determinations of α agree with the SU(6) prediction, α=0.4. See e.g. R.E. Cutcosky, Ann. Phys. (New York), 23, 415 (1963); A.W. Martin and K.C. Wali, N. Cim. 31, 1324 (1964); W. Willis, H. Courant, H. Filthuth, P. Franzini, A. Minguzzi-Ranzi, A. Segar, R. Engelmann, V. Hepp, E. Kluge, R.A. Burnstein, T.B. Day, R.G. Glasser, A.J. Herz, B. Sechi-Zorn, N. Seeman, and G.A. Snow, Phys. Rev. Letters 13, 291 (1964); F.J.M. von der Linden and C. Dullemond, N. Cim. 43, 615 (1966).
59) E.J. Kelly, Phys. Rev. 79, 399 (1950).
60) G.W. London, R.R. Rau, N.P. Samios, S.S. Yamamoto, M. Goldberg, S. Lichtman, M. Prime, and J. Leitner, Phys. Rev. 143, 1034 (1966).
61) B. Sakita, Phys. Rev. 136, 1756 (1964).
62) F. Gürsey, A. Pais, and L.A. Radicati, Phys. Rev. Letters 13, 299 (1964).
63) L. Wolfenstein, Ann. Rev. Nuclear Sci. 6, 43 (1956).
64) B.W. Downs and R. Schrils, Phys. Rev. 127, 1388 (1962).
65) M.H. Ross and G. Shaw, Ann. Phys. (New York) 13, 147 (1961).
66) See e.g. A. Messiah, Quantum Mechanics, Amsterdam 1961.
67) F.L. Jost, J.A. Wheeler, and G. Breit, Phys. Rev. 49, 174 (1936).
68) Tables of Coulomb Wave Functions, AMS 17, National Bureau of Standards, Washington 1952.
69) J.D. Jackson and J.M. Blatt, Rev. Mod. Phys. 22, 77 (1950).
70) B. Numerov, Publ. de l'Observ. Astrophys. Central de Russie, 2, 188 (1933); J.J. de Swart and P.J. Eberlein, Univ. of Rochester Report NYO-9030, March 1960 (unpublished).
71) J.L. Powell, Phys. Rev. 72, 626 (1947).
72) T.J. Stieltjes, Acta Math. Stockholm 10, 299 (1887) (reprinted in: Oevres Complètes de Thomas Jan Stieltjes II, Groningen 1918).
73) E.E. Allen, MTAC 10, 162 (1956).
74) This routine is due to Veltman. See also M.J.G. Veltman, Thesis University of Utrecht, 1963, Stelling XI.
75) J.C. Helder and J.J. de Swart, Physics Letters 21, 109 (1966). The values of the core radii obtained from Ref. 9 of this Letter have been corrected. Hence, the numerical results reported are no longer accurate.
76) Ref. 30, first entry.
77) O. Dahl, N. Horwitz, D. Miller, and J. Murray, Phys. Rev. Letters 4, 77 (1960).
78) R.G. Ammar, N. Crayton, K.P. Jain, R. Levi Setti, J.E. Mott, P.E. Schlein, O. Skjeggestad, and P.K. Srivastava, Phys. Rev. 120, 1914 (1960).
79) R. Chand, N. Cim. 36, 337 (1965).
80) J.J. Sakurai, Phys. Rev. Letters 17, 1021 (1966).
81) P. Signell and J.W. Durso, Phys. Rev. Letters 18, 185 (1967).
82) See e.g. F.M. Pipkin, Proceedings of the Oxford International Conference on Elementary Particles 1965, Oxford 1966.
83) E.B. Hughes, T.A. Griffy, M.R. Yearian, and R. Hofstadter, Phys. Rev. 139, B458 (1965).
84) L.H. Chan, K.W. Chen, J.R. Dunning, Jr., N.F. Ramsey, J.K. Walker, and R. Wilson, Phys. Rev. 141, 1298 (1966).
85) G.L. Kane and R.A. Zdanis, Phys. Rev. 151, 1239 (1966).
86) R.A. Bryan and B.L. Scott, preprint (March 1967).
87) M. Moravcsik, Phys. Rev. Letters 2, 352 (1959); M. Rimpault, N. Cim. 31, 56 (1964); J. Dufour, N. Cim. 34, 645 (1964); M. Lussignoli, M. Restignoli, G.A. Snow, and G. Violini, Physics Letters 21, 229 (1966); N. Zovko, Physics Letters 23, 143 (1966); H.P.C. Rood, N. Cim. 50A, 493 (1967).
88) I.G. Aznauryan and L.D. Soloviev, Dubna Report No. E-2544 (1966).
89) Y.C. Tang and R.C. Herndon, Phys. Rev. 151, 1116 (1966).